Title

Search for top-squark pair production in final states with one lepton, jets, and missing transverse momentum using 36 fb−1 of s=13 TeV pp collision data with the ATLAS detector

Journal

Journal of High Energy Physics, 2018(6)

ISSN

1126-6708

Authors

The ATLAS collaboration
Aaboud, M
Aad, G
et al.

Publication Date

2018-06-01

DOI

10.1007/jhep06(2018)108

EUROPEAN ORGANISATION FOR NUCLEAR RESEARCH (CERN)

Submitted to: JHEP

CERN-EP-2017-246
1st December 2017

Search for top-squark pair production in final states with one lepton, jets, and missing transverse momentum using 36 fb^{-1} of $\sqrt{s}$ = 13 TeV pp collision data with the ATLAS detector

The ATLAS Collaboration

The results of a search for the direct pair production of top squarks, the supersymmetric partner of the top quark, in final states with one isolated electron or muon, several energetic jets, and missing transverse momentum are reported. The analysis also targets spin-0 mediator models, where the mediator decays into a pair of dark-matter particles and is produced in association with a pair of top quarks. The search uses data from proton–proton collisions delivered by the Large Hadron Collider in 2015 and 2016 at a centre-of-mass energy of $\sqrt{s}$ = 13 TeV and recorded by the ATLAS detector, corresponding to an integrated luminosity of 36 fb^{-1}. A wide range of signal scenarios with different mass-splittings between the top squark, the lightest neutralino and possible intermediate supersymmetric particles are considered, including cases where the W bosons or the top quarks produced in the decay chain are off-shell. No significant excess over the Standard Model prediction is observed. The null results are used to set exclusion limits at 95% confidence level in several supersymmetry benchmark models. For pair-produced top-squarks decaying into top quarks, top-squark masses up to 940 GeV are excluded. Stringent exclusion limits are also derived for all other considered top-squark decay scenarios. For the spin-0 mediator models, upper limits are set on the visible cross-section.

1 Introduction

The hierarchy problem [1–4] has gained additional attention with the observation of a particle consistent with the Standard Model (SM) Higgs boson [5, 6] at the Large Hadron Collider (LHC) [7]. Supersymmetry (SUSY) [8–16], which extends the SM by introducing supersymmetric partners for every SM particle, can provide an elegant solution to the hierarchy problem. The partner particles have identical quantum numbers except for a half-unit difference in spin. The superpartners of the left- and right-handed top quarks, $\tilde{t}_{\mathrm{L}}$ and $\tilde{t}_{\mathrm{R}}$, mix to form the two mass eigenstates $\tilde{t}_1$ and $\tilde{t}_2$ (top squark or stop), where $\tilde{t}_1$ is the lighter of the two.[1] If the supersymmetric partners of the top quarks have masses $\lesssim 1$ TeV, loop diagrams involving top quarks, which are the dominant divergent contribution to the Higgs-boson mass, can largely cancel out [17–24].

Significant mass-splitting between the $\tilde{t}_1$ and $\tilde{t}_2$ is possible due to the large top-quark Yukawa coupling. Furthermore, effects of the renormalisation group equations are strong for the third-generation squarks, usually driving their masses to values significantly lower than those of the other generations. These considerations suggest a light stop[2] [25, 26] which, together with the stringent LHC limits excluding other coloured supersymmetric particles with masses below the TeV level, motivates dedicated stop searches.

The conservation of baryon number and lepton number can be violated in SUSY models, resulting in a proton lifetime shorter than current experimental limits [27]. This is commonly resolved by introducing a multiplicative quantum number called R-parity, which is 1 and -1 for all SM and SUSY particles (sparticles), respectively. A generic R-parity-conserving minimal supersymmetric extension of the SM (MSSM) [17, 28–31] predicts pair production of SUSY particles and the existence of a stable lightest supersymmetric particle (LSP).

The charginos $\tilde{\chi}^{\pm}_{1,2}$ and neutralinos $\tilde{\chi}^{0}_{1,2,3,4}$ are the mass eigenstates formed from the linear superposition of the charged and neutral SUSY partners of the Higgs and electroweak gauge bosons (higgsinos, winos and binos). They are referred to in the following as electroweakinos. In a large variety of SUSY models, the lightest neutralino ($\tilde{\chi}^{0}_{1}$) is the LSP, which is also the assumption throughout this paper. The LSP provides a particle dark-matter (DM) candidate, as it is stable and interacts only weakly [32, 33].

This paper presents a search for direct $\tilde{t}_1$ pair production in final states with exactly one isolated charged lepton (electron or muon,[3] henceforth referred to simply as 'lepton') from the decay of either a real or a virtual W boson. In addition the search requires several jets and a significant amount of missing transverse momentum $\vec{p}_{\mathrm{T}}^{\,\mathrm{miss}}$, the magnitude of which is referred to as $E_{\mathrm{T}}^{\mathrm{miss}}$, from the two weakly interacting LSPs that escape detection. Results are also interpreted in an alternative model where a spin-0 mediator is produced in association with top quarks and subsequently decays into a pair of DM particles.

Searches for direct $\tilde{t}_1$ pair production were previously reported by the ATLAS [34–38] and CMS [39–47] collaborations, as well as by the CDF and DØ collaborations (for example [48, 49]) and the LEP collaborations [50]. The exclusion limits obtained by previous ATLAS searches for stop models with massless neutralinos reach ~ 950 GeV for direct two-body decays $\tilde{t}_1 \to t\tilde{\chi}^{0}_{1}$, ~ 560 GeV for the three-body process $\tilde{t}_1 \to bW\tilde{\chi}^{0}_{1}$, and ~ 400 GeV for four-body decays $\tilde{t}_1 \to bff'\tilde{\chi}^{0}_{1}$, all at the 95% confidence level.

[1] Similarly the $\tilde{b}_1$ and $\tilde{b}_2$ (bottom squark or sbottom) are formed by the superpartners of the bottom quarks, $\tilde{b}_{\mathrm{L}}$ and $\tilde{b}_{\mathrm{R}}$.

[2] The soft mass term of the superpartner of the left-handed bottom quark can be as light as that of the superpartner of the left-handed top quark in certain scenarios as they are both governed mostly by a single mass parameter in SUSY models at tree level. The mass of the superpartner of the right-handed bottom quark is governed by a separate mass parameter from the stop mass parameters, and it is assumed to be larger than 3 TeV having no impact on the signal models considered in this paper.

[3] Electrons and muons from τ decays are included.

Searches for spin-0 mediators decaying into a pair of DM particles and produced in association with heavy-flavour quarks have also been reported with zero or two leptons in the final state by the ATLAS collaboration [51], and by the CMS collaboration [52].

2 Search strategy

2.1 Signal models

The experimental signatures of stop pair production can vary dramatically, depending on the spectrum of low-mass SUSY particles. Figure 1 illustrates two typical stop signatures: $\tilde{t}_1 \to t\tilde{\chi}_1^0$ and $\tilde{t}_1 \to b\tilde{\chi}_1^\pm$. Other decay and production modes such as $\tilde{t}_1 \to t\tilde{\chi}_2^0$ and $\tilde{t}_1 \to t\tilde{\chi}_3^0$, and sbottom direct pair production are also considered. The analysis attempts to probe a broad range of possible scenarios, taking the approach of defining dedicated search regions to target specific but representative SUSY models. The phenomenology of each model is largely driven by the composition of its lightest sparticles, which are considered to be some combination of the electroweakinos. In practice, this means that the most important parameters of the SUSY models considered are the masses of the electroweakinos and of the colour-charged third-generation sparticles.

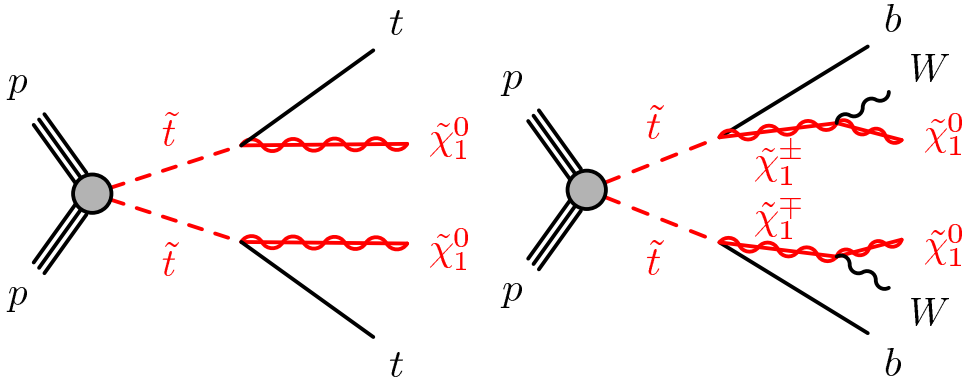

Figure 1: Diagrams illustrating the stop decay modes, which are referred to as (left) $\tilde{t}_1 \to t\tilde{\chi}_1^0$ and (right) $\tilde{t}_1 \to b\tilde{\chi}_1^\pm$. Sparticles are shown as red lines. In these diagrams, the charge-conjugate symbols are omitted for simplicity. The direct stop production begins with a top squark–antisquark pair.

In this search, the targeted signal scenarios are either simplified models [53–55], in which the masses of all sparticles are set to high values except for the few sparticles involved in the decay chain of interest, or models based on the phenomenological MSSM (pMSSM) [56, 57], in which all of the 19 pMSSM parameters are set to fixed values, except for two which are scanned. The set of models used are chosen to give a broad coverage of the possible stop decay patterns and phenomenology that can be realised in the MSSM, in order to best demonstrate the sensitivity of the search for direct stop production. The simplified models used are designed with a goal of covering distinct phenomenologically different regions of pMSSM parameter space.

The pMSSM parameters m_{tR} and m_{q3L} specify the $\tilde{t}_\mathrm{R}$ and $\tilde{t}_\mathrm{L}$ soft mass terms, with the smaller of the two controlling the $\tilde{t}_1$ mass. In models where the $\tilde{t}_1$ is primarily composed of $\tilde{t}_\mathrm{L}$, the production of light

sbottoms ($\tilde{b}_1$) with a similar mass is also considered. The mass spectrum of electroweakinos and the gluino is given by the running mass parameters M_1, M_2, M_3, and μ, which set the masses of the bino, wino, gluino, and higgsino, respectively. If the mass parameters, M_1, M_2, and μ, are comparably small, the physical LSP is a mixed state, composed of multiple electroweakinos. Other relevant pMSSM parameters include β, which gives the ratio of vacuum expectation values of the up- and down-type Higgs bosons influencing the preferred decays of the stop, the SUSY breaking scale (M_S) defined as $M_S = \sqrt{m_{\tilde{t}_1} m_{\tilde{t}_2}}$, and the top-quark trilinear coupling (A_t). In addition, a maximal $\tilde{t}_L$–$\tilde{t}_R$ mixing condition, $X_t/M_S \sim \sqrt{6}$ (where $X_t = A_t - \mu/\tan\beta$), is assumed to obtain a low-mass stop ($\tilde{t}_1$) while the models remain consistent with the observed Higgs boson mass of 125 GeV [5, 6].

In this search, four scenarios[4] are considered, where each signal scenario is defined by the nature of the LSP and the next-to-lightest supersymmetric particle (NLSP): (a) pure bino LSP, (b) bino LSP with a light wino NLSP, (c) higgsino LSP, and (d) mixed bino/higgsino LSP, which are detailed below with the corresponding sparticle mass spectra illustrated in Figure 2. Complementary searches target scenarios where the LSP is a pure wino (yielding a disappearing track signature [58] common in anomaly-mediated models [59, 60] of SUSY breaking) as well as other LSP hypotheses (such as gauge-mediated models [61–63]), which are not discussed further.

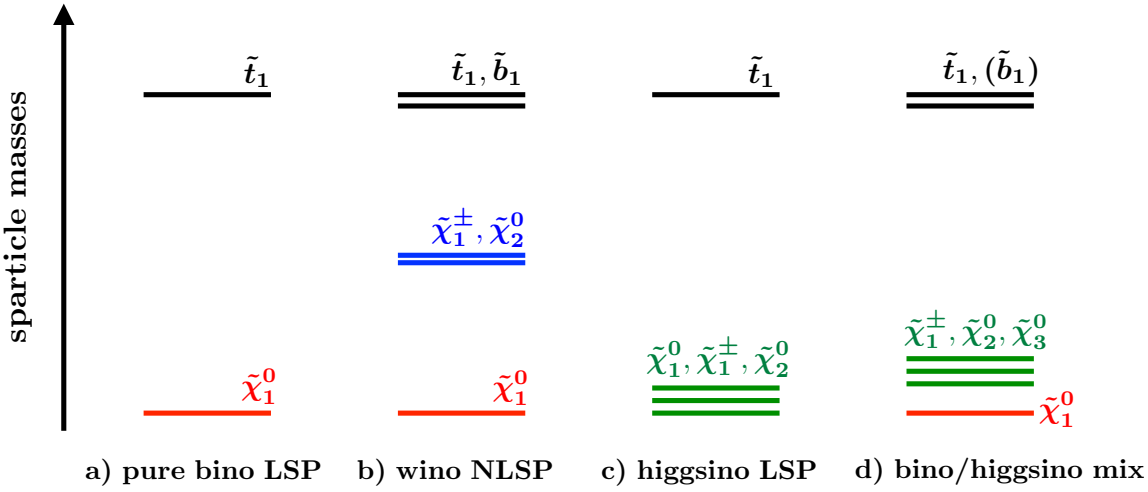

Figure 2: Illustration of the sparticle mass spectrum for various LSP scenarios: a) pure bino LSP, b) wino NLSP, c) higgsino LSP, and d) bino/higgsino mixed LSP. The $\tilde{t}_1$ and $\tilde{b}_1$, shown as black lines, decay into various electroweakino states: the bino state (red lines), wino state (blue lines), or higgsino state (green lines), possibly with the subsequent decay into the LSP. The light sbottom ($\tilde{b}_1$) is considered only for pMSSM models with $m_{q3L} < m_{tR}$.

(a) Pure bino LSP model:

A simplified model is considered for the scenario where the only light sparticles are the stop (composed mainly of $\tilde{t}_R$) and the lightest neutralino. When the stop mass is greater than the sum of the top quark and LSP masses, the dominant decay channel is via $\tilde{t}_1 \to t\tilde{\chi}_1^0$. If this decay is

[4] For the higgsino LSP scenarios, three sets of model assumptions are considered, each giving rise to different stop branching ratios for $\tilde{t}_1 \to b\tilde{\chi}_1^{\pm}$, $\tilde{t}_1 \to t\tilde{\chi}_1^0$, and $\tilde{t}_1 \to t\tilde{\chi}_2^0$.

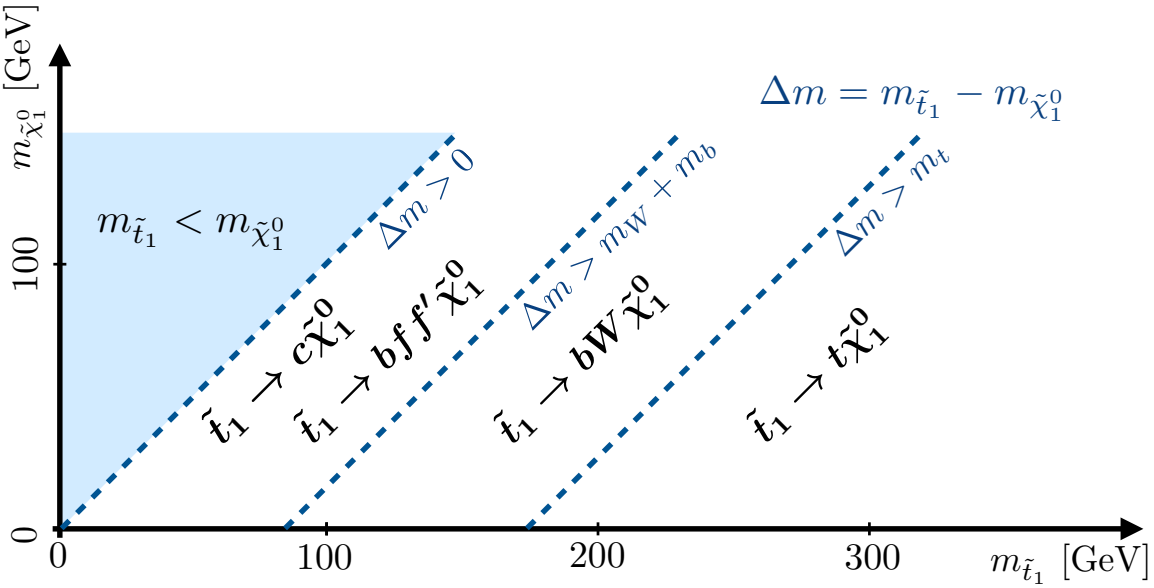

Figure 3: Illustration of the preferred stop decay modes in the plane spanned by the masses of the stop ($\tilde{t}_1$) and the lightest neutralino ($\tilde{\chi}_1^0$), where the latter is assumed to be the lightest supersymmetric particle. Stop decays into supersymmetric particles other than the lightest supersymmetric particle are not displayed.

kinematically disallowed, the stop can undergo a three-body decay, $\tilde{t}_1 \to bW\tilde{\chi}_1^0$, when the stop mass is above the sum of masses of the bottom quark, W boson, and $\tilde{\chi}_1^0$. Otherwise the decay proceeds via a four-body process, $\tilde{t}_1 \to bff'\tilde{\chi}_1^0$, where f and f' are two distinct fermions, or via a flavour-changing neutral current (FCNC) process, such as the loop-suppressed $\tilde{t}_1 \to c\tilde{\chi}_1^0$. Given the very different final state, the FCNC decay is not considered further in this search, and therefore a 100% branching ratio to $\tilde{t}_1 \to bff'\tilde{\chi}_1^0$ is assumed. The various $\tilde{t}_1$ decay modes in this scenario are illustrated in Figure 3. The region of phase space along the line of $m_{\tilde{t}_1} = m_{\tilde{\chi}_1^0} + m_{\text{top}}$ is especially challenging to target because of the similarity of the stop signature to the $t\bar{t}$ process, and is referred to in the following as the 'diagonal region'.

(b) Wino NLSP model:

A pMSSM model is designed such that a wino-like chargino ($\tilde{\chi}_1^\pm$) and neutralino ($\tilde{\chi}_2^0$) are mass-degenerate, with the bino as the LSP. This scenario is motivated by models with gauge unification at the GUT scale such as the cMSSM or mSugra [64–66], where M_2 is assumed to be twice as large as M_1, leading to the $\tilde{\chi}_1^\pm$ and $\tilde{\chi}_2^0$ having masses nearly twice as large as that of the bino-like LSP.

In this scenario, additional decay modes for the stop (composed mainly of $\tilde{t}_L$) become relevant, such as the decay into a bottom quark and the lightest chargino ($\tilde{t}_1 \to b\tilde{\chi}_1^\pm$) or the decay into a top quark and the second neutralino ($\tilde{t}_1 \to t\tilde{\chi}_2^0$). The $\tilde{\chi}_1^\pm$ and $\tilde{\chi}_2^0$ subsequently decay into $\tilde{\chi}_1^0$ via emission of a (potentially off-shell) W boson or Z/Higgs (h) boson, respectively. The $\tilde{t}_1 \to b\tilde{\chi}_1^\pm$ decay is considered for a chargino mass above about 100 GeV since the LEP limit on the lightest chargino is $m_{\tilde{\chi}_1^\pm} > 103.5$ GeV [67].

An additional $\tilde{t}_1 \to b\tilde{\chi}_1^\pm$ decay signal model (simplified model) is designed, motivated by a scenario

with nearly equal masses of the $\tilde{t}_1$ and $\tilde{\chi}_1^\pm$. The model considered assumes the mass-splitting between the $\tilde{t}_1$ and $\tilde{\chi}_1^\pm$, $\Delta m(\tilde{t}_1, \tilde{\chi}_1^\pm) = 10$ GeV and that the top squark decays via the process $\tilde{t}_1 \to b\tilde{\chi}_1^\pm$ with a branching ratio of 100%. In this scenario, the jets originating from the bottom quarks are too low in energy (soft) to be reconstructed and hence the signature is characterised by large $E_{\mathrm{T}}^{\mathrm{miss}}$ and no jets initiated by bottom quarks (referred to as b-jets).

(c) Higgsino LSP model:

'Natural' models of SUSY [23, 24, 68] suggest low-mass stops and a higgsino-like LSP. In such scenarios, a typical $\Delta m(\tilde{\chi}_1^\pm, \tilde{\chi}_1^0)$ varies between a few hundred MeV to several tens of GeV depending mainly on the mass relations amongst the electroweakinos. For this analysis, a simplified model is designed for various $\Delta m(\tilde{\chi}_1^\pm, \tilde{\chi}_1^0)$ of up to 30 GeV satisfying the mass relation as follows:

$$\Delta m(\tilde{\chi}_1^\pm, \tilde{\chi}_1^0) = 0.5 \times \Delta m(\tilde{\chi}_2^0, \tilde{\chi}_1^0).$$

The stop decays into either $b\tilde{\chi}_1^\pm$, $t\tilde{\chi}_1^0$, or $t\tilde{\chi}_2^0$, followed by the $\tilde{\chi}_1^\pm$ and $\tilde{\chi}_2^0$ decay through the emission of a highly off-shell W/Z boson. Hence the signature is characterised by low-momentum leptons or jets from off-shell W/Z bosons, and the analysis benefits from reconstructing low-momentum leptons (referred to as soft leptons). The stop decay branching ratio strongly depends on the $\tilde{t}_\mathrm{R}$ and $\tilde{t}_\mathrm{L}$ composition of the stop. Stops composed mainly of $\tilde{t}_\mathrm{R}$ have a large branching ratio $\mathcal{B}(\tilde{t}_1 \to b\tilde{\chi}_1^\pm)$, whereas stops composed mainly of $\tilde{t}_\mathrm{L}$ have a large $\mathcal{B}(\tilde{t}_1 \to t\tilde{\chi}_1^0)$ or $\mathcal{B}(\tilde{t}_1 \to t\tilde{\chi}_2^0)$. In this search, the three cases are considered separately: $\tilde{t}_1 \sim \tilde{t}_\mathrm{R}$, $\tilde{t}_1 \sim \tilde{t}_\mathrm{L}$, and a case in which the stop decays democratically into the three decay modes.

(d) Bino/higgsino mix model:

The 'well-tempered neutralino' [69] scenario seeks to provide a viable dark-matter candidate while simultaneously addressing the problem of naturalness by targeting an LSP that is an admixture of bino and higgsino. The mass spectrum of the electroweakinos (higgsinos and bino) is expected to be slightly compressed, with a typical mass-splitting between the bino and higgsino states of 20–50 GeV. A pMSSM signal model is designed such that only a low level of fine-tuning [70, 71] of the pMSSM parameters is needed and the annihilation rate of neutralinos is consistent with the observed dark-matter relic density[5] ($0.10 < \Omega h^2 < 0.12$) [72].

The final state produced by many of the models described above is consistent with a $t\bar{t} + E_{\mathrm{T}}^{\mathrm{miss}}$ final state. Exploiting the similarity, signal models with a spin-0 mediator decaying into dark-matter particles produced in association with $t\bar{t}$ are also studied assuming either a scalar (ϕ) or a pseudoscalar (a) mediator [51, 73]. An example diagram for this process is shown in Figure 4.

2.2 Analysis strategy

The search presented is based on 16 dedicated analyses that target the various scenarios mentioned above. Each of these analyses corresponds to a set of event selection criteria, referred to as a signal region (SR), and is optimised to target one or more signal scenarios. Two different analysis techniques are employed in the definition of the SRs, which are referred to as 'cut-and-count' and 'shape-fit'. The former is based on counting events in a single region of phase space, and is employed in the 16 analyses. The latter is used

[5] The quantities Ω and h are the density parameter and Hubble constant, respectively.

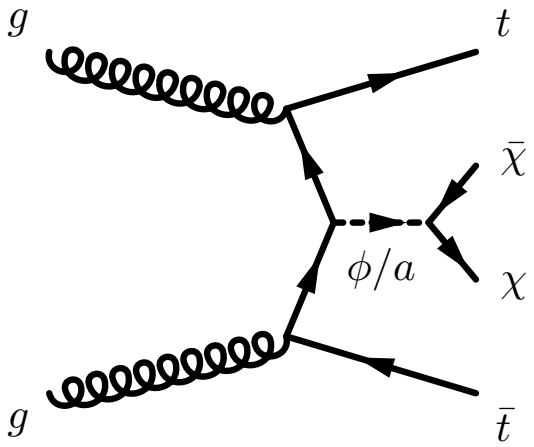

Figure 4: A representative Feynman diagram for spin-0 mediator production. The ϕ/a is the scalar/pseudoscalar mediator, which decays into a pair of dark-matter (χ) particles.

in some SRs in addition to the 'cut-and-count' technique and employs SRs split into multiple bins in a specific discriminating kinematic variable, that can cover a range that is larger than the 'cut-and-count' SR. By utilising different signal-to-background ratios in the various bins, the search sensitivity is enhanced in challenging scenarios where it is particularly difficult to separate signal from background.

The main background processes after the signal selections include $t\bar{t}$, single-top Wt, $t\bar{t} + Z(\rightarrow \nu\bar{\nu})$, and W+jets. Each of those SM processes are estimated by building dedicated control regions (CRs) enhanced in each of the processes, making the analysis more robust against potential mis-modelling effects in simulated events and reducing the uncertainties in the background estimates. The backgrounds are then simultaneously normalised in data using a likelihood fit for each SR with its associated CRs. The background modelling as predicted by the fits is tested in a series of validation regions (VRs).

3 ATLAS detector and data collection

The ATLAS detector [74] is a multipurpose particle physics detector with nearly 4π coverage in solid angle around the collision point.[6] It consists of an inner tracking detector (ID), surrounded by a superconducting solenoid providing a 2 T axial magnetic field, a system of calorimeters, and a muon spectrometer (MS) incorporating three large superconducting toroid magnets.

The ID provides charged-particle tracking in the range $|\eta| < 2.5$. During the LHC shutdown between Run 1 (2010–2012) and Run 2 (2015–2018), a new innermost layer of silicon pixels was added [75], which improves the track impact parameter resolution, vertex position resolution and b-tagging performance [76].

[6] ATLAS uses a right-handed coordinate system with its origin at the nominal interaction point (IP) in the centre of the detector and the z-axis along the beam pipe. The x-axis points from the IP to the centre of the LHC ring, and the y-axis points upwards. Cylindrical coordinates (r, ϕ) are used in the transverse plane, ϕ being the azimuthal angle around the z-axis. The pseudorapidity is defined in terms of the polar angle θ as $\eta = -\ln\tan(\theta/2)$. Angular distance is measured in units of $\Delta R \equiv \sqrt{(\Delta\eta)^2 + (\Delta\phi)^2}$.The transverse momentum, p_{T}, is defined with respect to the beam axis (x–y plane).

High-granularity electromagnetic and hadronic calorimeters cover the region $|\eta| < 4.9$. The central hadronic calorimeter is a sampling calorimeter with scintillator tiles as the active medium and steel absorbers. All the electromagnetic calorimeters, as well as the endcap and forward hadronic calorimeters, are sampling calorimeters with liquid argon as the active medium and lead, copper, or tungsten absorbers. The MS consists of three layers of high-precision tracking chambers with coverage up to $|\eta| = 2.7$ and dedicated chambers for triggering in the region $|\eta| < 2.4$. Events are selected by a two-level trigger system [77]: the first level is a hardware-based system and the second is a software-based system.

This analysis is based on a dataset collected in 2015 and 2016 at a collision energy of $\sqrt{s} = 13\,\text{TeV}$. The data contain an average number of simultaneous pp interactions per bunch crossing, or "pile-up", of approximately 23.7 across the two years. After the application of beam, detector and data-quality requirements, the total integrated luminosity is $36.1\,\text{fb}^{-1}$ with an associated uncertainty of 3.2%. The uncertainty is derived following a methodology similar to that detailed in Ref. [78] from a preliminary calibration of the luminosity scale using a pair of x–y beam separation scans performed in August 2015 and June 2016.

The events were primarily recorded with a trigger logic that accepts events with $E_{\text{T}}^{\text{miss}}$ above a given threshold. The trigger is fully efficient for events passing an offline-reconstructed $E_{\text{T}}^{\text{miss}} > 230\,\text{GeV}$ requirement, which is the minimum requirement deployed in the signal regions and control regions relying on the $E_{\text{T}}^{\text{miss}}$ triggers. To recover acceptance for signals with moderate $E_{\text{T}}^{\text{miss}}$, events having a well-identified lepton with a minimum p_{T} at trigger level are also accepted for several selections. Events in which the offline reconstructed $E_{\text{T}}^{\text{miss}}$ is measured to be less than 230 GeV are collected using single-lepton triggers, where the thresholds are set to obtain a constant efficiency as a function of the lepton p_{T} of ≈90% (≈80%) for electrons (muons).

4 Simulated event samples

Samples of Monte Carlo (MC) simulated events are used for the description of the SM background processes and to model the signals. Details of the simulation samples used, including the matrix element (ME) event generator and parton distribution function (PDF) set, the parton shower (PS) and hadronisation model, the set of tuned parameters (tune) for the underlying event (UE) and the order of the cross-section calculation, are summarised in Table 1.

Table 1: Overview of the nominal simulated samples.

Process	ME event generator	ME PDF	PS and hadronisation	UE tune	Cross-section calculation
$t\bar{t}$	Powheg-Box v2 [79]	CT10 [80]	Pythia 6 [81]	P2012 [82]	NNLO+NNLL [83–88]
Single-top					
t-channel	Powheg-Box v1	CT104f	Pythia 6	P2012	NNLO+NNLL [89]
s- and Wt-channel	Powheg-Box v2	CT10	Pythia 6	P2012	NNLO+NNLL [90, 91]
V+jets ($V = W/Z$)	Sherpa 2.2.0 [92]	NNPDF3.0 [93]	Sherpa	Default	NNLO [94]
Diboson	Sherpa 2.1.1 – 2.2.1	CT10/NNPDF3.0	Sherpa	Default	NLO
$t\bar{t} + V$	MG5_aMC@NLO 2.2.2 [95]	NNPDF3.0	Pythia 8 [96]	A14 [97]	NLO [95]
SUSY signal	MG5_aMC@NLO 2.2 – 2.4	NNPDF2.3 [98]	Pythia 8	A14	NLO+NLL [99]
DM signal	MG5_aMC@NLO 2.3.3	NNPDF2.3	Pythia 8	A14	NLO

The samples produced with MG5_aMC@NLO [95] and Powheg-Box [79, 100–103] used EvtGen v1.2.0 [104] for the modelling of b-hadron decays. The signal samples were all processed with a fast simulation [105], whereas all background samples were processed with the full simulation of the ATLAS detector [105] based on GEANT4 [106]. All samples were produced with varying numbers of minimum-bias interactions overlaid on the hard-scattering event to simulate the effect of multiple pp interactions in the same or nearby bunch crossings. The number of interactions per bunch crossing was reweighted to match the distribution in data.

4.1 Background samples

The nominal $t\bar{t}$ sample and single-top sample cross-sections were calculated to next-to-next-to-leading order (NNLO) with the resummation of soft gluon emission at next-to-next-to-leading-logarithm (NNLL) accuracy and were generated with Powheg-Box (NLO) interfaced to Pythia6 for parton showering and hadronisation. Additional $t\bar{t}$ samples were generated with MG5_aMC@NLO (NLO)+Pythia8, Sherpa, and Powheg-Box+Herwig++ [107, 108] for modelling comparisons and evaluation of systematic uncertainties.

Additional samples for $WWbb$, $Wt + b$, and $t\bar{t}$ were generated with MG5_aMC@NLO leading order (LO) interfaced to Pythia8, in order to assess the effect of interference between the singly and doubly resonant processes as a part of the Wt theoretical modelling systematic uncertainty.

Samples for W+ jets, Z + jets and diboson production were generated with Sherpa 2.2.0 [92] (and Sherpa 2.1.1 – 2.2.1 for the latter) using Comix [109] and OpenLoops [110], and merged with the Sherpa parton shower [111] using the ME+PS@NLO prescription [112]. The NNPDF30 PDF set [93] was used in conjunction with a dedicated parton shower tuning developed by the Sherpa authors. The W/Z + jets events were further normalised with the NNLO cross-sections.

The $t\bar{t} + V$ samples were generated with MG5_aMC@NLO (NLO) interfaced to Pythia8 for parton showering and hadronisation. Sherpa (NLO) samples were used to evaluate the systematic uncertainties related to the modelling of $t\bar{t} + V$ production.

More details of the $t\bar{t}$, W+ jets, Z + jets, diboson and $t\bar{t} + V$ samples can be found in Refs. [113–116].

4.2 Signal samples

Signal SUSY samples were generated at leading order (LO) with MG5_aMC@NLO including up to two extra partons, and interfaced to Pythia8 for parton showering and hadronisation. For the pMSSM models, the sparticle mass spectra were calculated using Softsusy 3.7.3 [117, 118]. The output mass spectrum was then interfaced to HDECAY 3.4 [119] and SDECAY 1.5/1.5a [120] to generate decay tables for each of the sparticles. The decays of the $\tilde{\chi}_2^0$ and $\tilde{\chi}_1^\pm$ via highly off-shell W/Z bosons were computed by taking into account the mass of τ leptons and charm quarks in the low $\Delta m(\tilde{\chi}_1^\pm/\tilde{\chi}_2^0, \tilde{\chi}_1^0)$ regime. For all models considered the decays of SUSY particles are prompt. The details of the various simulated samples in the four LSP scenarios targeted are given below. The input parameters for the pMSSM models are summarised in Table 2.

(a) Pure bino LSP:

For the $\tilde{t}_1 \to t\tilde{\chi}_1^0$ samples, the stop was decayed in PYTHIA8 using only phase space considerations and not the full matrix element. Since the decay products of the samples generated did not preserve spin information, a polarisation reweighting was applied[7] following Refs. [121, 122]. For the $\tilde{t}_1 \to bW\tilde{\chi}_1^0$ and $\tilde{t}_1 \to bff'\tilde{\chi}_1^0$ samples, the stop was decayed with MadSpin [123], interfaced to PYTHIA8. MadSpin emulates kinematic distributions such as the mass of the bW system to a good approximation without calculating the full ME. For the MadSpin samples, the stop was assumed to be composed mainly of $\tilde{t}_R$(~70%), consistent with the $\tilde{t}_1 \to t\tilde{\chi}_1^0$ samples.

(b) Wino NLSP:

In the wino NLSP model, the $\tilde{t}_1$ was assumed to be composed mainly of $\tilde{t}_L$ (i.e. $m_{q3L} < m_{tR}$). The stop was decayed according to $\mathcal{B}(\tilde{t}_1 \to b\tilde{\chi}_1^\pm) \sim 66\%$, or $\mathcal{B}(\tilde{t}_1 \to t\tilde{\chi}_2^0) \sim 33\%$, followed by $\tilde{\chi}_1^\pm$ and $\tilde{\chi}_2^0$ decays into the LSP, in a large fraction of the phase space. Since the coupling of $\tilde{t}_L$ to the wino states is larger than the one to the bino state, the stop decay into the bino state ($\tilde{t}_1 \to t\tilde{\chi}_1^0$) is suppressed. The BR can be significantly different in the regions of phase space where one of the decays is kinematically inaccessible. In the case that a mass-splitting between the $\tilde{t}_1$ and $\tilde{\chi}_2^0$ is smaller than the top-quark mass ($\Delta m(\tilde{t}_1, \tilde{\chi}_2^0) < m_{\text{top}}$), for instance, the $\tilde{t}_1 \to t\tilde{\chi}_2^0$ decay is suppressed, while the $\tilde{t}_1 \to b\tilde{\chi}_1^\pm$ decay is enhanced. Similarly, the $\tilde{t}_1 \to b\tilde{\chi}_1^\pm$ decay is suppressed near the boundary of $m_{\tilde{t}_1} = m_b + m_{\tilde{\chi}_1^\pm}$ while the $\tilde{t}_1 \to t\tilde{\chi}_1^0$ decay is enhanced.

The signal model was constructed by performing a two-dimensional scan of the pMSSM parameters M_1 and m_{q3L}. For the models considered, $M_3 = 2.2$ TeV and $M_S = 1.2$ TeV were assumed in order for the produced models to evade the current gluino and stop mass limits [124–127].

The $\tilde{\chi}_2^0$ decay modes are very sensitive to the sign of μ. The $\tilde{\chi}_2^0$ decays into the lightest Higgs boson and the LSP (with $\mathcal{B}(\tilde{\chi}_2^0 \to h\tilde{\chi}_1^0) \sim 95\%$) if $\mu > 0$ and decays into a Z boson and the LSP (with $\mathcal{B}(\tilde{\chi}_2^0 \to Z\tilde{\chi}_1^0) \sim 75\%$) if $\mu < 0$. Hence, the two μ scenarios were considered separately.[8]

Both the stop and sbottom pair production modes were included. The stop and sbottom masses are roughly the same since they are both closely related to m_{q3L}. The sbottom decays largely via $\tilde{b}_1 \to t\tilde{\chi}_1^\pm$ and $\tilde{b}_1 \to b\tilde{\chi}_2^0$ with a similar BR as for $\tilde{t}_1 \to b\tilde{\chi}_1^\pm$ and $\tilde{t}_1 \to t\tilde{\chi}_2^0$, respectively.

(c) Higgsino LSP:

For the higgsino LSP case, a simplified model was built. Similar input parameters to those of the wino NLSP pMSSM model were assumed when evaluating the stop decay branching ratios, except for the electroweakino mass parameters, M_1, M_2, and μ. These mass parameters were changed to satisfy $\mu \ll M_1, M_2$.

The stop decay BR in scenarios with $m_{tR} < m_{q3L}$ were found to be ~ 50% for $\mathcal{B}(\tilde{t}_1 \to b\tilde{\chi}_1^\pm)$ and ~ 25% for both $\mathcal{B}(\tilde{t}_1 \to t\tilde{\chi}_1^0)$ and $\mathcal{B}(\tilde{t}_1 \to t\tilde{\chi}_2^0)$, independent of $\tan\beta$. On the other hand, in scenarios with $m_{q3L} < m_{tR}$ and $\tan\beta = 20$, the $\mathcal{B}(\tilde{t}_1 \to b\tilde{\chi}_1^\pm)$ was suppressed to ~ 10% while $\mathcal{B}(\tilde{t}_1 \to t\tilde{\chi}_1^0)$ and $\mathcal{B}(\tilde{t}_1 \to t\tilde{\chi}_2^0)$ were each increased to ~ 45%. A third scenario with $\tan\beta = 60$

[7] A value of $\cos\theta_t = 0.553$ is assumed, corresponding to a $\tilde{t}_1$ composed mainly of $\tilde{t}_R$(~70%)

[8] When the $\tilde{\chi}_2^0$ decay into the LSP via Z/Higgs boson is kinematically suppressed, the decay is instead determined by the LSP coupling to squarks. In the low-m_{q3L} scenario considered, the decay via a virtual sbottom becomes dominant due to the large sbottom–bottom–LSP coupling, resulting in a $\tilde{\chi}_2^0 \to b\bar{b}\tilde{\chi}_1^0$ decay with a branching ratio up to 95%.

and $m_{q3L} < m_{tR}$ was also studied. In this scenario, the stop BR was found to be $\sim$ 33% for each of the three decay modes. The $\tilde{\chi}_1^{\pm}$ and $\tilde{\chi}_2^0$ subsequently decayed into the $\tilde{\chi}_1^0$ via a highly off-shell W/Z boson. The exact decay BR of $\tilde{\chi}_1^{\pm}$ and $\tilde{\chi}_2^0$ depend on the size of the mass-splitting amongst the triplet of higgsino states. For the baseline model, $\Delta m(\tilde{\chi}_1^{\pm}, \tilde{\chi}_1^0) = 5$ GeV and $\Delta m(\tilde{\chi}_2^0, \tilde{\chi}_1^0) = 10$ GeV were assumed, which roughly corresponds to $M_1 = M_2 \sim 1.2$–1.5 TeV. An additional signal model with $\Delta m(\tilde{\chi}_1^{\pm}, \tilde{\chi}_1^0)$ varying between 0 and 30 GeV was also considered.

In the signal generation, the stop decay BR was set to 33% for each of the three decay modes ($\tilde{t}_1 \to b\tilde{\chi}_1^{\pm}$, $\tilde{t}_1 \to t\tilde{\chi}_2^0$, $\tilde{t}_1 \to t\tilde{\chi}_1^0$). The polarisation and stop BR were reweighted to match the BR described above for each scenario. Samples were simulated down to $\Delta m(\tilde{\chi}_1^{\pm}, \tilde{\chi}_1^0) = 2$ GeV for the Δm scan. The $\tilde{t}_1 \to t\tilde{\chi}_1^0$ samples generated for the pure bino scenario were used in the region below 2 GeV, scaling the cross section by $\left[\mathcal{B}(\tilde{t}_1 \to t\tilde{\chi}_1^0) + \mathcal{B}(\tilde{t}_1 \to t\tilde{\chi}_2^0)\right]^2$, under the assumption that the decay products from $\tilde{\chi}_1^{\pm}$ and $\tilde{\chi}_2^0$ are too soft to be reconstructed.

(d) Bino/higgsino mix:

For the well-tempered neutralino, the signal model was built in a similar manner to the wino NLSP model. Signals were generated by scanning in M_1 and m_{q3L} parameter space, with $\tan\beta = 20$, $M_2 = 2.0$ TeV and $M_3 = 1.8$ TeV (corresponding to a gluino mass of ~ 2.0 TeV).[9] The value of M_S was varied in the range of 700–1300 GeV in the large $\tilde{t}_L$–$\tilde{t}_R$ mixing regime in order for the lightest Higgs boson to have a mass consistent with the observed mass. Since the dark-matter relic density is very sensitive to the mass-splitting $\Delta m(\mu, M_1)$, μ was chosen to satisfy $0.10 < \Omega h^2 < 0.12$ given the value of M_1 considered ($-\mu \sim M_1$), which resulted in $\Delta m(\mu, M_1) = 20$–50 GeV.

The dark-matter relic density was computed using MicrOMEGAs 4.3.1f [128, 129]. Softsusy-3.3.3 was used to evaluate the level of fine-tuning (Δ) [70] of the pMSSM parameters. The signal models were required to have a low level of fine-tuning corresponding to $\Delta < 100$ (at most 1% fine-tuning).

For scenarios with $m_{tR} < m_{q3L}$, only stop pair production was considered while both stop and sbottom pair production were considered in scenarios with $m_{tR} > m_{q3L}$. The sbottom mass was found to be close to the stop mass as they were both determined mainly by m_{q3L}. The stop and sbottom decay largely into a higgsino state, $\tilde{\chi}_1^{\pm}$, $\tilde{\chi}_2^0$, and $\tilde{\chi}_3^0$ with BR similar to those of the higgsino models. The stop and sbottom decay BR to the bino state were found to be small.

Signal cross-sections for stop/sbottom pair production were calculated to next-to-leading order in the strong coupling constant, adding the resummation of soft gluon emission at next-to-leading-logarithm accuracy (NLO+NLL) [130–132]. The nominal cross-section and the uncertainty were taken from an envelope of cross-section predictions using different PDF sets and factorisation and renormalisation scales, as described in Ref. [99].

Signal events for the spin-0 mediator model were generated with MG5_aMC@NLO (LO) with up to one additional parton, interfaced to Pythia8. The couplings of the mediator to the DM and SM particles (g_χ and g_v) were assumed to be equal and a common coupling with value $g = g_\chi = g_v = 1$ is used. The

[9] The light sbottom and/or stop become tachyonic when their radiative corrections are large in the low-m_{q3L} regime, as the correction to squark masses is proportional to $(M_3/m_{q3L})^2$, which can change the sign of the physical mass. This was an important consideration when choosing the value of M_3.

Table 2: Overview of the input parameters and typical stop decay branching ratios (BR) for the signal models. Lists of mass parameters scanned are provided in between parentheses. The pMSSM mass parameters that are not shown below were set to values above 3 TeV. The table represents seven different models that are used in the interpretation of the results (two for the wino NLSP, three for the higgsino LSP, and two for the bino/higgsino admixture). For the higgsino LSP scenarios, a simplified model is used instead of a pMSSM model, although the stop decay BR are based on pMSSM scans with the parameters shown in the table. For the higgsino and bino/higgsino mix scenarios, the stop decay BR change depending on the $\tilde{t}_L$–$\tilde{t}_R$ composition of the $\tilde{t}_1$, hence the BR for various scenarios corresponding to (a) $\tilde{t}_1 \sim \tilde{t}_R$ and (b) $\tilde{t}_1 \sim \tilde{t}_L$ (and (c) $\tilde{t}_1 \sim \tilde{t}_L$ with $\tan\beta = 60$ in the higgsino model) are shown separately. For the wino NLSP model, only the $\tilde{t}_1 \sim \tilde{t}_L$ scenario is considered. Sbottom pair production is also considered where $\tilde{b}_1 \sim \tilde{b}_L$ for the wino NLSP and bino/higgsino mix scenarios.

Scenario	Wino NLSP	Higgsino LSP	Bino/higgsino mix
Models	pMSSM	simplified	pMSSM
Mixing parameters		$X_t/M_S \sim \sqrt{6}$	
$\tan\beta$	20	20 or 60	20
M_S [TeV]	0.9–1.2	1.2	0.7–1.3
M_3 [TeV]	2.2	2.2	1.8
Scanned mass parameters	(M_1, m_{q3L})	$(\mu, m_{q3L}/m_{tR})$	$(M_1, m_{q3L}/m_{tR})$
Electroweakino masses [TeV]	$\mu = \pm 3.0$	$M_2 = M_1 = 1.5$	$M_2 = 2.0$
	$M_2 = 2M_1 \ll \lvert\mu\rvert$	$\mu \ll M_1 = M_2$	$M_1 \sim -\mu$, $M_1 < M_2$
Additional requirements	–	–	$0.10 < \Omega h^2 < 0.12$
	–	–	$\Delta < 100$
Sbottom pair production	considered	–	considered
$\tilde{t}_1$ decay modes and their BR [%]	$\tilde{t}_1 \sim \tilde{t}_L$	(a) / (b) / (c)	(a) / (b)
$\tilde{t}_1 \to t\tilde{\chi}_1^0$	< 5	~ 25/~ 45/~ 33	< 10/< 10
$\tilde{t}_1 \to b\tilde{\chi}_1^\pm$	~ 65	~ 50/~ 10/~ 33	~ 50/~ 10
$\tilde{t}_1 \to t\tilde{\chi}_2^0$	~ 30	~ 25/~ 45/~ 33	~ 20/~ 40
$\tilde{t}_1 \to t\tilde{\chi}_3^0$	–	–	~ 20/~ 40
$\tilde{b}_1$ decay modes and their BR [%]	$\tilde{b}_1 \sim \tilde{t}_L$	–	$\tilde{b}_1 \sim \tilde{b}_L$
$\tilde{b}_1 \to b\tilde{\chi}_1^0$	< 5	–	< 5
$\tilde{b}_1 \to t\tilde{\chi}_1^\pm$	~ 65	–	~ 85
$\tilde{b}_1 \to b\tilde{\chi}_2^0$	~ 30	–	< 5
$\tilde{b}_1 \to b\tilde{\chi}_3^0$	–	–	< 5

kinematics of the decay was found not to depend strongly on the values of these couplings. The cross-section was computed at NLO [133, 134] and decreased significantly when the mediator was produced off-shell.

5 Event reconstruction

Events used in the analysis must satisfy a series of beam, detector and data-quality criteria. The primary vertex, defined as the reconstructed vertex with the highest $\sum_{\text{tracks}} p_T^2$, must have at least two associated

tracks with $p_{\mathrm{T}} > 400\,\mathrm{MeV}$.

Depending on the quality and kinematic requirements imposed, reconstructed physics objects are labelled either as *baseline* or *signal*, where the latter describes a subset of the former. Baseline objects are used when classifying overlapping physics objects and to compute the missing transverse momentum. Baseline leptons (electrons and muons) are also used to impose a veto on events with more than one lepton, which suppresses background contibutions from $t\bar{t}$ and Wt production where both W-bosons decay leptonically, referred to as dileptonic $t\bar{t}$ or Wt events. Signal objects are used to construct kinematic and multiplicity discriminating variables needed for the event selection.

Electron candidates are reconstructed from electromagnetic calorimeter cell clusters that are matched to ID tracks. Baseline electrons are required to have $p_{\mathrm{T}} > 5\,\mathrm{GeV}$, $|\eta| < 2.47$, and to satisfy 'VeryLoose' likelihood identification criteria that are defined following the methodology described in Ref. [135]. Signal electrons must pass all baseline requirements and in addition satisfy the 'LooseAndBLayer' or 'Tight' likelihood identification criteria depending on the signal region selection, and are classified as 'loose' or 'tight' signal electrons, respectively. They must also have a transverse impact parameter evaluated at the point of closest approach between the track and the beam axis in the transverse plane (d_0) that satisfies $|d_0|/\sigma_{d_0} < 5$, where σ_{d_0} is the uncertainty in d_0, and the distance from this point to the primary vertex along the beam direction (z_0) must satisfy $|z_0 \sin\theta| < 0.5\,\mathrm{mm}$. Furthermore, lepton isolation, defined as the sum of the transverse energy deposited in a cone with a certain size ΔR excluding the energy of the lepton itself, is required. The isolation criteria for 'loose' electrons use only track-based information, while the 'tight' electron isolation criteria rely on both track- and calorimeter-based information with a fixed requirement on the isolation energy divided by the electron's p_{T}.

Muon candidates are reconstructed from combined tracks that are formed from ID and MS tracks, ID tracks matched to MS track segments, stand-alone MS tracks, or ID tracks matched to an energy deposit in the calorimeter compatible with a minimum-ionising particle (referred to as calo-tagged muon) [136]. Baseline muons up to $|\eta| = 2.7$ are used and they are required to have $p_{\mathrm{T}} > 4\,\mathrm{GeV}$ and to satisfy the 'Loose' identification criteria. Signal muons must pass all baseline requirements and in addition have impact parameters $|z_0 \sin\theta| < 0.5\,\mathrm{mm}$ and $|d_0|/\sigma_{d_0} < 3$, and satisfy the 'Medium' identification criteria. Furthermore, signal muons must be isolated according to criteria similar to those used for signal electrons, but with a fixed requirement on track-based isolation energy divided by the muon's p_{T}. No separation into 'loose' and 'tight' classes is performed for signal muons.

Dedicated scale factors for the requirements of identification, impact parameters, and isolation are derived from $Z \to \ell\ell$ and $J/\Psi \to \ell\ell$ data samples for electrons and muons to correct for minor mis-modelling in the MC samples [136, 137]. The p_{T} thresholds of signal leptons are raised to 25 GeV for electrons and muons in all signal regions except those that target higgsino LSP scenarios.

Jet candidates are built from topological clusters [138, 139] in the calorimeters using the anti-k_t algorithm [140] with a jet radius parameter $R = 0.4$ implemented in the FastJet package [141]. Jets are corrected for contamination from pile-up using the jet area method [142–144] and are then calibrated to account for the detector response [145, 146]. Jets in data are further calibrated according to *in situ* measurements of the jet energy scale [146]. Baseline jets are required to have $p_{\mathrm{T}} > 20\,\mathrm{GeV}$. Signal jets must have $p_{\mathrm{T}} > 25\,\mathrm{GeV}$ and $|\eta| < 2.5$. Furthermore, signal jets with $p_{\mathrm{T}} < 60\,\mathrm{GeV}$ and $|\eta| < 2.4$ are required to satisfy track-based criteria designed to reject jets originating from pile-up [144]. Events containing a jet that does not pass specific jet quality requirements ("jet cleaning") are vetoed from the analysis in order to suppress detector noise and non-collision backgrounds [147, 148].

Jets containing b-hadrons are identified using the MV2c10 b-tagging algorithm (and those identified are referred to as b-tagged jets), which incorporates quantities such as the impact parameters of associated tracks and reconstructed secondary vertices [76, 149]. The algorithm is used at a working point that provides a 77% b-tagging efficiency in simulated $t\bar{t}$ events, and corresponds to a rejection factor of about 130 for jets originating from gluons and light-flavour quarks (light jets) and about 6 for jets induced by charm quarks. Corrections derived from data control samples are applied to account for differences between data and simulation for the efficiency and mis-tag rate of the b-tagging algorithm [149].

Jets and associated tracks are also used to identify hadronically decaying τ leptons using the 'Loose' identification criteria described in Refs. [146, 150], which have a 60% (50%) efficiency for reconstructing τ leptons decaying into one (three) charged pions. These τ candidates are required to have one or three associated tracks, with total electric charge opposite to that of the selected electron or muon, $p_{\mathrm{T}} > 20$ GeV, and $|\eta| < 2.5$. The τ candidate p_{T} requirement is applied after a dedicated energy calibration [146, 150].

To avoid labelling the same detector signature as more than one object, an overlap removal procedure is applied. Table 3 summarises the procedure. Given a set of baseline objects, the procedure checks for overlap based on either a shared track, ghost-matching [143], or a minimum distance[10] ΔR between pairs of objects. For example, if a baseline electron and a baseline jet are separated by $\Delta R < 0.2$, then the electron is retained (as stated in the 'Precedence' row) and the jet is discarded, unless the jet is b-tagged (as stated in the 'Condition' row) in which case the electron is assumed to originate from a heavy-flavour decay and is hence discarded while the jet is retained. If the matching requirement in Table 3 is not met, then both objects under consideration are kept. The order of the steps in the procedure is given by the columns in Table 3, which are executed from left to right. The second (ej) and the third (μj) steps of the procedure ensure that leptons and jets have a minimum ΔR separation of 0.2. Jets overlapping with muons that satisfy one or more of the following conditions are not considered in the third step: the jet is b-tagged, the jet contains more than three tracks ($n^{j}_{\mathrm{track}} > 3$), or the ratio of muon p_{T} to jet p_{T} satisfies $p^{\mu}_{\mathrm{T}}/p^{j}_{\mathrm{T}} < 0.7$. Therefore, the fourth step (ℓj) is applied only to the jets that satisfy the above criteria or that are well separated from leptons with $\Delta R > 0.2$. For the remainder of the paper, all baseline and signal objects are those that have passed the overlap removal procedure.

The missing transverse momentum is reconstructed from the negative vector sum of the transverse momenta of baseline electrons, muons, jets, and a soft term built from high-quality tracks that are associated with the primary vertex but not with the baseline physics objects [151, 152]. Photons and hadronically decaying τ leptons are not explicitly included but enter either as jets, electrons, or via the soft term.

6 Discriminating variables

The background processes contributing to a final state with one isolated lepton, jets and $E^{\mathrm{miss}}_{\mathrm{T}}$ are primarily semileptonic $t\bar{t}$ events with one of the W bosons from two top quarks decaying leptonically, and W+jets events with a leptonic decay of the W boson. Both backgrounds can be effectively reduced by requiring the transverse mass of the event, m_{T},[11] to be larger than the W-boson mass. In most signal regions,

[10] Rapidity ($y \equiv 1/2 \ln(E + p_z/E - p_z)$) is used instead of pseudorapidity (η) when computing ΔR in the overlap removal procedure.

[11] The transverse mass m_{T} is defined as $m^2_{\mathrm{T}} = 2p^{\ell}_{\mathrm{T}}E^{\mathrm{miss}}_{\mathrm{T}}[1 - \cos(\Delta\phi)]$, where $\Delta\phi$ is the azimuthal angle between the lepton and missing transverse momentum directions. The quantity p^{ℓ}_{T} is the transverse momentum of the charged lepton.

Table 3: Overlap removal procedure for physics objects. The first two rows list the types of overlapping objects: electron (e), muon (μ), electron or muon (ℓ), jet (j), and hadronically decaying τ lepton (τ). All objects refer to the baseline definitions, except for τ where no distinction between baseline and signal definition is made. The third row specifies when an object pair is considered to be overlapping. The fourth row describes an optional condition which must also be met for the pair of objects to be considered overlapping. The last row lists the object given precedence. Object 1 is retained and Object 2 is discarded if the condition is not met, and vice versa. More information is given in the text.

Object 1	e	e	μ	j	e
Object 2	μ	j	j	ℓ	τ
Matching criteria	shared track	$\Delta R < 0.2$	ghost-matched	$\Delta R < \min\left(0.4, 0.04 + \frac{10}{p_{\mathrm{T}}^{\ell}/\mathrm{GeV}}\right)$	$\Delta R < 0.1$
Condition	calo-tagged μ	j not b-tagged	j not b-tagged and $\left(n_{\mathrm{track}}^{j} < 3 \text{ or } \frac{p_{\mathrm{T}}^{\mu}}{p_{\mathrm{T}}^{j}} > 0.7\right)$	–	–
Precedence	e	e	μ	j	e

the dominant background after this requirement arises from dileptonic $t\bar{t}$ events, in which one lepton is not identified, is outside the detector acceptance, or is a hadronically decaying τ lepton. On the other hand, the m_{T} selection is not applied in the signal regions targeting the higgsino LSP scenarios, hence the background is dominated by semileptonic $t\bar{t}$ events. A series of additional variables described below are used to discriminate between the $t\bar{t}$ background and the signal processes.

6.1 Common discriminating variables

The asymmetric m_{T2} (am_{T2}) [153–156] and m_{T2}^{τ} are both variants of the variable m_{T2} [157], a generalisation of the transverse mass applied to signatures where two particles are not directly detected. The am_{T2} variable targets dileptonic $t\bar{t}$ events where one lepton is not reconstructed, while the m_{T2}^{τ} variable targets $t\bar{t}$ events where one of the two W bosons decays via a hadronically decaying τ lepton. In addition, the $H_{\mathrm{T,sig}}^{\mathrm{miss}}$ variable is used in some signal regions to reject background processes without invisible particles in the final state. It is defined as:

$$H_{\mathrm{T,sig}}^{\mathrm{miss}} = \frac{|\vec{H}_{\mathrm{T}}^{\mathrm{miss}}| - M}{\sigma_{|\vec{H}_{\mathrm{T}}^{\mathrm{miss}}|}},$$

where $\vec{H}_{\mathrm{T}}^{\mathrm{miss}}$ is the negative vectorial sum of the momenta of the signal jets and signal lepton. The denominator is computed from the per-event jet energy uncertainties, while the lepton is assumed to be well measured. The offset parameter M, which is a characteristic scale of the background processes, is fixed at 100 GeV in this analysis. These variables are detailed in Ref. [158]. Figure 5 shows distributions of the am_{T2} and $H_{\mathrm{T,sig}}^{\mathrm{miss}}$ variables.

Reconstructing the hadronic top-quark decay (top-tagging) can provide additional discrimination against dileptonic $t\bar{t}$ events, which do not contain a hadronically decaying top quark. In events where the top quark is produced with moderate p_{T}, a χ^2 technique is used to reconstruct candidate hadronic top-quark decays. For every selected event with four jets of which at least one is b-tagged, the m_{top}^{χ} variable is defined as the invariant mass of the three jets in the event most compatible with the hadronic decay products of a top quark, where the three jets are selected by a χ^2 minimisation using the jet momenta and energy resolutions.

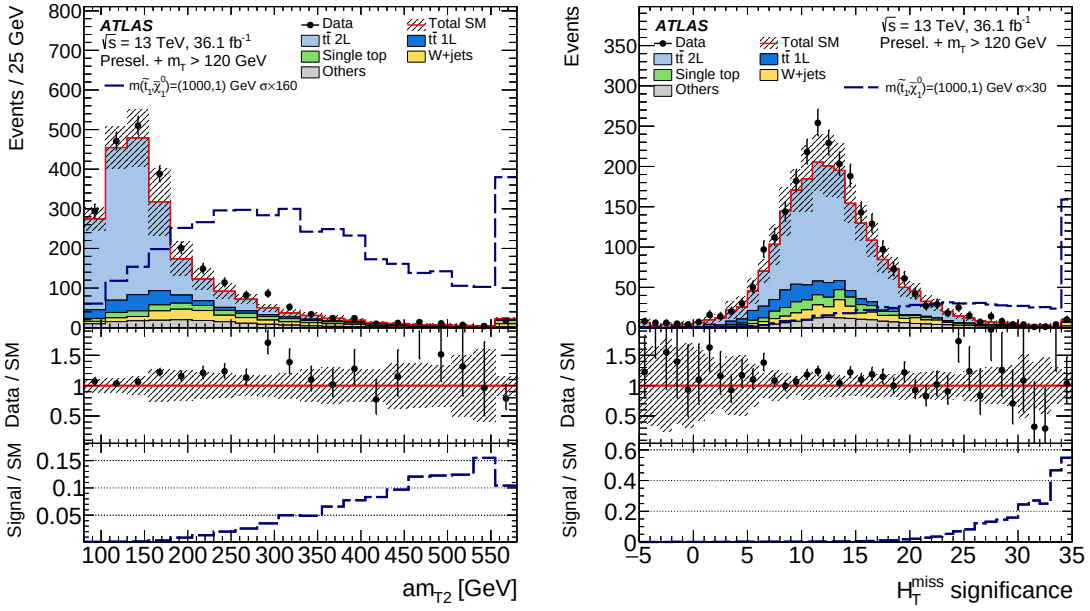

Figure 5: Distributions of discriminating variables: (left) am_{T2} and (right) $H_{\mathrm{T,sig}}^{\mathrm{miss}}$ after the high-$E_{\mathrm{T}}^{\mathrm{miss}}$ preselection shown in Table 4 and $m_{\mathrm{T}} > 120\,\mathrm{GeV}$. In addition to the SM background prediction, a bino LSP signal model is shown for a stop mass of 1 TeV, with a neutralino mass of 1 GeV, in the upper panel this component is scaled up by a factor of 160 (left) or 30 (right) for visibility. The $t\bar{t}$ 2L and $t\bar{t}$ 1L in the legend refer to dileptonic and semileptonic $t\bar{t}$, respectively. The lower panels show the ratio of data to total SM background and the ratio of expected signal to total SM background. The category labelled 'Others' stands for minor SM backgrounds that contribute less than 5% of the total SM background. The hatched area around the total SM prediction and the hatched band in the Data/SM ratio include statistical and experimental uncertainties. The last bin contains overflows.

After reconstructing the hadronic top-quark decay through the χ^2 minimisation, the remaining b-tagged jet[12] is paired with the lepton to reconstruct the semileptonically decaying top quark candidate (leptonic top quark). Based on these objects, the azimuthal separation between the p_{T} of hadronic and of leptonic top-quark candidates, $\Delta\phi(t_{\mathrm{had}}^{\chi}, t_{\mathrm{lep}}^{\chi})$ and between the missing transverse momentum vector and the p_{T} of hadronic top-quark candidate, $\Delta\phi(\vec{p}_{\mathrm{T}}^{\,\mathrm{miss}}, t_{\mathrm{had}}^{\chi})$, are defined.

An alternative top-tagging method is used to target events where the top quark is produced with a significant boost. The top-quark candidates are reconstructed by considering all small-radius jets in the event and clustering them into large-radius jets using the anti-k_t algorithm with a radius parameter $R_0 = 3.0$. The radius of each jet is then iteratively reduced to an optimal radius, $R(p_{\mathrm{T}}) = 2 \times m_{\mathrm{top}}/p_{\mathrm{T}}$, that matches their p_{T}. If a candidate loses a large fraction of its p_{T} in the shrinking process, it is discarded. In events where two or more top-quark candidates are found, the one with the mass closest to the top-quark mass is taken. The same algorithm is also used to define boosted hadronic W-boson candidates, where only non-b-tagged jets are considered, and the mass of the W boson is used to define the optimal radius. The masses of the reclustered top-quark and W-boson candidates are referred to as $m_{\mathrm{top}}^{\mathrm{reclustered}}$ and $m_{W}^{\mathrm{reclustered}}$, respectively.

The $\vec{p}_{\mathrm{T}}^{\,\mathrm{miss}}$ in semileptonic $t\bar{t}$ events is expected to be closely aligned with the direction of the leptonic top quark. After boosting the leptonic top-quark candidate and the $\vec{p}_{\mathrm{T}}^{\,\mathrm{miss}}$ into the $t\bar{t}$ rest frame, the magnitude of the perpendicular component of the $\vec{p}_{\mathrm{T}}^{\,\mathrm{miss}}$ with respect to the leptonic top quark is computed. This $E_{\mathrm{T},\perp}^{\mathrm{miss}}$

[12] If the event has exactly one b-tagged jet, the highest-p_{T} jet is used instead of the second highest-p_{T} b-tagged jet.

is expected to be small for the background, as the dominant contribution to the total $E_{\mathrm{T}}^{\mathrm{miss}}$ is due to the neutrino emitted in the leptonic top-quark decay.

6.2 Discriminating variables for boosted decision trees

In the diagonal region where $m_{\tilde{t}_1} \approx m_{\mathrm{top}} + m_{\tilde{\chi}_1^0}$, the momentum transfer from the $\tilde{t}_1$ to the $\tilde{\chi}_1^0$ is small, and the stop signal is kinematically very similar to the $t\bar{t}$ process. In order to achieve good separation between $t\bar{t}$ and signal, a boosted decision tree (BDT) implemented in the TMVA framework [159] is used. Additional discriminating variables are developed to use as inputs to the BDT, or as a part of the preselection in the BDT analyses.

Some of the selections targeting the diagonal region in the pure bino LSP scenarios rely on the presence of high-p_{T} initial-state radiation (ISR) jets, which serves to boost the di-stop system. A powerful technique to discriminate these signal models from the $t\bar{t}$ background is to attempt to reconstruct the ratio of the transverse momenta of the the di-neutralino and di-stop systems. This ratio α can be directly related to the ratio of the masses of the $\tilde{t}_1$ and the $\tilde{\chi}_1^0$ [160, 161]:

$$\alpha \equiv \frac{m_{\tilde{\chi}_1^0}}{m_{\tilde{t}_1}} \sim \frac{p_{\mathrm{T}}(\tilde{\chi}_1^0 \tilde{\chi}_1^0)}{p_{\mathrm{T}}(\tilde{t}_1 \tilde{t}_1)}.$$

The observed $E_{\mathrm{T}}^{\mathrm{miss}}$ would also include a contribution from the neutrino produced in the leptonic W-boson decay, in addition to that due to the LSPs. A light $\tilde{\chi}_1^0$ and a $\tilde{t}_1$ mass close to the mass of the top quark would result in the neutralinos having low momenta, making the reconstruction of the neutrino momentum and its subtraction from the $\vec{p}_{\mathrm{T}}^{\,\mathrm{miss}}$ vital. In the signal region targeting this scenario, a modified χ^2 minimisation using jet momenta only is applied to define the hadronic top-quark candidate $t_{\mathrm{had}}^{\mathrm{ISR}}$. One or two light jets and one b-tagged jet are selected in such a way that they are most compatible with originating from hadronic W-boson and top-quark decays. The leading-p_{T} light jet is excluded, as it is assumed to originate from ISR.

Out of the two jets with the highest probabilities of being a b-jet according to the b-tagging algorithm, the one not assigned to $t_{\mathrm{had}}^{\mathrm{ISR}}$ is assigned to the leptonic top-quark candidate, together with the lepton. For the determination of the neutrino momentum, two hypotheses are considered: that of a $t\bar{t}$ event and that of a signal event. For the $t\bar{t}$ hypothesis, the entire $\vec{p}_{\mathrm{T}}^{\,\mathrm{miss}}$ is attributed to the neutrino. Under the signal hypothesis, collinearity of each $\tilde{t}_1$ with both of its decay products is assumed. This results in the transverse-momentum vector of the neutrino from the leptonic W-boson decay being calculable by subtracting the momenta of the LSPs from $\vec{p}_{\mathrm{T}}^{\,\mathrm{miss}}$, when assuming a specific mass ratio α:

$$\vec{p}_{\mathrm{T}}(\nu^{\alpha}) = (1-\alpha)\vec{p}_{\mathrm{T}}^{\,\mathrm{miss}} - \alpha \vec{p}_{\mathrm{T}}(t_{\mathrm{had}}^{\mathrm{ISR}} + b_{\mathrm{lep}} + \ell),$$

where ν^{α} represents the neutrino four-vector for a given value of α, b_{lep} is the b-jet candidate assigned to the semileptonic top-quark candidate and ℓ is the charged lepton. The resulting momentum of ν^{α} is then used to calculate further variables under the signal hypothesis, such as the leptonically decaying W boson's transverse mass m_{T}^{α} or the mass of the top-quark candidate including the leptonic W-boson decay, $m(t_{\mathrm{lep}}^{\alpha})$. The lepton pseudorapidity is used as a proxy for the neutrino pseudorapidity in the calculation. Further variables are the difference in m_{T} between the calculation under the hypothesis of a $t\bar{t}$ event and under the signal hypothesis, $\Delta m_{\mathrm{T}}^{\alpha} = m_{\mathrm{T}} - m_{\mathrm{T}}^{\alpha}$, where m_{T}^{α} is calculated using the lepton and ν^{α}, and the p_{T} of the reconstructed $t\bar{t}$ system under the SM hypothesis, $p_{\mathrm{T}}(t\bar{t})$. The mass ratio $\alpha = 0.135$ is used

throughout the paper, as is calculated from $m_{\tilde{t}_1} = 200\,\text{GeV}$ and $m_{\tilde{\chi}_1^0} = 27\,\text{GeV}$. This signal point was chosen since it is close to the exclusion limit from previous analyses.

Larger stop-mass values in compressed bino LSP scenarios boost the $\tilde{\chi}_1^0$ such that neglecting the neutrino momentum in the determination of α is a good approximation. A recursive jigsaw reconstruction (RJR) technique [162] is used to divide each event into an ISR hemisphere and a sparticle (S) hemisphere, where the latter contains both the invisible (I) and visible (V) decay products of the stops. Objects are grouped together according to their proximity in the lab frame's transverse plane by maximising the p_{T} of the S and ISR hemispheres over all choices of object assignment. In events with high-p_{T} ISR jets, the axis of maximum back-to-back p_{T}, also known as the thrust axis, should approximate the direction of the ISR and the di-stop system's back-to-back recoil.

The RJR variables used in the corresponding signal regions are the transverse mass of the S system, M_{T}^{S}, the ratio of the momenta of the I and ISR systems, R_{ISR} (an approximation of α), the azimuthal separation between the momenta of the ISR and I systems, $\Delta\phi(\text{ISR}, I)$, and the number of jets assigned to the V system, N_j^{V}.

Figures 6 and 7 show example kinematic distributions of the variables used for the BDT trainings.

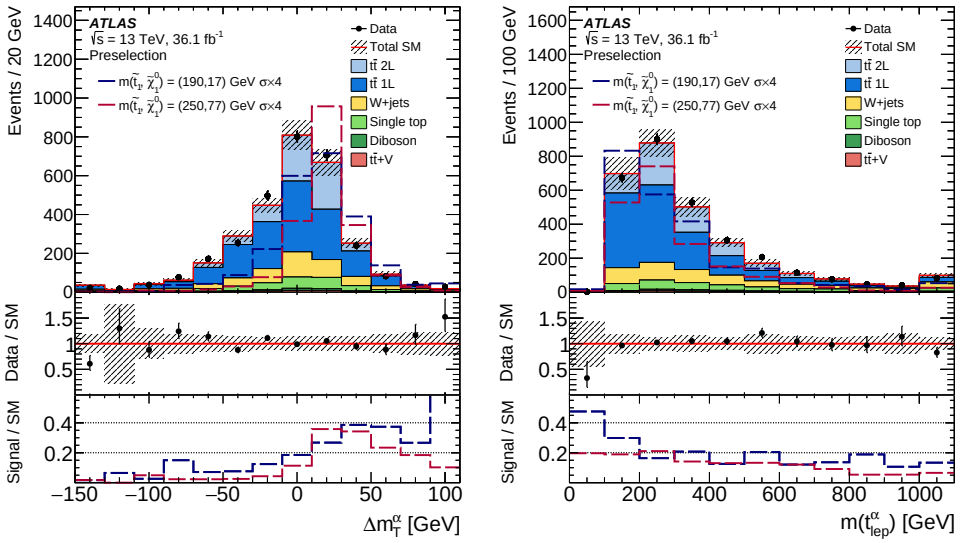

Figure 6: Distributions of discriminating variables: (left) $\Delta m_{\text{T}}^{\alpha}$ and (right) $m(t_{\text{lep}}^{\alpha})$. They are used in the `tN_diag_low` signal region, which is defined in Section 7.1.2. Preselection refers to the signal region selection but without any requirements on the BDT output score. In addition to the SM background prediction, signal models are shown, denoted by $m(\tilde{t}_1, \tilde{\chi}_1^0)$, and scaled by a factor of four for visibility. The lower panels show the ratio of data to total SM background and the ratio of expected signal to total SM background. The hatched area around the total SM prediction and the hatched band in the Data/SM ratio include statistical and experimental uncertainties. The last bin contains overflows.

7 Signal selections

SR selections are optimised using simulated MC event samples. The metric of the optimisation is the discovery sensitivity for the various decay modes and for different regions of SUSY parameter space and

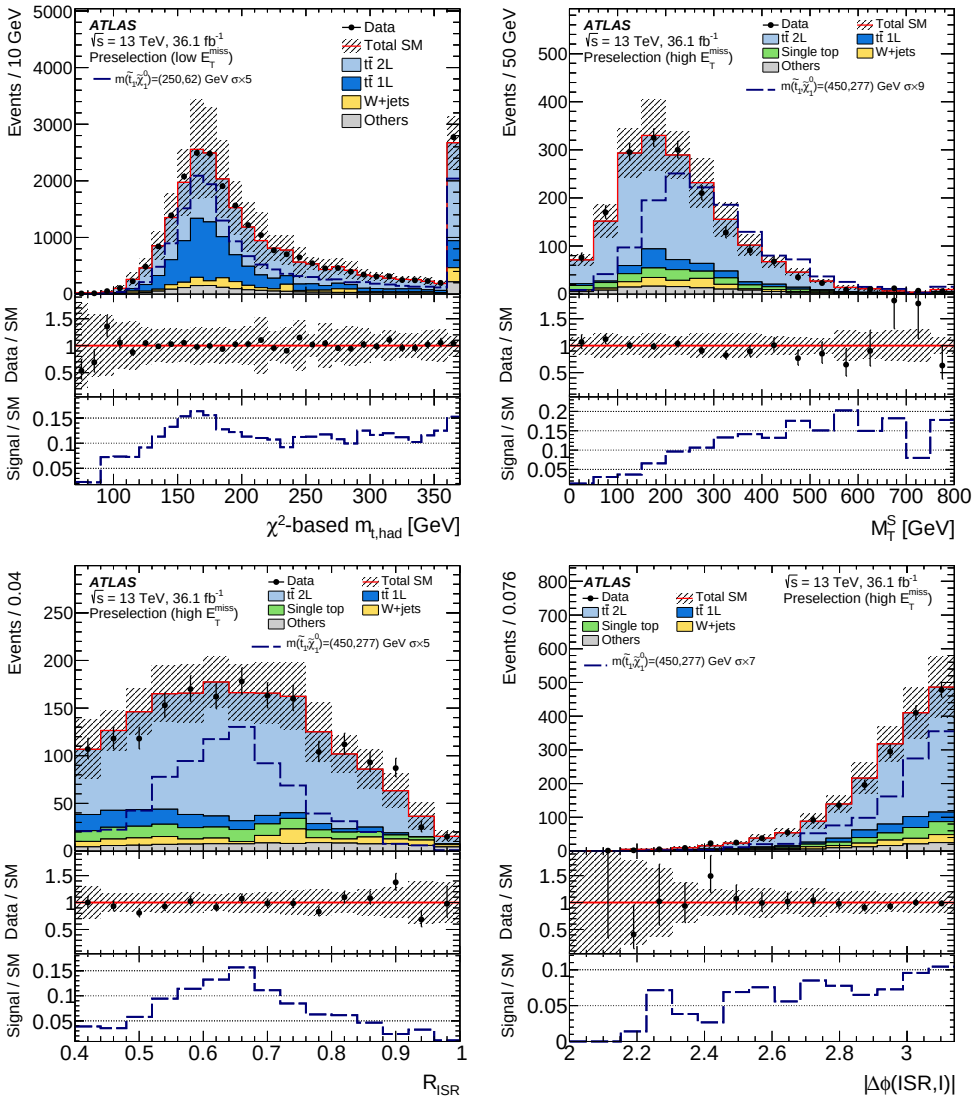

Figure 7: Distributions of discriminating variables: (top left) reconstructed mass of the hadronic top-quark candidates with χ^2-based minimisation method (m_{top}^{χ}), (top right) M_{T}^{S}, (bottom left) R_{ISR}, and (bottom right) $|\Delta\phi(\text{ISR}, I)|$. The m_{top}^{χ} variable is used in the `tN_diag_med` signal region and the others are used in the `tN_diag_high` signal region, which are defined in Section 7.1.2. In addition to the SM background prediction, signal models are shown, denoted by $m(\tilde{t}_1, \tilde{\chi}_1^0)$, and scaled by a certain factor for visibility. The lower panels show the ratio of data to total SM background and the ratio of expected signal to total SM background. The category labelled 'Others' stands for minor SM backgrounds that contribute less than 5% of the total SM background. The hatched area around the total SM prediction and the hatched band in the Data/SM ratio include statistical and experimental uncertainties. The last bin contains overflows.

Table 4: Preselection criteria used for the high-$E_{\mathrm{T}}^{\mathrm{miss}}$ signal regions (left), the low-$E_{\mathrm{T}}^{\mathrm{miss}}$ signal regions (middle) and the soft-lepton signal regions (right). For the soft-lepton selection, $p_{\mathrm{T}} \geq 5$ GeV is required for electrons. List values are provided in between parentheses.

Selection	**high-$E_{\mathrm{T}}^{\mathrm{miss}}$**	**low-$E_{\mathrm{T}}^{\mathrm{miss}}$**	**soft-lepton**
Trigger	$E_{\mathrm{T}}^{\mathrm{miss}}$ triggers only	$E_{\mathrm{T}}^{\mathrm{miss}}$ and lepton triggers	$E_{\mathrm{T}}^{\mathrm{miss}}$ triggers only
Data quality	jet cleaning, primary vertex		
Second-lepton veto	no additional baseline leptons		
Number of leptons, tightness	= 1 'loose' lepton	= 1 'tight' lepton	= 1 'tight' lepton
Lepton p_{T} [GeV]	> 25	> 27	> 4 for μ > 5 for e
Number of (jets, b-tags)	$(\geq 2, \geq 0)$	$(\geq 4, \geq 1)$	$(\geq 2, \geq 1)$
Jet p_{T} [GeV]	> (25, 25)	> (50, 25, 25, 25)	> (25, 25)
$E_{\mathrm{T}}^{\mathrm{miss}}$ [GeV]	> 230	> 100	> 230
m_{T} [GeV]	> 30	> 90	–

masses in the spin-0 mediator models. A set of benchmark signal models, selected to cover the various stop and spin-0 mediator scenarios, is used for the optimisation. The optimisations of signal-region selections are performed using an iterative algorithm and considering all studied discriminating variables, accounting for statistical and systematic uncertainties.

All regions are required to have exactly one signal lepton (except for the $t\bar{t}Z(\rightarrow \ell\ell)$ control regions, where three signal leptons are required), no additional baseline leptons, and at least four (or in some regions two or three) signal jets. In most cases, at least one b-tagged jet is also required. A set of preselection criteria (high-$E_{\mathrm{T}}^{\mathrm{miss}}$, low-$E_{\mathrm{T}}^{\mathrm{miss}}$, and soft-lepton) is defined for monitoring the MC modelling of the kinematic variables. The preselection criteria are also used as the starting point for the SR optimisation.

In the SRs relying only on the $E_{\mathrm{T}}^{\mathrm{miss}}$ trigger, all events are required to have $E_{\mathrm{T}}^{\mathrm{miss}} > 230$ GeV to ensure that the trigger is fully efficient. In SRs that use a combination of $E_{\mathrm{T}}^{\mathrm{miss}}$ and lepton triggers, this requirement is relaxed to $E_{\mathrm{T}}^{\mathrm{miss}} > 100$ GeV. In order to reject multijet events, requirements are imposed on the transverse mass (m_{T}) and the azimuthal angles between the leading and sub-leading jets (in p_{T}) and $E_{\mathrm{T}}^{\mathrm{miss}}$ ($|\Delta\phi(\mathrm{jet}_i, \vec{p}_{\mathrm{T}}^{\mathrm{miss}})|$) in most of SRs. For events with hadronic τ candidates, the requirement $m_{\mathrm{T2}}^{\tau} > 80$ GeV is applied in most SRs.

The exact preselection criteria can be found in Table 4. The preselections do not include requirements on the $|\Delta\phi(\mathrm{jet}_i, \vec{p}_{\mathrm{T}}^{\mathrm{miss}})|$ and m_{T2}^{τ} variables, but these are often used to define SRs. Figure 8 shows various relevant kinematic distributions at preselection level. The backgrounds are normalised with the theoretical cross-sections, except for the $E_{\mathrm{T}}^{\mathrm{miss}}$ distribution where the $t\bar{t}$ events are scaled with normalisation factors obtained from a simultaneous likelihood fit of the CRs, described in Section 10.

Table 5 summarises all SRs with a brief description of the targeted signal scenarios. For the pure bino LSP scenario, seven SRs are considered in total. Five SRs target the $\tilde{t}_1 \rightarrow t\tilde{\chi}_1^0$ decay. The corresponding SR labels begin with `tN`, which is an acronym for 'top neutralino'. Additional text in the label describes the stop mass region. For example, `tN_diag` targets the diagonal region where $m_{\tilde{t}_1} \sim m_{\tilde{\chi}_1^0} + m_{\mathrm{top}}$. The third part of the labels `low`, `med`, and `high` denote the targeted stop mass range, relative to other regions

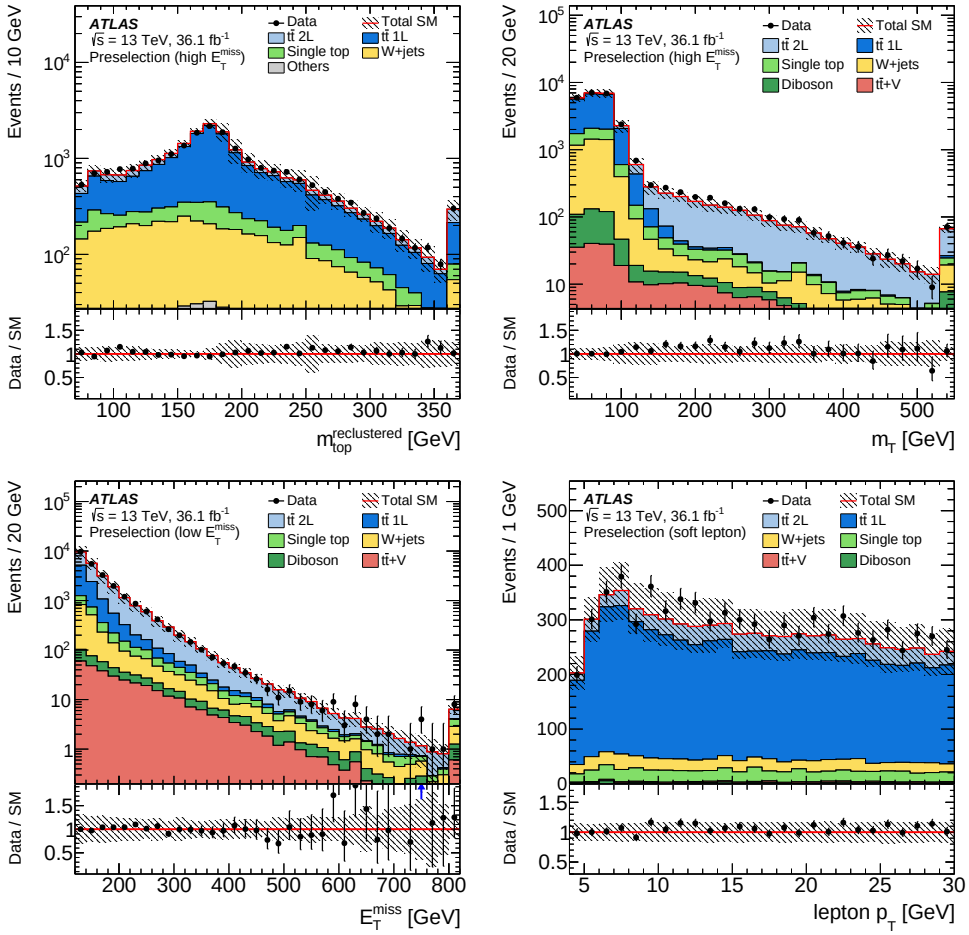

Figure 8: Kinematic distributions after the preselection: (top left) mass of the hadronic top-quark candidate with the recursive reclustering method ($m_{\text{top}}^{\text{reclustered}}$) after the high-$E_{\text{T}}^{\text{miss}}$ preselection, (top right) m_{T} after the high-$E_{\text{T}}^{\text{miss}}$ preselection, (bottom left) $E_{\text{T}}^{\text{miss}}$ after the low-$E_{\text{T}}^{\text{miss}}$ preselection, and (bottom right) lepton p_{T} after the soft-lepton preselection with an additional requirement of at least two b-tagged jets. The SM background predictions are normalised with the theoretical cross-sections (pre-fit), except for in the $E_{\text{T}}^{\text{miss}}$ distribution, where the $t\bar{t}$ events are scaled by the normalisation factors obtained from a simultaneous likelihood fit of the CRs. The category labelled 'Others' in the top left panel stands for the sum of minor SM backgrounds that contribute less than 5% of the total SM background. The hatched area around the total SM prediction and the hatched band in the Data/SM ratio include statistical and experimental uncertainties. The last bin contains overflows, except for the lepton p_{T} distribution.

of the same type (for example, `tN_diag_low` targets a stop mass of 190 GeV, while `tN_diag_high` is optimised for $m_{\tilde{t}_1} = 450$ GeV). Furthermore, two additional SRs labelled `bWN` and `bffN` are dedicated to the three-body ($\tilde{t}_1 \to bW\tilde{\chi}_1^0$) and four-body ($\tilde{t}_1 \to bff'\tilde{\chi}_1^0$) decay searches, respectively.

Six SRs target various $\tilde{t}_1 \to b\tilde{\chi}_1^{\pm}$ scenarios, and the SR labels follow the same logic: the first two characters `bC` stand for 'bottom chargino'. The consecutive labels, `2x`, `bv`, or `soft`, denote the targeted electroweakino spectrum. For the wino NLSP scenario, three SRs are designed with the label `bC2x` denoting the mass relation $m_{\tilde{\chi}_1^{\pm}} \sim 2{\times}m_{\tilde{\chi}_1^0}$ in the signal model. The label `bCbv` is used for the no b-tagged jets (b-veto) SR. For the higgsino LSP scenario, three SRs are labelled as `bCsoft` because their selections explicitly target soft-lepton signatures.

Table 5: Overview of all signal regions together with the targeted signal scenario, benchmarks used for the optimisation (with particle masses given in units of GeV), the analysis technique used for model-dependent exclusions, and a reference to the table with the event selection details. For the wino NLSP scenario, sbottom pair production (not shown) is also considered.

SR	Signal scenario	Benchmark	Exclusion technique	Table
tN_med	Pure bino LSP ($\tilde{t}_1 \to t\tilde{\chi}_1^0$)	m($\tilde{t}_1$, $\tilde{\chi}_1^0$)=(600,300)	shape-fit ($E_{\mathrm{T}}^{\mathrm{miss}}$)	6
tN_high	Pure bino LSP ($\tilde{t}_1 \to t\tilde{\chi}_1^0$)	m($\tilde{t}_1$, $\tilde{\chi}_1^0$)=(1000,1)	cut-and-count	6
tN_diag_low	Pure bino LSP ($\tilde{t}_1 \to t\tilde{\chi}_1^0$)	m($\tilde{t}_1$, $\tilde{\chi}_1^0$)=(190,17)	BDT cut-and-count	7
tN_diag_med	Pure bino LSP ($\tilde{t}_1 \to t\tilde{\chi}_1^0$)	m($\tilde{t}_1$, $\tilde{\chi}_1^0$)=(250,62)	BDT shape-fit	7
tN_diag_high	Pure bino LSP ($\tilde{t}_1 \to t\tilde{\chi}_1^0$)	m($\tilde{t}_1$, $\tilde{\chi}_1^0$)=(450,277)	BDT shape-fit	7
bWN	Pure bino LSP ($\tilde{t}_1 \to bW\tilde{\chi}_1^0$)	m($\tilde{t}_1$, $\tilde{\chi}_1^0$)=(350,230)	shape-fit (am_{T2})	8
bffN	Pure bino LSP ($\tilde{t}_1 \to bff'\tilde{\chi}_1^0$)	m($\tilde{t}_1$, $\tilde{\chi}_1^0$)=(400,350)	shape-fit ($p_{\mathrm{T}}^{\ell}/E_{\mathrm{T}}^{\mathrm{miss}}$)	8
bC2x_med	Wino NLSP ($\tilde{t}_1 \to b\tilde{\chi}_1^{\pm}, \tilde{t}_1 \to t\tilde{\chi}_2^0$)	m($\tilde{t}_1$, $\tilde{\chi}_1^{\pm}$, $\tilde{\chi}_1^0$)=(750,300,150)	cut-and-count	9
bC2x_diag	Wino NLSP ($\tilde{t}_1 \to b\tilde{\chi}_1^{\pm}, \tilde{t}_1 \to t\tilde{\chi}_2^0$)	m($\tilde{t}_1$, $\tilde{\chi}_1^{\pm}$, $\tilde{\chi}_1^0$)=(650,500,250)	cut-and-count	9
bCbv	Wino NLSP ($\tilde{t}_1 \to b\tilde{\chi}_1^{\pm}, \tilde{t}_1 \to t\tilde{\chi}_2^0$)	m($\tilde{t}_1$, $\tilde{\chi}_1^{\pm}$, $\tilde{\chi}_1^0$)=(700,690,1)	cut-and-count	9
bCsoft_diag	Higgsino LSP ($\tilde{t}_1 \to t\tilde{\chi}_1^0, \tilde{t}_1 \to t\tilde{\chi}_2^0, \tilde{t}_1 \to b\tilde{\chi}_1^{\pm}$)	m($\tilde{t}_1$, $\tilde{\chi}_1^{\pm}$, $\tilde{\chi}_1^0$)=(400,355,350)	shape-fit ($p_{\mathrm{T}}^{\ell}/E_{\mathrm{T}}^{\mathrm{miss}}$)	10
bCsoft_med	Higgsino LSP ($\tilde{t}_1 \to t\tilde{\chi}_1^0, \tilde{t}_1 \to t\tilde{\chi}_2^0, \tilde{t}_1 \to b\tilde{\chi}_1^{\pm}$)	m($\tilde{t}_1$, $\tilde{\chi}_1^{\pm}$, $\tilde{\chi}_1^0$)=(600,205,200)	shape-fit ($p_{\mathrm{T}}^{\ell}/E_{\mathrm{T}}^{\mathrm{miss}}$)	10
bCsoft_high	Higgsino LSP ($\tilde{t}_1 \to t\tilde{\chi}_1^0, \tilde{t}_1 \to t\tilde{\chi}_2^0, \tilde{t}_1 \to b\tilde{\chi}_1^{\pm}$)	m($\tilde{t}_1$, $\tilde{\chi}_1^{\pm}$, $\tilde{\chi}_1^0$)=(800,155,150)	shape-fit ($p_{\mathrm{T}}^{\ell}/E_{\mathrm{T}}^{\mathrm{miss}}$)	10
DM_low_loose	spin-0 mediator	m(Φ/a, χ)=(20,1)	cut-and-count	11
DM_low	spin-0 mediator	m(Φ/a, χ)=(20,1)	cut-and-count	11
DM_high	spin-0 mediator	m(Φ/a, χ)=(300,1)	cut-and-count	11

Finally, three SRs labelled as DM target the spin-0 mediator scenario, with the consecutive labels, low and low_loose for low mediator masses and high for high mediator masses.

With the exception of the tN and bCsoft regions, the above SRs are not designed to be mutually exclusive. A dedicated combined fit is performed using tN_med and bCsoft_med (or bCsoft_high) in the higgsino LSP and well-tempered neutralino scenarios in order to improve exclusion sensitivity. The SRs with the requirement of lepton $p_{\mathrm{T}} > 25$ GeV ($p_{\mathrm{T}} > 4$ GeV) are referred to as hard-lepton SRs (soft-lepton SRs) in the following sections.

7.1 Pure bino LSP scenario

The signature of stop pair production with subsequent $\tilde{t}_1$ decays is determined by the masses of the two sparticles, $\tilde{t}_1$ and $\tilde{\chi}_1^0$. It often leads to a final state similar to that of $t\bar{t}$ production, except for the additional $E_{\mathrm{T}}^{\mathrm{miss}}$ due to the two additional neutralinos in the event. A set of event selections is defined targeting various signals.

Two signal regions are designed to target the majority of signal models with $\Delta m(\tilde{t}_1, \tilde{\chi}_1^0) > m_{\mathrm{top}}$, tN_med and tN_high, which are optimised for medium and high $\tilde{t}_1$ mass, respectively. For the compressed region with $m_{\tilde{t}_1} \approx m_{\mathrm{top}} + m_{\tilde{\chi}_1^0}$, three BDT selections (tN_diag_low, tN_diag_med, and tN_diag_high) target different $\tilde{t}_1$ masses. For the $\tilde{t}_1 \to bW\tilde{\chi}_1^0$ region, a signal selection (bWN) is defined by utilising the

Table 6: Overview of the event selections for the tN_med and tN_high SRs. List values are provided in between parentheses and square brackets denote intervals.

Signal region	tN_med	tN_high
Preselection	high-$E_{\mathrm{T}}^{\mathrm{miss}}$ preselection	
Number of (jets, b-tags)	$(\geq 4, \geq 1)$	$(\geq 4, \geq 1)$
Jet p_{T} [GeV]	$> (60,\ 50,\ 40,\ 40)$	$> (100,\ 80,\ 50,\ 30)$
$E_{\mathrm{T}}^{\mathrm{miss}}$ [GeV]	> 250	> 550
$E_{\mathrm{T},\perp}^{\mathrm{miss}}$ [GeV]	> 230	–
$H_{\mathrm{T,sig}}^{\mathrm{miss}}$	> 14	> 27
m_{T} [GeV]	> 160	
am_{T2} [GeV]	> 175	
$m_{\mathrm{top}}^{\mathrm{reclustered}}$ [GeV]	> 150	> 130
$\Delta R(b, \ell)$	< 2.0	
$\lvert\Delta\phi(j_{1,2}, \vec{p}_{\mathrm{T}}^{\mathrm{miss}})\rvert$	> 0.4	
m_{T2}^{τ} based τ-veto [GeV]	> 80	
Exclusion technique	shape-fit in $E_{\mathrm{T}}^{\mathrm{miss}}$	cut-and-count
Bin boundaries	[250, 350, 450, 600, inf]	

distinctive shape of the invariant mass of the bW system. For the $\tilde{t}_1 \to bff'\tilde{\chi}_1^0$ region, the signal region (bffN) is defined by making use of the soft-lepton selection designed for the higgsino LSP scenarios. The event selection for each signal region is detailed in the following subsections.

7.1.1 $\tilde{t}_1 \to t\tilde{\chi}_1^0$ decay

Table 6 details the event selections for the tN_med and tN_high SRs. In addition to the high-$E_{\mathrm{T}}^{\mathrm{miss}}$ preselection described in Table 4, at least one reconstructed hadronic top-quark candidate based on the recursive reclustered jet algorithm is required in both SRs. Stringent requirements are also imposed on $E_{\mathrm{T}}^{\mathrm{miss}}$, m_{T} and $H_{\mathrm{T,sig}}^{\mathrm{miss}}$. Furthermore, a requirement is placed on am_{T2} to reduce the dileptonic $t\bar{t}$ background. The main background processes after all selection requirements are $ttZ(\nu\nu)$, dileptonic $t\bar{t}$ and W+heavy-flavour processes.

For the tN_med SR, a shape-fit technique is employed, with the SR subdivided in bins of $E_{\mathrm{T}}^{\mathrm{miss}}$, which allows the model-dependent exclusion fits to be more sensitive than the cut-and-count analysis.

7.1.2 Compressed $\tilde{t}_1 \to t\tilde{\chi}_1^0$ decay

The three BDT selections (tN_diag_low, tN_diag_med, and tN_diag_high) are summarised in Table 7 and detailed in the following.

Table 7: Overview of the signal selections using BDTs to target compressed $\tilde{t}_1 \rightarrow t\tilde{\chi}_1^0$ scenarios. List values are provided in between parentheses and square brackets denote intervals.

Variable	tN_diag_low	tN_diag_med	tN_diag_high
Preselection	low-$E_{\mathrm{T}}^{\mathrm{miss}}$	low-$E_{\mathrm{T}}^{\mathrm{miss}}$	high-$E_{\mathrm{T}}^{\mathrm{miss}}$
Number of (jets, b-tags)	$(\geq 4, \geq 1)$	$(\geq 4, \geq 1)$	$(\geq 5, \geq 1)$
Jet p_{T} [GeV]	$> (120,\ 25,\ 25,\ 25)$	$> (100,\ 50,\ 25,\ 25)$	$> (25,\ 25,\ 25,\ 25,\ 25)$
$E_{\mathrm{T}}^{\mathrm{miss}}$ [GeV]	> 100	> 120	> 230
m_{T} [GeV]	> 90	> 120	> 120
R_{ISR}	–	–	> 0.4
$p_{\mathrm{T}}(t\bar{t})$ [GeV]	> 400	–	–
$\lvert\Delta\phi(\ell, t\bar{t})\rvert$	> 1.0	–	–
$\lvert\Delta\phi(j_{1,2}, \vec{p}_{\mathrm{T}}^{\mathrm{miss}})\rvert$	> 0.4	> 0.4	–
m_{T2}^{τ} based τ-veto [GeV]	–	> 80	–
BDT score	BDT_low > 0.55	BDT_med > 0.75	BDT_high> 0.8
Exclusion technique	cut-and-count	shape-fit in BDT score	shape-fit in BDT score
Bin boundaries	–	$[0.4, 0.5, 0.6, 0.7, 0.8, 1.0]$	$[0.6, 0.7, 0.8, 1.0]$

Low $\tilde{t}_1$ mass For $\tilde{t}_1$ masses close to the top-quark mass a BDT is trained for the tN_diag_low signal region. The preselection is based on the low-$E_{\mathrm{T}}^{\mathrm{miss}}$ selection in Table 4.

The variables input to the BDT are $E_{\mathrm{T}}^{\mathrm{miss}}$ and m_{T}, the difference $\Delta m_{\mathrm{T}}^{\alpha}$ in m_{T} between the SM and signal hypothesis, the two top-quark candidate masses $m(t_{\mathrm{had}}^{\mathrm{ISR}})$ and $m(t_{\mathrm{lep}}^{\alpha})$ under the signal hypothesis, and the azimuthal angles between the lepton and the $t\bar{t}$ system, as well as between the lepton and $\vec{p}_{\mathrm{T}}(\nu^{\alpha})$.

The BDT output, from here on referred to as BDT_low, is used to define a single-bin cut-and-count signal region, using the optimal point of BDT_low > 0.55, determined by maximising the expected discovery significance. To avoid a significant extrapolation between control and signal regions an additional selection of $p_{\mathrm{T}}(t\bar{t}) \geq 400$ GeV and $\lvert\Delta\phi(\ell, t\bar{t})\rvert \geq 1.0$ is applied for all selected regions in the tN_diag_low .

Medium $\tilde{t}_1$ mass Stop masses from about 200 to 400 GeV in the compressed scenario are targeted by a BDT using the low-$E_{\mathrm{T}}^{\mathrm{miss}}$ preselection given in Table 4. The input variables of the BDT are $E_{\mathrm{T}}^{\mathrm{miss}}$ and $H_{\mathrm{T,sig}}^{\mathrm{miss}}$, the angular variables $\Delta\phi(\vec{p}_{\mathrm{T}}^{\mathrm{miss}}, t_{\mathrm{had}}^{\chi})$, $\Delta\phi(t_{\mathrm{had}}^{\chi}, t_{\mathrm{lep}}^{\chi})$ and $\Delta R(b, \ell)$, mass variables m_{T} and m_{top}^{χ}, as well as the number of jets and the third and fourth jet p_{T}.

The BDT output score, referred to in the following as BDT_med, is used to define a signal region called tN_diag_med, based on the expected significance for a $\tilde{t}_1$ mass of 250 GeV. The known signal shape is exploited for the exclusion of signal models, using five bins in the BDT score, including also BDT bins lower than the SR.

High $\tilde{t}_1$ mass For compressed bino LSP scenarios with high $\tilde{t}_1$ mass, a BDT is trained using the following variables: R_{ISR}, the angular variables $\Delta\phi(\mathrm{ISR, I})$, $\Delta\phi(t_{\mathrm{had}}^{\chi}, t_{\mathrm{lep}}^{\chi})$, and $\Delta R(b, \ell)$, masses m_{T}, $M_{\mathrm{T}}^{\mathrm{S}}$ and m_{top}^{χ} as well as the number of jets in the di-stop decay system and the third and fourth jet p_{T}, derived using the RJR techniques as described in Section 5. In addition to the high-$E_{\mathrm{T}}^{\mathrm{miss}}$ preselection, a tightened

selection of $m_{\mathrm{T}} > 120\,\mathrm{GeV}$ is imposed to control the multijet background. An additional selection of $R_{\mathrm{ISR}} > 0.4$ is applied to further reduce the background while retaining high efficiency for the considered signal events.

The resulting BDT output score, hereafter called BDT_high, is used to define the `tN_diag_high` signal region. In addition, three BDT bins are employed in a shape-fit to improve the exclusion sensitivity.

7.1.3 $\tilde{t}_1 \to bW\tilde{\chi}_1^0$ and $\tilde{t}_1 \to bff'\tilde{\chi}_1^0$ decays

When the mass difference between the $\tilde{t}_1$ and the $\tilde{\chi}_1^0$ is smaller than the top-quark mass but greater than the sum of the W-boson and bottom-quark masses, the $\tilde{t}$ decays dominantly through the three-body channel into a bottom quark, a W boson, and a neutralino. The `bWN` SR is optimised to search for these events. Compared to the scenario with on-shell top quarks, the three-body decay yields the same final-state leptons and jets but with significantly lower momenta, although typically still above the reconstruction thresholds.

The am_{T2} variable is a powerful discriminant for separating dileptonic $t\bar{t}$ background from signal models in this region of phase space. Because $m_{\tilde{t}_1} - m_{\tilde{\chi}_1^0}$ is below the top-quark mass for signal, am_{T2} peaks at low values, while dileptonic $t\bar{t}$ events typically saturate at values nearer to the top-quark mass. A shape-fit technique is employed, using five bins of am_{T2}, similar to the shape-fit employed in the `tN_med` SR.

When the $\tilde{t}_1$ mass is much closer to the $\tilde{\chi}_1^0$ mass, the stop undergoes a four-body decay with an off-shell W boson, characterised by events having even lower momentum leptons and jets than in the three-body decay. A soft-lepton SR, `bCsoft_diag`, designed for the higgsino LSP scenario with a relaxed m_{T} requirement, provides good sensitivity to this scenario. A shape-fit is performed in the $p_{\mathrm{T}}^{\ell}/E_{\mathrm{T}}^{\mathrm{miss}}$ variable, using three bins for the model-dependent exclusion fit.

The event selections for `bWN` and `bffN` are summarised in Table 8.

7.2 Wino NLSP scenario

If the wino mass parameter M_2 is small enough, the stop may decay directly into $\tilde{\chi}_1^{\pm}$ and $\tilde{\chi}_2^0$ (in addition to the $\tilde{\chi}_1^0$, as the bino is still assumed to be the LSP). In this case, the decays $\tilde{t}_1 \to b\tilde{\chi}_1^{\pm}$ and $\tilde{t}_1 \to t\tilde{\chi}_2^0$ become relevant, leading to a more complex phenomenology than that probed in the pure bino LSP scenario. The SRs targeting this scenario are referred to as `bC2x`.

Two SRs target the $\tilde{t}_1 \to b\tilde{\chi}_1^{\pm}$ decay: the `bC2x_med` and `bC2x_diag` SRs. The kinematics of the decay products are governed by the different mass-splittings, with high-p_{T} b-jets produced from large $\Delta m(\tilde{t}_1,\tilde{\chi}_1^{\pm})$ and high-p_{T} W bosons from large $\Delta m(\tilde{\chi}_1^{\pm},\tilde{\chi}_1^0)$. In addition to the high-$E_{\mathrm{T}}^{\mathrm{miss}}$ preselection, two b-tagged jets and a hadronic W-boson candidate with a mass satisfying $m_W^{\mathrm{reclustered}} > 50\,\mathrm{GeV}$ are required. Tight requirements on m_{T} and am_{T2} are placed to reduce the $t\bar{t}$ background. The main backgrounds after the full signal selection are the $ttZ(\nu\nu)$, dileptonic $t\bar{t}$, and single-top Wt processes.

An additional SR, `bCbv`, is designed for the simplified model $\tilde{t}_1 \to b\tilde{\chi}_1^{\pm}$ scenario with $\Delta m(\tilde{t}_1,\tilde{\chi}_1^{\pm}) = 10\,\mathrm{GeV}$, leading to a signature where the b-jets are too soft to be reconstructed.

The event selections for `bC2x_diag`, `bC2x_med` and `bCbv` are summarised in Table 9.

Table 8: Overview of the event selections for the bWN and bffN SRs. List values are provided in between parentheses and square brackets denote intervals. The veto on the reclustered hadronic top-quark candidate is satisfied for events where no reclustered jet candidate is found, or where the mass of the hadronic top-quark candidate ($m_{\text{top}}^{\text{reclustered}}$) is below 150 GeV. For the bffN SR, the leading jet is required to not be b-tagged.

Signal region	bWN	bffN
Preselection	high-$E_{\text{T}}^{\text{miss}}$	soft-lepton
Number of (jets, b-tags)	$(\geq 4, \geq 1)$	$(\geq 2, \geq 1)$
Jet p_{T} [GeV]	$> (50,\ 25,\ 25,\ 25)$	$> (400,\ 25)$
b-tagged jet p_{T} [GeV]	> 25	> 25
$E_{\text{T}}^{\text{miss}}$ [GeV]	> 300	> 300
m_{T} [GeV]	> 130	< 160
am_{T2} [GeV]	< 110	–
$m_{\text{top}}^{\text{reclustered}}$ [GeV]	–	top veto
$p_{\text{T}}^{\ell}/E_{\text{T}}^{\text{miss}}$	–	< 0.02
$\Delta\phi(\ell, \vec{p}_{\text{T}}^{\text{miss}})$	< 2.5	–
$\min(\Delta\phi(\vec{p}_{\text{T}}^{\text{miss}}, b\text{-jet}_i))$	–	< 1.5
$\lvert\Delta\phi(j_{1,2}, \vec{p}_{\text{T}}^{\text{miss}})\rvert$	> 0.4	
m_{T2}^{τ} based τ-veto [GeV]	> 80	–
Exclusion technique	shape-fit in am_{T2}	shape-fit in $p_{\text{T}}^{\ell}/E_{\text{T}}^{\text{miss}}$
Bin boundaries	[0, 91, 97, 106, 118, 130]	[0, 0.01, 0.015, 0.02]

7.3 Higgsino LSP scenario

The SRs optimised for the pure bino LSP scenarios such as tN_med have sensitivity to the higgsino model in events where a lepton is produced by a top quark from the stop decay. However, three additional SRs, bCsoft_diag, bCsoft_med, and bCsoft_high, are designed to target the case when the lepton is soft, originating instead from a $\tilde{\chi}_1^{\pm}$ decay via a highly off-shell W boson ($\tilde{\chi}_1^{\pm} \rightarrow \tilde{\chi}_1^0 + W^*(\ell\nu)$). This is particularly important in scenarios with $m_{tR} < m_{q3L}$ where the $\mathcal{B}(\tilde{t}_1 \rightarrow b\tilde{\chi}_1^{\pm})$ is large. These soft-lepton SRs are defined to be orthogonal to the tN_med SR so that they can be statistically combined to profit from covering both decay chains.

The bCsoft_diag SR targets a region where the mass difference between the stop and higgsinos is less than the mass of the top quark, so the stop must decay via the $\tilde{t}_1 \rightarrow b\tilde{\chi}_1^{\pm}$ mode. Since none of the decay products receive a large momentum transfer, a high-p_{T} ISR jet is required, resulting in a boost of the $\tilde{t}_1\tilde{t}_1$ system in order to achieve better separation between the signal and background. As a result, the signature is characterised by a high-p_{T} jet, large $E_{\text{T}}^{\text{miss}}$, and a soft lepton. The main background after all selection requirements is semileptonic $t\bar{t}$ and W+jets processes. The bCsoft_diag SR with relaxed m_{T} requirement is found to be sensitive to the $\tilde{t}_1 \rightarrow bff'\tilde{\chi}_1^0$ signature and is described further in Section 7.1.3.

The second SR, bCsoft_med, targets generic higgsino models where each of the decays $\tilde{t}_1 \rightarrow b\tilde{\chi}_1^{\pm}$, $\tilde{t}_1 \rightarrow t\tilde{\chi}_1^0$, and $\tilde{t}_1 \rightarrow t\tilde{\chi}_2^0$ are allowed. In particular, it is designed to select the large fraction of events that produce "mixed" decays, where one $\tilde{t}_1$decays via a chargino and the other via a neutralino. In such cases, the $\tilde{t}_1 \rightarrow b\tilde{\chi}_1^{\pm}$ decay produces a high-p_{T} b-jet, while the b-jet from the other branch, $\tilde{t}_1 \rightarrow t\tilde{\chi}_1^0$

Table 9: Overview of the event selections for the bC2x_med, bC2x_diag, and bCbv SRs. List values are provided in between parentheses and square brackets denote intervals.

Signal region	bC2x_diag	bC2x_med	bCbv
Preselection	high-$E_{\mathrm{T}}^{\mathrm{miss}}$ preselection		
Number of (jets, b-tags)	(≥ 4, ≥ 2)	(≥ 4, ≥ 2)	(≥ 2, $= 0$)
Jet p_{T} [GeV]	$>$ (75, 75, 75, 30)	$>$ (200, 140, 25, 25)	$>$ (120, 80)
b-tagged jet p_{T} [GeV]	$>$ (30, 30)	$>$ (140, 140)	–
$E_{\mathrm{T}}^{\mathrm{miss}}$ [GeV]	> 230	> 230	> 360
$H_{\mathrm{T,sig}}^{\mathrm{miss}}$	> 13	> 10	> 16
m_{T} [GeV]	> 180	> 120	> 200
am_{T2} [GeV]	> 175	> 300	–
$\lvert\Delta\phi(j_1, \vec{p}_{\mathrm{T}}^{\mathrm{miss}})\rvert$	> 0.7	> 0.9	> 2.0
$\lvert\Delta\phi(j_2, \vec{p}_{\mathrm{T}}^{\mathrm{miss}})\rvert$	> 0.7	> 0.9	> 0.8
$m_W^{\mathrm{reclustered}}$ [GeV]	> 50	> 50	[70, 100]
$\Delta\phi(\ell, \vec{p}_{\mathrm{T}}^{\mathrm{miss}})$	–	–	> 1.2
$\lvert\Delta\phi(j_{1,2}, \vec{p}_{\mathrm{T}}^{\mathrm{miss}})\rvert$		> 0.4	
m_{T2}^{τ} based τ-veto [GeV]	> 80	> 80	–
Lepton p_{T} [GeV]	–	–	> 60
Exclusion technique	cut-and-count	cut-and-count	cut-and-count

or $\tilde{t}_1 \to t\tilde{\chi}_2^0$, can be much softer. The third SR, bCsoft_high, targets the higher stop masses, focusing on the $\tilde{t}_1 \to b\tilde{\chi}_1^{\pm}$ signature. The b-jet is boosted due to the large mass difference between the stop and higgsino states, and therefore the signature is characterised by two high-p_{T} b-jets, large $E_{\mathrm{T}}^{\mathrm{miss}}$, and a soft lepton. The remaining background after all signal selection requirements is dominated by semileptonic $t\bar{t}$, single-top Wt, and W+heavy-flavour jets events.

In all three SRs, $p_{\mathrm{T}}^{\ell}/E_{\mathrm{T}}^{\mathrm{miss}}$ is a powerful discriminant as the higgsino signature is characterised by low-p_{T} leptons and large $E_{\mathrm{T}}^{\mathrm{miss}}$, while the SM backgrounds are dominated by events where the $E_{\mathrm{T}}^{\mathrm{miss}}$ arises from a leptonic W-boson decay, producing lepton p_{T} and $E_{\mathrm{T}}^{\mathrm{miss}}$ of a similar magnitude. A shape-fit in $p_{\mathrm{T}}^{\ell}/E_{\mathrm{T}}^{\mathrm{miss}}$ is performed, similar to the shape-fits implemented for the tN_med and bWN SRs.

The event selections for bCsoft_diag, bCsoft_med, and bCsoft_high are detailed in Table 10.

7.4 Bino/higgsino mix scenario

For the bino/higgsino mix scenario, the SRs designed for other scenarios are found to have good sensitivity for this scenario, and are therefore used.

7.5 Spin-0 mediator scenario

Two SRs, DM_low and DM_high, are designed to search for dark matter particles that are pair-produced via a spin-0 mediator (either scalar or pseudoscalar) produced in association with $t\bar{t}$. The DM_low SR

Table 10: Overview of the event selections for the bCsoft_diag, bCsoft_med, and bCsoft_high SRs. List values are provided in between parentheses and square brackets denote intervals. The veto on the reclustered hadronic top-quark candidate is satisfied for events where no reclustered jet candidate is found, or where the mass of the hadronic top-quark candidate ($m_{\text{top}}^{\text{reclustered}}$) is below 150 GeV. For the bCsoft_diag SR, the leading jet is required not to be b-tagged.

Signal region	bCsoft_diag	bCsoft_med	bCsoft_high
Preselection	soft-lepton preselection		
Number of (jets, b-tags)	$(\geq 2, \geq 1)$	$(\geq 3, \geq 2)$	$(\geq 2, \geq 2)$
Jet p_{T} [GeV]	$> (400,\ 25)$	$> (120,\ 60,\ 40)$	$> (100,\ 100)$
b-tagged jet p_{T} [GeV]	> 25	$> (120,\ 60)$	$> (100,\ 100)$
$E_{\text{T}}^{\text{miss}}$ [GeV]	> 300	> 230	> 230
m_{T} [GeV]	< 50	< 160	< 160
p_{T}^{W} [GeV]	–	> 400	> 500
$p_{\text{T}}^{\ell}/E_{\text{T}}^{\text{miss}}$	< 0.02	< 0.03	< 0.03
am_{T2} [GeV]	–	> 200	> 300
$m_{\text{top}}^{\text{reclustered}}$ [GeV]	top veto	–	–
$\min(\Delta\phi(\vec{p}_{\text{T}}^{\text{miss}}, b\text{-jet}_i))$	< 1.5	> 0.8	> 0.4
$\Delta R(b_1, b_2)$	–	–	> 0.8
$\lvert\Delta\phi(j_{1,2}, \vec{p}_{\text{T}}^{\text{miss}})\rvert$		> 0.4	
Exclusion technique	shape-fit in $p_{\text{T}}^{\ell}/E_{\text{T}}^{\text{miss}}$	shape-fit in $p_{\text{T}}^{\ell}/E_{\text{T}}^{\text{miss}}$	shape-fit in $p_{\text{T}}^{\ell}/E_{\text{T}}^{\text{miss}}$
Bin boundaries	$[0, 0.01, 0.015, 0.02]$	$[0, 0.015, 0.03, 0.1]$	$[0, 0.015, 0.03, 0.1]$

is optimised for mediator masses around $m_\phi = 20$ GeV, while the DM_high SR targets mediator masses around $m_\phi = 300$ GeV.

In addition, a predecessor to the DM_low signal region, originally designed for a search using a smaller data set (13.2 fb^{-1}), has been retained, as in that search the number of observed events exceeded the background prediction. This signal region, which was previously called DM_low, is referred to here as DM_low_loose.

Table 11 details the event selections for each of the three SRs. At least one reconstructed hadronic top-quark candidate is required with $m_{\text{top}}^{\text{reclustered}} > 130$ GeV in the newly defined SRs. A high am_{T2} requirement and an angular selection requirement of $|\Delta\phi(\text{jet}_i, \vec{p}_{\text{T}}^{\text{miss}})|$ are further imposed to reduce the $t\bar{t}$ background. The main backgrounds after all signal selection requirements are the $ttZ(\nu\nu)$, dileptonic $t\bar{t}$, and W+heavy-flavour processes.

The event selections for DM_low_loose, DM_low, and DM_high are summarised in Table 11.

8 Background estimates

The dominant background processes in this analysis originate from $t\bar{t}$, single-top Wt, $t\bar{t} + Z(\rightarrow \nu\bar{\nu})$, and W+jets production. Most of the $t\bar{t}$ and Wt events in the hard-lepton signal regions have both W bosons decaying leptonically, where one lepton is 'lost' (meaning it is either not reconstructed, not identified,

Table 11: Overview of the event selections for the DM_low_loose, DM_low, and DM_high SRs. List values are provided in between parentheses.

Signal region	DM_low_loose	DM_low	DM_high
Preselection	high-$E_{\mathrm{T}}^{\mathrm{miss}}$ preselection		
Number of (jets, b-tags)	$(\geq 4, \geq 1)$	$(\geq 4, \geq 1)$	$(\geq 4, \geq 1)$
Jet p_{T} [GeV]	$> (60,\ 60,\ 40,\ 25)$	$> (120,\ 85,\ 65,\ 25)$	$> (125,\ 75,\ 65,\ 25)$
b-tagged jet p_{T} [GeV]	> 25	> 60	> 25
$E_{\mathrm{T}}^{\mathrm{miss}}$ [GeV]	> 300	> 320	> 380
m_{T} [GeV]	> 120	> 170	> 225
$H_{\mathrm{T,sig}}^{\mathrm{miss}}$	> 14	> 14	–
am_{T2} [GeV]	> 140	> 160	> 190
$m_{\mathrm{top}}^{\mathrm{reclustered}}$ [GeV]	–	> 130	> 130
$\Delta\phi(\ell, \vec{p}_{\mathrm{T}}^{\mathrm{miss}})$	> 0.8	> 1.2	> 1.2
$\lvert\Delta\phi(\mathrm{jet}_i, \vec{p}_{\mathrm{T}}^{\mathrm{miss}})\rvert$	> 1.4	> 1.0	> 1.0
m_{T2}^{τ} based τ-veto [GeV]		> 80	
Exclusion technique	cut-and-count	cut-and-count	cut-and-count

or removed by the overlap removal procedure) or one W boson decaying leptonically and the other via a hadronically decaying τ lepton. This is in contrast to the soft-lepton signal regions, where most of the $t\bar{t}$ and Wt contribution arises from semileptonic decays.

These $t\bar{t}$ background decay components are treated separately, referred to as 1L and 2L, which also includes the dileptonic $t\bar{t}$ process where a W boson decays into a τ lepton that subsequently decays hadronically. The $t\bar{t}+Z$ background combined with the subdominant $t\bar{t}+W$ contribution is referred to as $t\bar{t}+V$. Other background contributions arise from dibosons, Z+jets, and multijet production. The multijet background is estimated from data using a fake-factor method [163], and it is found to be negligible in all regions.

The main background processes are estimated via a dedicated CR, used to normalise the simulation to the data with a simultaneous fit, discussed in Section 10. The CRs are defined with event selections that are kinematically close to the SRs but with a few key variable requirements inverted to significantly reduce the potential signal contribution and enhance the yield and purity of a particular background. Each SR has dedicated CRs for the background processes that have the largest contributions. The following background processes are normalised in dedicated CRs: semileptonic $t\bar{t}$ (T1LCR), dileptonic $t\bar{t}$ (T2LCR), W+jets (WCR), single-top (STCR), and $t\bar{t}+V$ (TZCR) processes. All other backgrounds are normalised with the most accurate theoretical cross-sections available.

Several signal regions (bWN, tN_diag_low, and tN_diag_high) that are dominated exclusively by either semileptonic or dileptonic $t\bar{t}$ events have only one associated CR, denoted generically TCR. Signal regions can have fewer associated CRs when the fractional contribution of the corresponding background is small. For the shape-fit analyses, the CRs of each background are not binned and only one normalisation factor is extracted for each background process, which is applied in all SR bins.[13]

[13] The binned CR approach has been tested by comparing the results to a one-bin CR. The normalisation factors were found to be consistent with each other within the statistical uncertainties.

Table 12: Overview of various approaches for the background estimates in all signal regions together with the targeted signal scenario. The $t\bar{t} + Z(\ell\ell)$ control region (CR) described in Section 8.6 is also defined in the top-tagging and W-tagging approaches, except for the bCbv SR where the contribution of the $t\bar{t} + V$ background is negligible.

SR	Signal scenario	Background strategy	Sections
tN_med	Pure bino LSP	top-tagging + $t\bar{t}Z$ CR	8.1
tN_high	Pure bino LSP	top-tagging + $t\bar{t}Z$ CR	8.1
tN_diag_low	Pure bino LSP	BDT	8.2
tN_diag_med	Pure bino LSP	BDT	8.2
tN_diag_high	Pure bino LSP	BDT	8.2
bWN	Pure bino LSP	three-body	8.3
bffN	Pure bino LSP	soft-lepton	8.5
bC2x_med	Wino NLSP	W-tagging + $t\bar{t}Z$ CR	8.4
bC2x_diag	Wino NLSP	W-tagging + $t\bar{t}Z$ CR	8.4
bCbv	Wino NLSP	W-tagging	8.4
bCsoft_diag	Higgsino LSP	soft-lepton	8.5
bCsoft_med	Higgsino LSP	soft-lepton	8.5
bCsoft_high	Higgsino LSP	soft-lepton	8.5
DM_low_loose	DM+$t\bar{t}$	m_{T} extrapolation + $t\bar{t}Z$ CR	8.1
DM_low	DM+$t\bar{t}$	top-tagging + $t\bar{t}Z$ CR	8.1
DM_high	DM+$t\bar{t}$	top-tagging + $t\bar{t}Z$ CR	8.1

The background estimates are tested using VRs, which are disjoint from both the CRs and SRs. Background normalisations determined in the CRs are extrapolated to the VRs and compared with the observed data. Each SR has associated VRs for the $t\bar{t}$ (T1LVR and T2LVR) and W+jets (WVR) processes, which are constructed by inverting or relaxing the selection requirements to be orthogonal to the corresponding SR and CRs. A single-top Wt VR (STVR) is defined for the bCsoft_med and bCsoft_high SRs, where Wt is one of the dominant background processes.

The VRs are not used to constrain parameters in the fit, but provide a statistically independent test of the background estimates made using the CRs. The potential signal contamination in the VRs is studied for all considered signal models and mass ranges, and is found to be less than a few percent in most of the VRs, and less than 15% in VRs for the tN_diag SRs.

The background estimation techniques are categorised using several different approaches. The requirement of the presence of hadronic top-quark candidates (top-tagging) is used for the background estimate in the SRs targeting signals with high-p_{T} top quarks. Compared to previous analyses this background estimation technique has the advantage that the $t\bar{t}$ background composition does not change in the extrapolation from CR to SR. Similarly hadronic W-boson reconstruction (W-tagging) is employed for the background estimate in the SRs targeting signals with high-p_{T} W bosons decaying hadronically. In the following subsections the two approaches are described in detail together with the background estimates for the remaining SRs. Table 12 summarises the approaches for each SR with a brief description of the targeted signal scenarios, and each of those approaches are detailed in Sections 8.1–8.5.

8.1 Hadronic top-tagging approach

In SRs targeting signals with high-p_{T} top quarks (`tN_med`, `tN_high`, `DM_low`, and `DM_high`), a requirement is made that events contain a recursively reclustered jet with a mass consistent with the top-quark mass. While the requirement on $m_{\mathrm{top}}^{\mathrm{reclustered}}$ is powerful for identifying signals, it is also useful in defining CRs that are enriched in background processes with hadronically decaying top quarks ("top-tagged") or depleted in such backgrounds ("top-vetoed").

The CR for dileptonic $t\bar{t}$ (T2LCR) requires m_{T} above the W-boson endpoint. The SR requirement on am_{T2} is inverted (to select events with values below the top-quark mass) and a hadronic top-quark veto is required to reduce the potential signal contamination and improve the purity. The semileptonic $t\bar{t}$ CR (T1LCR) requires a tagged hadronic top-quark candidate and that the m_{T} be within a window around the W-boson mass. The background from semileptonic $t\bar{t}$ events is negligible in the SR but can be sizeable in the other CRs.

The CRs for W+jets (WCR) and single-top (STCR) require m_{T} to be below the W-boson mass. Both CRs also require large am_{T2} and a hadronic top-quark veto. The STCR also requires two b-tagged jets to reduce the W+jets contribution, and a minimum separation between the b-tagged jets, $\Delta R(b_1, b_2) > 1.2$. This latter requirement is useful to suppress the semileptonic $t\bar{t}$ contribution, which can evade the am_{T2} endpoint when a charm quark from the hadronic W-boson decay is misidentified as a b-tagged jet, often leading to a small separation between the two identified b-tagged jets. Events with exactly one b-tagged jet or $\Delta R(b_1, b_2) < 1.2$ are assigned to the WCR. In order to increase the W+jets purity, only events with a positively charged lepton are selected. This requirement exploits the asymmetry in the production of W^+ over W^- events in LHC proton–proton collisions. The asymmetry is further enhanced by the requirement of large $E_{\mathrm{T}}^{\mathrm{miss}}$, as neutrinos from decays of the mostly left-handed W^+ boson are preferentially emitted in the momentum direction of the W boson.

In addition, the background contribution from $t\bar{t} + V$ is large and a dedicated control region is designed, and is described in Section 8.6.

Figure 9 shows various kinematic distributions in the CRs associated with the `tN_med` SR. The backgrounds are scaled with normalisation factors obtained from a simultaneous likelihood fit of the CRs, described in Section 10.

A set of VRs associated with the corresponding CRs is defined by modifying the requirements on the m_{T}, am_{T2}, and hadronic top-tagging variables. The semileptonic $t\bar{t}$ validation region (T1LVR) and W+jets validation region (WVR) slide the m_{T} window from 30–90 GeV to 90–120 GeV. The dileptonic $t\bar{t}$ VR (T2LVR) inverts the requirement of the hadronic top-quark veto (so that a hadronic top-quark tag is required) and relaxes the requirement on am_{T2}. Since the $t\bar{t}$ events are mostly dileptonic after the large m_{T} requirement, the purity of dileptonic $t\bar{t}$ events remains high, despite the hadronic top-quark tag requirement. The relaxed am_{T2} requirement significantly reduces the potential signal contamination. There is no single-top Wt VR (STVR) for these CRs. The m_{T} window for the STCR extends to 120 GeV in order to increase the number of data events entering the CR.

In Figure 9, various kinematic distributions in the VRs associated with `tN_med` are compared to the observed data. The backgrounds are scaled with normalisation factors obtained from a simultaneous likelihood fit of the CRs, described in Section 10.

Tables 13 and 14 detail the definitions of the CRs and VRs associated with the SRs `tN_med`, `tN_high`, `DM_low`, and `DM_high`.

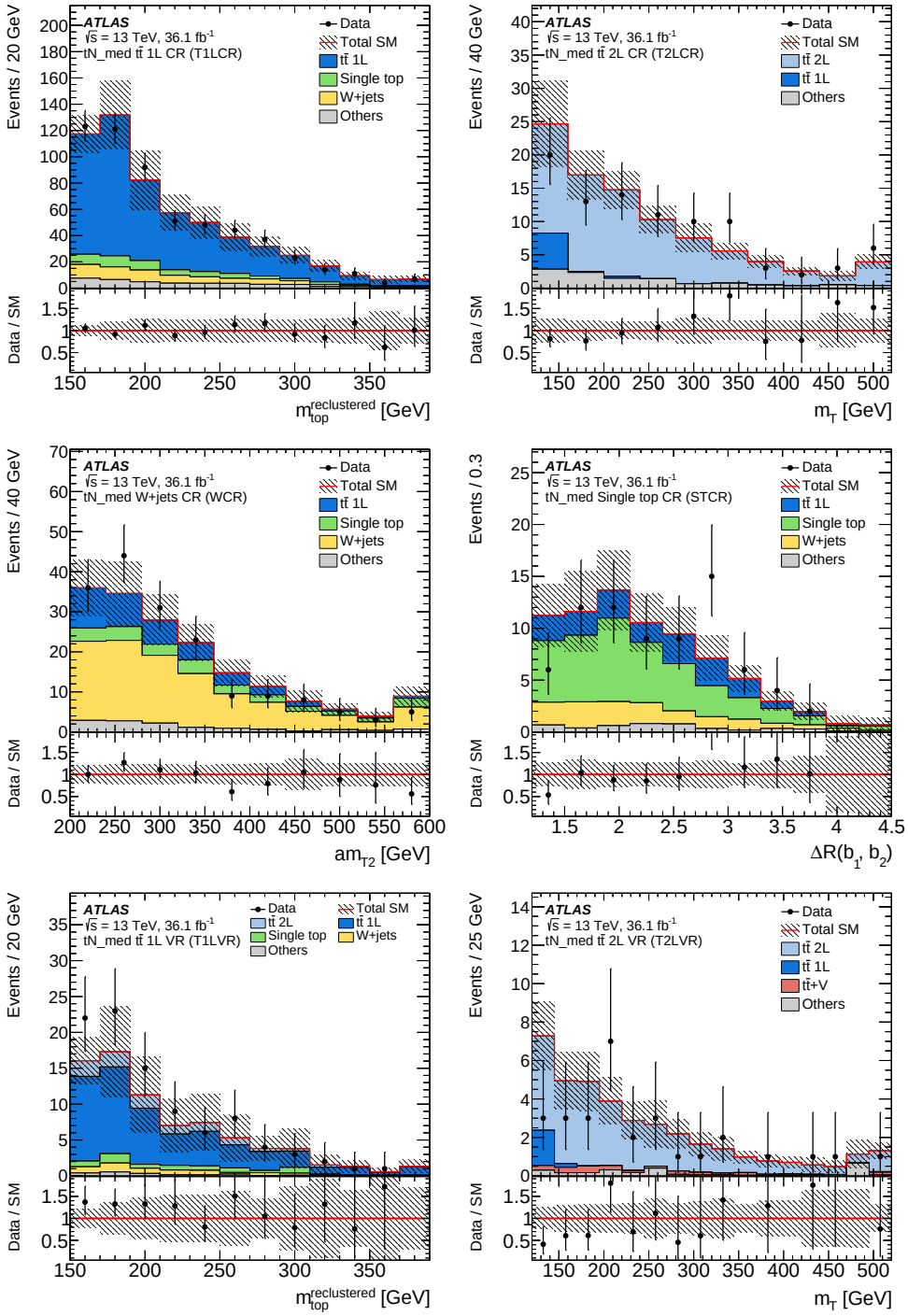

Figure 9: Various kinematic distributions in the `tN_med` control and validation regions: (top left) reclustered jet mass ($m_{\text{top}}^{\text{reclustered}}$) in the semileptonic $t\bar{t}$ control region, (top right) m_{T} in the dileptonic $t\bar{t}$ control region, (middle left) am_{T2} in the W+jets control region, (middle right) $\Delta R(b_1,b_2)$ in the single-top control region, (bottom left) reclustered jet mass ($m_{\text{top}}^{\text{reclustered}}$) in the semileptonic $t\bar{t}$ validation region, and (bottom right) m_{T} in the dileptonic $t\bar{t}$ validation region. Each of the backgrounds is scaled by a normalisation factor obtained from a simultaneous likelihood fit of the CRs. The category labelled 'Others' stands for minor SM backgrounds that contribute less than 5% of the total SM background. The hatched area around the total SM prediction and the hatched band in the Data/SM ratio include statistical and experimental uncertainties. The last bin contains overflows.

The CRs and VRs associated with `DM_low_loose` are retained unchanged from the previous analysis, and are described in Table 15. The $t\bar{t}$ and W+jets backgrounds are estimated from a low m_{T} region, $m_{\mathrm{T}} \in [30, 90]$ GeV, with and without a b-tag requirement, respectively. The corresponding VRs are defined with $m_{\mathrm{T}} \in [90, 120]$ GeV. The single-top Wt, and $t\bar{t}Z$ backgrounds are estimated using the same strategy as the rest of the regions described in this section.

8.2 BDT analyses

For the signal regions `tN_diag_low`, `tN_diag_med` and `tN_diag_high`, control regions use the signal selections but change the requirements on the BDT output scores. Due to its large fractional contribution, only the $t\bar{t}$ background is constrained using data, with all other backgrounds using predictions from samples of simulated events.

Although the main background is always the $t\bar{t}$ process in all three SRs, the fraction of dileptonic $t\bar{t}$ events varies. Therefore, a different strategy is employed for each SR.

For the signal regions `tN_diag_low` and `tN_diag_high`, the $t\bar{t}$ background is treated as a single component, with a single normalisation factor being derived. One $t\bar{t}$ control region (TCR) is used for `tN_diag_low`, while three control-region bins (TCR1, TCR2, and TCR3) are used for `tN_diag_high` in order to improve the stability of the simultaneous fit by reducing the correlation between the signal and $t\bar{t}$ background.

For `tN_diag_med`, the $t\bar{t}$ background is split into semileptonic and dileptonic $t\bar{t}$ contributions. Two control-region bins (TCR1 and TCR2, enriched in dileptonic and semileptonic $t\bar{t}$ events respectively) are defined to constrain the $t\bar{t}$ background and determine two separate normalisation factors for its two components in all fits to the data. Selected kinematic distributions in the `tN_diag_low` and `tN_diag_med` CRs are shown in Figure 10.

An overview of the CR selections for the BDT analyses can be found in Table 16.

8.3 $\tilde{t}_1 \to bW\tilde{\chi}_1^0$ analysis

Almost all of the background in the `bWN` SR consists of dileptonic $t\bar{t}$ events (where one of the leptons is lost or a hadronically decaying τ lepton). Therefore, a single high-purity TCR is defined by relaxing the selection requirements on $E_{\mathrm{T}}^{\mathrm{miss}}$ and am_{T2}. In addition, the requirement on $\Delta\phi(\ell, \vec{p}_{\mathrm{T}}^{\mathrm{miss}})$ is inverted to reduce the potential signal contamination. The TVR is defined by sliding the am_{T2} window to 110–130 GeV in order to validate the background normalisation obtained from the TCR.

Figure 11 shows kinematic distributions in the CRs associated with the `bWN` SR. Table 17 details the corresponding CR and VR selections together with the SR selection.

8.4 Hadronic W-tagging approach

Control regions for the `bC2x_diag` and `bC2x_med` SRs exploit hadronic W-boson tagging (W-tagging) with the $m_W^{\mathrm{reclustered}}$ variable, closely following the strategy described in Section 8.1. The CRs invert two out of three requirements on m_{T}, am_{T2}, and the hadronic W-boson candidate mass.

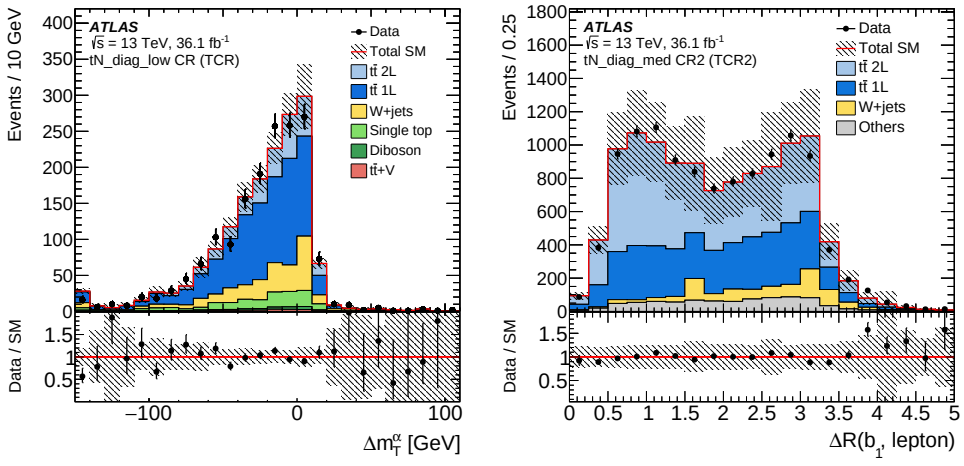

Figure 10: Kinematic distributions in the `tN_diag_low` and `tN_diag_med` control regions: (left) $\Delta m_{\mathrm{T}}^{\alpha}$ in the `tN_diag_low` top control region (TCR) and (right) $\Delta R(b_1, \ell)$ in the `tN_diag_med` top control region (TCR2). Values of $m_{\tilde{t}_1} = 200\,\mathrm{GeV}$ and $m_{\tilde{\chi}_1^0} = 27\,\mathrm{GeV}$ are used, resulting in $\alpha = 0.135$. The $t\bar{t}$ background is scaled by a normalisation factor obtained from the control region. The category labelled 'Others' stands for minor SM backgrounds that contribute less than 5% of the total SM background. The hatched area around the total SM prediction and the hatched band in the Data/SM ratio include statistical and experimental uncertainties. The last bin contains overflows.

For the `bCbv` SR, since the veto on b-tagged jets is required in the signal-region selection, a different CR strategy is used. The WCR and TCR remove the selection requirement on $\Delta\phi(\ell, \vec{p}_{\mathrm{T}}^{\,\mathrm{miss}})$ and select a m_{T} window of 30–90 GeV to increase the number of events in the region while suppressing potential signal contamination. A b-tagged jet is further required in the TCR to improve the purity of $t\bar{t}$ events.

Figure 12 shows selected kinematic distributions in associated CRs for `bC2x_med`.

A set of VRs associated with the CRs is defined following the approach taken for the top-tagging VRs in Section 8.1, i.e. by modifying the requirements on the m_{T}, am_{T2}, and hadronic W-tagging variables. Tables 18 and 19 detail the CR and VR selections for the corresponding SRs.

8.5 Soft-lepton analyses

For the soft-lepton SRs (`bCsoft_diag`, `bCsoft_med`, `bCsoft_high`, and `bffN`), a single TCR, dominated by semileptonic $t\bar{t}$ events, is defined for the $t\bar{t}$ background since the fraction of dileptonic $t\bar{t}$ background is small compared to the other SRs because there is no m_{T} requirement.

For `bCsoft_med` and `bCsoft_high` SRs, three CRs (TCR, WCR, and STCR) are defined by inverting the requirements on am_{T2}, $p_{\mathrm{T}}^{\ell}/E_{\mathrm{T}}^{\mathrm{miss}}$, and the number of b-tagged jets, while requiring the same p_{T}^{W} threshold as the corresponding SR to ensure similar kinematics in the SR and CRs for the p_{T} of the top quark and the W boson, which might be poorly modelled by the simulation. The TCR is designed by inverting the selection requirement on am_{T2} and relaxing the $p_{\mathrm{T}}^{\ell}/E_{\mathrm{T}}^{\mathrm{miss}}$ requirement to minimise potential signal contamination while improving the purity. Similarly, the WCR and STCR are defined by relaxing $p_{\mathrm{T}}^{\ell}/E_{\mathrm{T}}^{\mathrm{miss}}$, and requiring exactly one or at least two b-tagged jets respectively.

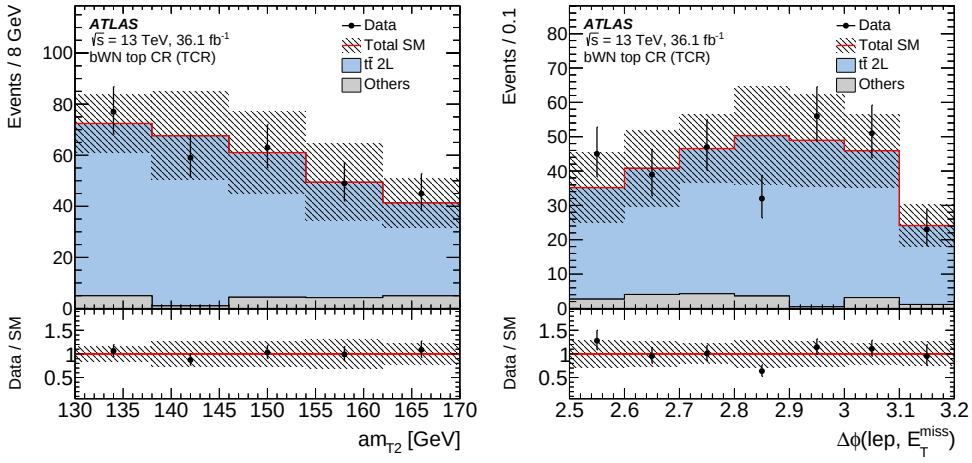

Figure 11: Kinematic distributions in the bWN top control region (TCR): (left) am_{T2} and (right) $\Delta\phi(\ell, \vec{p}_{\mathrm{T}}^{\,\mathrm{miss}})$. The $t\bar{t}$ process is scaled by a normalisation factor obtained in the corresponding control region. The category labelled 'Others' stands for minor SM backgrounds that contribute less than 5% of the total SM background. The hatched area around the total SM prediction and the hatched band in the Data/SM ratio include statistical and experimental uncertainties. The last bin contains overflows.

For the bCsoft_diag SR, the CR strategy using top-tagging is employed, based on the $m_{\mathrm{top}}^{\mathrm{reclustered}}$ variable as described in Section 8.1. The TCR is defined by requiring a tagged hadronic top-quark candidate and relaxing the requirement on m_{T} to increase the number of $t\bar{t}$ events, while the WCR is defined by requiring a hadronic top-quark veto. For the WCR, an additional requirement is imposed on $\min(\Delta\phi(\vec{p}_{\mathrm{T}}^{\,\mathrm{miss}}, b\text{-jet}_i))$ to increase the purity of W+jets events. A STCR is not defined for this SR, as the Wt contribution is small compared to other backgrounds. The CRs for the bffN SR are identical to those for bCsoft_diag because of the similarity in the SR selections.

Figure 13 shows selected kinematic distributions in the CRs associated with bCsoft_med. The backgrounds are scaled with normalisation factors obtained from the simultaneous likelihood fit of the CRs as described in Section 10.

A set of VRs associated with corresponding CRs is also defined by inverting the requirement on $p_{\mathrm{T}}^{\ell}/E_{\mathrm{T}}^{\mathrm{miss}}$. For the soft-lepton SRs, an STVR is defined together with the TVR and WVR. In Figure 13, selected kinematic distributions in the VRs associated with bCsoft_high are compared to the observed data. The backgrounds are scaled with normalisation factors. Tables 20 and 21 detail the soft-lepton CR and VR selections.

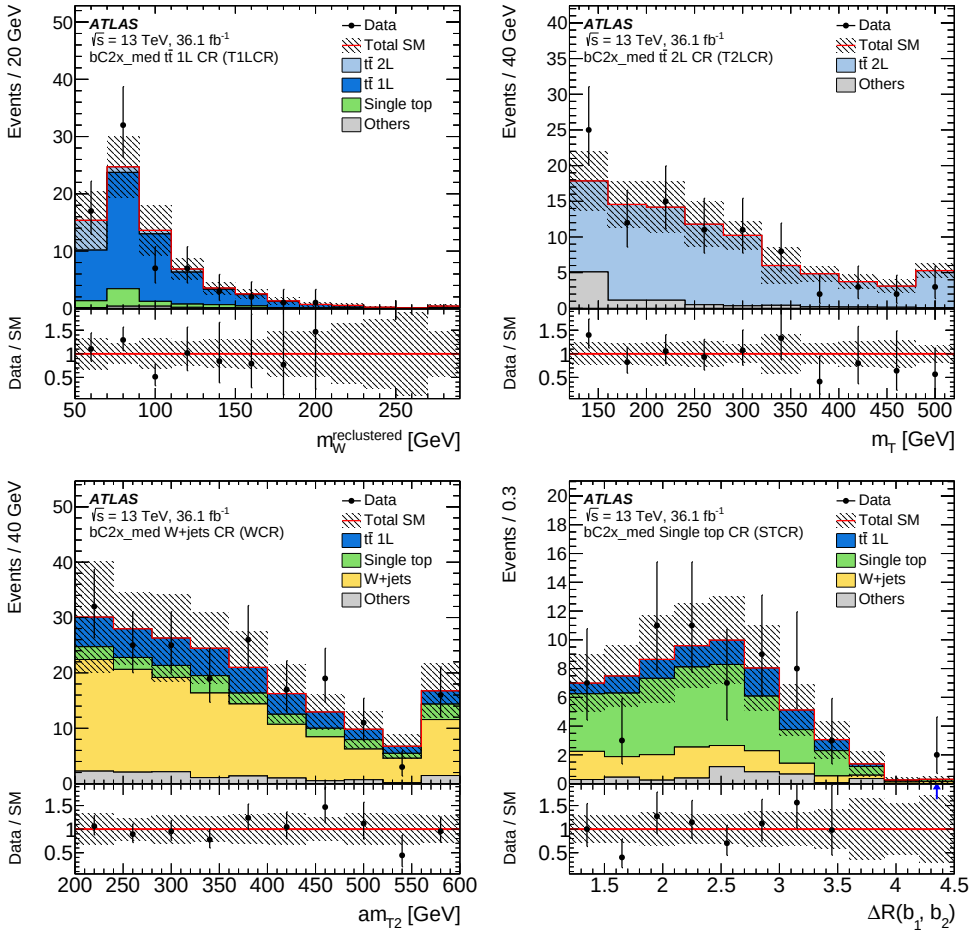

Figure 12: Kinematic distribution of the `bC2x_med` control regions: (top left) reclustered jet mass ($m_W^{\text{reclustered}}$) in the semileptonic $t\bar{t}$ control region, (top right) m_{T} in the dileptonic $t\bar{t}$ control region, (bottom left) am_{T2} in the W+jets control region, and (bottom right) $\Delta R(b_1,b_2)$ in the single-top control region. Each of these backgrounds is scaled by normalisation factors obtained from the corresponding control region. The category labelled 'Others' stands for minor SM backgrounds that contribute less than 5% of the total SM background. The hatched area around the total SM prediction and the hatched band in the Data/SM ratio include statistical and experimental uncertainties. The last bin contains overflows.

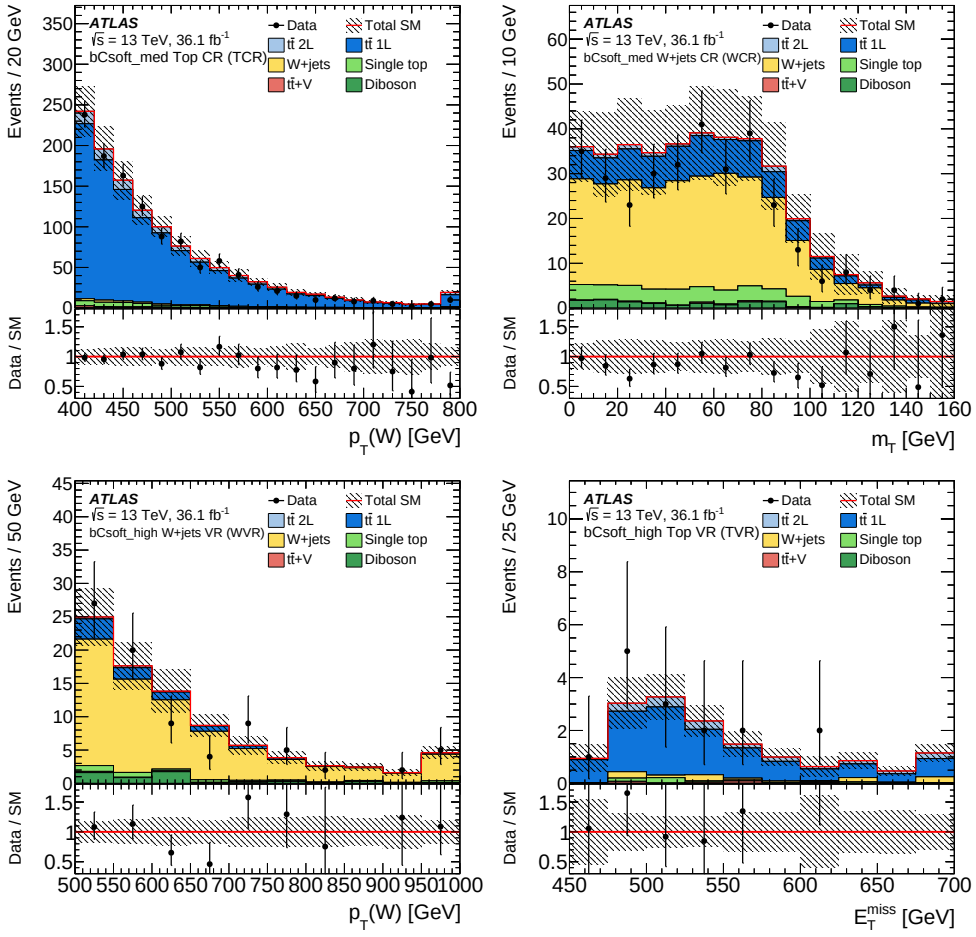

Figure 13: Kinematic distributions in the control regions associated with `bCsoft_med` and the validation regions associated with `bCsoft_high`: (top left) p_{T}^{W} in the top control region, (top right) m_{T} in the W+jets control region, (bottom left) p_{T} of the leptonically decaying W boson (p_{T}^{W}) in the W+jets validation region, and (bottom right) $E_{\mathrm{T}}^{\mathrm{miss}}$ in the top validation region. Each of the backgrounds is scaled by a normalisation factor obtained from the corresponding control region. The hatched area around the total SM prediction and the hatched band in the Data/SM ratio include statistical and experimental uncertainties. The last bin contains overflows.

Table 13: Overview of the selections for the `tN_med` and `tN_high` signal regions as well as the associated control and validation regions. The control regions include the semileptonic $t\bar{t}$ control region (T1LCR), the dileptonic $t\bar{t}$ control region (T2LCR), the W+jets control region (WCR), and the single-top Wt control region (STCR). The validation regions include the semileptonic $t\bar{t}$ validation region (T1LVR), the dileptonic $t\bar{t}$ validation region (T2LVR), and the W+jets validation region (WVR). List values are provided in between parentheses and square brackets denote intervals. The veto on the reclustered hadronic top-quark candidate is satisfied for events where no reclustered jet candidate is found, or where the mass of the hadronic top-quark candidate ($m_{\text{top}}^{\text{reclustered}}$) is below the specified tag threshold. For the WCR, $\Delta R(b_1,b_2) < 1.2$ is not required when the event has only one b-tagged jet. The selection of the $t\bar{t}+V$ control region (TZCR) is detailed in Section 8.6.

	`tN_med`	T1LCR/VR	T2LCR/VR	WCR/VR	STCR
Preselection	high-$E_{\text{T}}^{\text{miss}}$ preselection				
Number of (jets, b-tags)	($\geq 4, \geq 1$)	($\geq 4, \geq 1$)	($\geq 4, \geq 1$)	($\geq 4, \geq 1$)	($\geq 4, \geq 2$)
Jet p_{T} [GeV]	$> (60,\ 50,\ 40,\ 40)$				
b-tagged jet p_{T} [GeV]	> 25				$> (25,\ 25)$
$E_{\text{T}}^{\text{miss}}$ [GeV]	> 250				
$E_{\text{T},\perp}^{\text{miss}}$ [GeV]	> 230				
m_{T} [GeV]	> 160	[30, 90] / [90, 120]	> 120	[30, 90] / [90, 120]	[30, 120]
$H_{\text{T,sig}}^{\text{miss}}$	> 14	> 10	> 10	> 10	> 10
$m_{\text{top}}^{\text{reclustered}}$ [GeV]	> 150	> 150	top veto / > 150	top veto	top veto
am_{T2} [GeV]	> 175	< 200	< 200 / < 130	> 200	> 200
$\Delta R(b,\ell)$	< 2.0	–	–	–	–
$\Delta R(b_1,b_2)$	–	–	–	< 1.2	> 1.2
Lepton charge	–	–	–	+1	–
$\lvert\Delta\phi(j_{1,2},\vec{p}_{\text{T}}^{\text{miss}})\rvert$	> 0.4				
m_{T2}^{τ} based τ-veto [GeV]	> 80				
	`tN_high`	T1LCR/VR	T2LCR/VR	WCR/VR	STCR
Preselection	high-$E_{\text{T}}^{\text{miss}}$ preselection				
Number of (jets, b-tags)	($\geq 4, \geq 1$)	($\geq 4, \geq 1$)	($\geq 4, \geq 1$)	($\geq 4, \geq 1$)	($\geq 4, \geq 2$)
Jet p_{T} [GeV]	$> (100,\ 80,\ 50,\ 30)$				
b-tagged jet p_{T} [GeV]	> 25				$> (25,\ 25)$
$E_{\text{T}}^{\text{miss}}$ [GeV]	> 550	> 350	> 350	> 350	> 350
m_{T} [GeV]	> 160	[30, 90] / [90, 120]	> 120	[30, 90] / [90, 120]	[30, 120]
$H_{\text{T,sig}}^{\text{miss}}$	> 27	> 10	> 10	> 10	> 10
$m_{\text{top}}^{\text{reclustered}}$ [GeV]	> 130	> 130	top veto / > 130	top veto	top veto
am_{T2} [GeV]	> 175	< 200	< 200 / < 130	> 200	> 200
$\Delta R(b,\ell)$	< 2.0	–	–	–	–
$\Delta R(b_1,b_2)$	–	–	–	< 1.2	> 1.2
Lepton charge	–	–	–	+1	–
$\lvert\Delta\phi(j_{1,2},\vec{p}_{\text{T}}^{\text{miss}})\rvert$	> 0.4				
m_{T2}^{τ} based τ-veto [GeV]	> 80				

Table 14: Overview of the selections for the DM_low and DM_high signal regions as well as the associated control and validation regions. The control regions include the semileptonic $t\bar{t}$ control region (T1LCR), the dileptonic $t\bar{t}$ control region (T2LCR), the W+jets control region (WCR), and the single-top Wt control region (STCR). The validation regions include the semileptonic $t\bar{t}$ validation region (T1LVR), the dileptonic $t\bar{t}$ validation region (T2LVR), and the W+jets validation region (WVR). List values are provided in between parentheses and square brackets denote intervals. The veto on the reclustered hadronic top-quark candidate is satisfied for events where no reclustered jet candidate is found, or where the mass of the hadronic top-quark ($m_{\text{top}}^{\text{reclustered}}$) is below a certain threshold. For the WCR, $\Delta R(b_1,b_2) < 1.2$ is not required when the event has only one b-tagged jet. The selection of the $t\bar{t}+V$ control region (TZCR) is detailed in Section 8.6.

	DM_low	T1LCR/VR	T2LCR/VR	WCR/VR	STCR
Preselection	high-$E_{\text{T}}^{\text{miss}}$ preselection				
Number of (jets, b-tags)	($\geq 4, \geq 1$)	($\geq 4, \geq 1$)	($\geq 4, \geq 1$)	($\geq 4, \geq 1$)	($\geq 4, \geq 2$)
Jet p_{T} [GeV]	$> (120,\ 85,\ 65,\ 60)$				
b-tagged jet p_{T} [GeV]	> 25				$> (25,\ 25)$
$E_{\text{T}}^{\text{miss}}$ [GeV]	> 320	> 250	> 230	> 250	> 250
m_{T} [GeV]	> 170	[30, 90] / [90, 120]	> 120	[30, 90] / [90, 120]	[30, 120]
$H_{\text{T,sig}}^{\text{miss}}$	> 14	> 10	> 10	> 10	> 10
$m_{\text{top}}^{\text{reclustered}}$ [GeV]	> 130	> 130	top veto / > 130	top veto	top veto
am_{T2} [GeV]	> 160	< 200	< 160	> 160	> 200
$\Delta\phi(\ell, \vec{p}_{\text{T}}^{\text{miss}})$	> 1.2	–	> 1.2	–	–
$\lvert\Delta\phi(\text{jet}_i, \vec{p}_{\text{T}}^{\text{miss}})\rvert$	> 1.0	–	–	–	–
$\Delta R(b_1,b_2)$	–	–	–	< 1.2	> 1.2
Lepton charge	–	–	–	+1	–
$\lvert\Delta\phi(j_{1,2}, \vec{p}_{\text{T}}^{\text{miss}})\rvert$	> 0.4				
m_{T2}^{τ} based τ-veto [GeV]	> 80				

	DM_high	T1LCR/VR	T2LCR/VR	WCR/VR	STCR
Preselection	high-$E_{\text{T}}^{\text{miss}}$ preselection				
Number of (jets, b-tags)	($\geq 4, \geq 1$)	($\geq 4, \geq 1$)	($\geq 4, \geq 1$)	($\geq 4, \geq 1$)	($\geq 4, \geq 2$)
Jet p_{T} [GeV]	$> (125,\ 75,\ 65,\ 25)$				
b-tagged jet p_{T} [GeV]	> 25				$> (25,\ 25)$
$E_{\text{T}}^{\text{miss}}$ [GeV]	> 380	> 280	> 280	> 280	> 280
m_{T} [GeV]	> 225	[30, 90] / [90.120]	> 120	[30, 90] / [90, 120]	[30, 120]
$m_{\text{top}}^{\text{reclustered}}$ [GeV]	> 130	> 130	top veto / > 130	top veto	top veto
am_{T2} [GeV]	> 190	< 200	< 200 / < 190	> 190	> 200
$\Delta\phi(\ell, \vec{p}_{\text{T}}^{\text{miss}})$	> 1.2	–	> 1.2	–	–
$\lvert\Delta\phi(\text{jet}_i, \vec{p}_{\text{T}}^{\text{miss}})\rvert$	> 1.0	> 1.0	–	> 1.0	–
$\Delta R(b_1,b_2)$	–	–	–	< 1.2	> 1.2
Lepton charge	–	–	–	+1 / –	–
$\lvert\Delta\phi(j_{1,2}, \vec{p}_{\text{T}}^{\text{miss}})\rvert$	> 0.4			> 0.4 / –	> 0.4
m_{T2}^{τ} based τ-veto [GeV]	> 80				

Table 15: Overview of the selections for the DM_low_loose signal region as well as the associated control and validation regions. The control regions include the $t\bar{t}$ control region (TCR), the W+jets control region (WCR), and the single-top Wt control region (STCR). The validation regions include the $t\bar{t}$ validation region (TVR) and the W+jets validation region (WVR). List values are provided in between parentheses and square brackets denote intervals. The selection of the $t\bar{t}+V$ control region (TZCR) is detailed in Section 8.6.

	DM_low_loose	TCR/VR	WCR/VR	STCR
Preselection	high-$E_{\mathrm{T}}^{\mathrm{miss}}$ preselection			
Number of (jets, b-tags)	($\geq 4, \geq 1$)	($\geq 4, \geq 1$)	($\geq 4, = 0$)	($\geq 4, \geq 2$)
Jet p_{T} [GeV]	$>$ (60, 60, 40, 25)			
b-tagged jet p_{T} [GeV]	$>$ 25			$>$ (25, 25)
$E_{\mathrm{T}}^{\mathrm{miss}}$ [GeV]	$>$ 300	$>$ 230	$>$ 230	$>$ 230
$H_{\mathrm{T,sig}}^{\mathrm{miss}}$	$>$ 14	$>$ 8	$>$ 8	$>$ 8
m_{T} [GeV]	$>$ 120	[30,90] / [90,120]	[30,90] / [90,120]	[30,120]
am_{T2} [GeV]	$>$ 140	[100, 200]	$>$ 100	$>$ 200
$\lvert\Delta\phi(\mathrm{jet}_i, \vec{p}_{\mathrm{T}}^{\mathrm{miss}})\rvert$	$>$ 1.4	$>$ 1.4	$>$ 1.4	$>$ 1.4
$\Delta\phi(\ell, \vec{p}_{\mathrm{T}}^{\mathrm{miss}})$	$>$ 0.8	$>$ 0.8	$>$ 0.8	–
$\Delta R(b_1, b_2)$	–	–	–	$>$ 1.8
m_{T2}^{τ} based τ-veto [GeV]	$>$ 80			

Table 16: Overview of signal region and control region definitions for the BDT analyses targeting the compressed bino LSP scenarios. The selections described in Table 7 are applied, except for the BDT score. Square brackets denote intervals.

Signal Region	tN_diag_low	tN_diag_med		tN_diag_high		
BDT score	≥ 0.55	≥ 0.4		≥ 0.6		
Associated CRs	TCR	TCR1	TCR2	TCR1	TCR2	TCR3
BDT score	[−1, 0.1]	[−1, −0.4]	[−0.4, 0.4]	[−1, −0.5]	[−0.5, 0]	[0, 0.4]

Table 17: Overview of the selections for the bWN signal region and associated control and validation regions. List values are provided in between parentheses and square brackets denote intervals.

	bWN	TCR/VR
Preselection	high-$E_{\mathrm{T}}^{\mathrm{miss}}$ preselection	
Number of (jets, b-tags)	($\geq 4, \geq 1$)	($\geq 4, \geq 1$)
Jet p_{T} [GeV]	$>$ (50, 25, 25, 25)	
b-tagged jet p_{T} [GeV]	$>$ 25	
$E_{\mathrm{T}}^{\mathrm{miss}}$ [GeV]	$>$ 300	$>$ 230
m_{T} [GeV]	$>$ 130	$>$ 130
am_{T2} [GeV]	$<$ 110	[130, 170] / [110, 130]
$\Delta\phi(\ell, \vec{p}_{\mathrm{T}}^{\mathrm{miss}})$	$<$ 2.5	$>$ 2.5
$\lvert\Delta\phi(j_{1,2}, \vec{p}_{\mathrm{T}}^{\mathrm{miss}})\rvert$	$>$ 0.4	
m_{T2}^{τ} based τ-veto [GeV]	$>$ 80	

Table 18: Overview of the selections for the bC2x_diag and bC2x_med signal regions as well as the associated control and validation regions. The control regions include the semileptonic $t\bar{t}$ control region (T1LCR), the dileptonic $t\bar{t}$ control region (T2LCR), the W+jets control region (WCR), and the single-top Wt control region (STCR). The validation regions include the semileptonic $t\bar{t}$ validation region (T1LVR), the dileptonic $t\bar{t}$ validation region (T2LVR), and the W+jets validation region (WVR). List values are provided in between parentheses and square brackets denote intervals. The veto on the reclustered hadronic W-boson candidate is satisfied for events where no reclustered jet candidate is found, or where the mass of the hadronic top-quark candidate ($m_{\text{top}}^{\text{reclustered}}$) is below the specified tag threshold. For the WCR, $\Delta R(b_1,b_2) < 1.2$ is not required when the event has only one b-tagged jet. The selection of the $t\bar{t} + V$ control region (TZCR) is detailed in Section 8.6.

	bC2x_diag	T1LCR/VR	T2LCR/VR	WCR/VR	STCR
Preselection	high-$E_{\text{T}}^{\text{miss}}$ preselection				
Number of (jets, b-tags)	($\geq 4, \geq 2$)	($\geq 4, \geq 2$)	($\geq 4, \geq 2$)	($\geq 4, \geq 1$)	($\geq 4, \geq 2$)
Jet p_{T} [GeV]			$> (75,\ 75,\ 75,\ 30)$		
b-tagged jet p_{T} [GeV]	$> (30,\ 30)$	$> (30,\ 30)$	$> (30,\ 30)$	$> (30,\ -)$	$> (30,\ 30)$
$E_{\text{T}}^{\text{miss}}$ [GeV]			> 230		
$H_{\text{T,sig}}^{\text{miss}}$	> 13	> 13	> 10	> 13	> 10
m_{T} [GeV]	> 180	[30, 90] / [90, 120]	> 120	[30, 90] / [90, 120]	[30, 120]
am_{T2} [GeV]	> 175	< 200	< 200 / < 130	> 200	> 200
$\lvert\Delta\phi(\text{jet}_i, \vec{p}_{\text{T}}^{\text{miss}})\rvert (i = 1, 2)$			> 0.7		
$m_W^{\text{reclustered}}$ [GeV]	> 50	> 50	W veto / > 50	W veto	W veto
$\Delta R(b_1, b_2)$	–	–	–	< 1.2	> 1.2
Lepton charge	–	–	–	$= +1$	–
$\lvert\Delta\phi(j_{1,2}, \vec{p}_{\text{T}}^{\text{miss}})\rvert$			> 0.4		
m_{T2}^{τ} based τ-veto [GeV]			> 80		

	bC2x_med	T1LCR/VR	T2LCR/VR	WCR/VR	STCR
Preselection	high-$E_{\text{T}}^{\text{miss}}$ preselection				
Number of (jets, b-tags)	($\geq 4, \geq 2$)	($\geq 4, \geq 2$)	($\geq 4, \geq 1$)	($\geq 4, \geq 1$)	($\geq 4, \geq 2$)
Jet p_{T} [GeV]			$> (200,\ 140,\ 25,\ 25)$		
b-tagged jet p_{T} [GeV]	$> (140,\ 140)$	$> (140,\ 140)$	$> (140,\ -)$	$> (140,\ -)$	$> (140,\ 140)$
$E_{\text{T}}^{\text{miss}}$ [GeV]			> 230		
$H_{\text{T,sig}}^{\text{miss}}$	> 10	> 10	> 10	> 10	> 6
m_{T} [GeV]	> 120	[30, 90] / [90, 120]	> 120	[30, 90] / [90, 120]	[30, 120]
am_{T2} [GeV]	> 300	< 200	< 200 / < 130	> 200	> 200
$\lvert\Delta\phi(\text{jet}_i, \vec{p}_{\text{T}}^{\text{miss}})\rvert (i = 1, 2)$			> 0.9		
$m_W^{\text{reclustered}}$ [GeV]	> 50	> 50	W veto / > 50	W veto	W veto
$\Delta R(b_1, b_2)$	–	–	–	< 1.2	> 1.2
Lepton charge	–	–	–	$= +1$	–
$\lvert\Delta\phi(j_{1,2}, \vec{p}_{\text{T}}^{\text{miss}})\rvert$			> 0.4		
m_{T2}^{τ} based τ-veto [GeV]			> 80		

Table 19: Overview of the selections for the bCbv signal region, as well as the associated control regions for $t\bar{t}$ (TCR) and W+jets (WCR), and the validation regions targeting $t\bar{t}$ (TVR) and W+jets (WVR) backgrounds. List values are provided in between parentheses and square brackets denote intervals.

	bCbv	TCR/VR	WCR/VR
Preselection		high-$E_{\mathrm{T}}^{\mathrm{miss}}$ preselection	
Lepton p_{T} [GeV]		> 60	
Number of (jets, b-tags)	$(\geq 2, = 0)$	$(\geq 2, \geq 1)$	$(\geq 2, = 0)$
Jet p_{T} [GeV]		$> (120,\ 80)$	
b-tagged jet p_{T} [GeV]	–	> 25	–
$E_{\mathrm{T}}^{\mathrm{miss}}$ [GeV]		> 360	
$H_{\mathrm{T,sig}}^{\mathrm{miss}}$		> 16	
m_{T} [GeV]	> 200	$[30, 90]$ / $[90, 120]$	$[30, 90]$ / $[90, 120]$
$\lvert\Delta\phi(\mathrm{jet}_i, \vec{p}_{\mathrm{T}}^{\mathrm{miss}})\rvert (i = 1)$		> 2.0	
$\lvert\Delta\phi(\mathrm{jet}_i, \vec{p}_{\mathrm{T}}^{\mathrm{miss}})\rvert (i = 2)$		> 0.8	
$\Delta\phi(\ell, \vec{p}_{\mathrm{T}}^{\mathrm{miss}})$	> 1.2	–	–
$m_W^{\mathrm{reclustered}}$ [GeV]		$[70, 100]$	
$\lvert\Delta\phi(j_{1,2}, \vec{p}_{\mathrm{T}}^{\mathrm{miss}})\rvert$		> 0.4	

Table 20: Overview of the selections for the bCsoft_diag and bffN signal regions, as well as the associated control regions for $t\bar{t}$ (TCR) and W+jets (WCR), and the validation regions targeting $t\bar{t}$ (TVR) and W+jets (WVR) backgrounds. List values are provided in between parentheses and square brackets denote intervals. The veto on the reclustered hadronic top-quark candidate is satisfied for events where no reclustered jet candidate is found, or where the mass of the hadronic top-quark candidate ($m_{\mathrm{top}}^{\mathrm{reclustered}}$) is below a certain threshold. The leading jet is required not to be b-tagged in all regions.

	bCsoft_diag/bffN	TCR/VR	WCR/VR
Preselection		soft-lepton preselection	
Number of (jets, b-tags)	$(\geq 2, \geq 1)$	$(\geq 2, \geq 1)$	$(\geq 2, = 1)$
Jet p_{T} [GeV]		$> (120,\ 25)$	
b-tagged jet p_{T} [GeV]		> 25	
$E_{\mathrm{T}}^{\mathrm{miss}}$ [GeV]		> 300	
m_{T} [GeV]	< 50 / < 160	< 160	< 160
$p_{\mathrm{T}}^{\ell}/E_{\mathrm{T}}^{\mathrm{miss}}$	< 0.02	$[0.03, 0.10]$ / < 0.03	$[0.03, 0.10]$ / < 0.03
$m_{\mathrm{top}}^{\mathrm{reclustered}}$ [GeV]	top veto	> 150	top veto
$\min(\Delta\phi(\vec{p}_{\mathrm{T}}^{\mathrm{miss}}, b\text{-jet}_i))$	< 1.5	< 1.5	> 1.5
$\lvert\Delta\phi(j_{1,2}, \vec{p}_{\mathrm{T}}^{\mathrm{miss}})\rvert$		> 0.4	

Table 21: Overview of the selections for the `bCsoft_med` and `bCsoft_high` signal regions, as well as the associated control regions for $t\bar{t}$ (TCR) and W+jets (WCR), and the validation regions targeting $t\bar{t}$ (TVR) and W+jets (WVR) backgrounds. List values are provided in between parentheses and square brackets denote intervals.

	`bCsoft_med`	TCR/VR	WCR/VR	STCR/VR
Preselection	soft-lepton preselection			
Number of (jets, b-tags)	$(\geq 3, \geq 2)$	$(\geq 3, \geq 2)$	$(\geq 3, = 1)$	$(\geq 3, \geq 2)$
Jet p_{T} [GeV]	$> (120,\ 60,\ 40,\ 25)$			
b-tagged jet p_{T} [GeV]	$> (120,\ 60)$	$> (120,\ 60)$	> 120	$> (120,\ 60)$
$E_{\mathrm{T}}^{\mathrm{miss}}$ [GeV]	> 230			
m_{T} [GeV]	< 160			
p_{T}^{W} [GeV]	> 400			
$p_{\mathrm{T}}^{\ell}/E_{\mathrm{T}}^{\mathrm{miss}}$	< 0.03	> 0.03 / < 0.03	> 0.20 / $[0.1, 0.2]$	> 0.20 / $[0.1, 0.2]$
am_{T2} [GeV]	> 200	< 200	> 200	> 200
$\min(\Delta\phi(\vec{p}_{\mathrm{T}}^{\mathrm{miss}}, b\text{-jet}_i))$	> 0.8	–	$[0.8, 2.5]$	> 0.8
$\Delta R(b_1, b_2)$	–	–	–	> 1.2
$\lvert\Delta\phi(j_{1,2}, \vec{p}_{\mathrm{T}}^{\mathrm{miss}})\rvert$	> 0.4			

	`bCsoft_high`	TCR/VR	WCR/VR	STCR/VR
Preselection	soft-lepton preselection			
Number of (jets, b-tags)	$(\geq 2, \geq 2)$	$(\geq 2, \geq 2)$	$(\geq 2, = 1)$	$(\geq 2, \geq 2)$
Jet p_{T} [GeV]	$> (100,\ 100)$			
b-tagged jet p_{T} [GeV]	$> (100,\ 100)$			
$E_{\mathrm{T}}^{\mathrm{miss}}$ [GeV]	> 230			
m_{T} [GeV]	< 160			
p_{T}^{W} [GeV]	> 500			
$p_{\mathrm{T}}^{\ell}/E_{\mathrm{T}}^{\mathrm{miss}}$	< 0.03	> 0.10 / < 0.10	$[0.1, 0.4]$ / < 0.10	> 0.30 / $[0.1, 0.3]$
am_{T2} [GeV]	> 300	< 300	> 300	> 300
$\min(\Delta\phi(\vec{p}_{\mathrm{T}}^{\mathrm{miss}}, b\text{-jet}_i))$	> 0.4			
$\Delta R(b_1, b_2)$	> 0.8	> 0.8	–	> 0.8
$\Delta R(b, \ell)$	–	–	> 0.8	–
$\lvert\Delta\phi(j_{1,2}, \vec{p}_{\mathrm{T}}^{\mathrm{miss}})\rvert$	> 0.4			

8.6 Control regions for $t\bar{t} + V$

Top-quark pair production in association with a Z boson that decays into neutrinos is an irreducible background to the $t\bar{t}$ +$E_{\mathrm{T}}^{\mathrm{miss}}$ signature. In order to estimate the $t\bar{t} + Z$ contribution in the SRs, Z-boson decays into charged leptons are exploited to define high-purity CRs (TZCR). The $t\bar{t} + V$ CRs require exactly three loose signal leptons, at least one of which must also satisfy the tight criteria. Two leptons are required to have same flavour and opposite charge, and the mass of the dilepton system ($m_{\ell\ell}$) is required to be in the range 81 GeV $< m_{\ell\ell} <$ 101 GeV. In addition, at least four jets, one of which is b-tagged, are required. The minimum jet p_{T} of the four leading jets is required to match the thresholds used in the corresponding SR. The diboson process ($WZ \rightarrow \ell\nu\ell\ell$) is a dominant background in the TZCR, and is normalised to data in a region identical to the TZCR, except for the requirement that no jet is b-tagged. A constant diboson normalisation factor of 0.8, derived in this region, is applied to all TZCRs.

The $t\bar{t} + Z$ control region is defined for SRs where the $t\bar{t} + Z$ contribution is sizeable: `tN_med`, `tN_high`, `bC2x_med`, `bC2x_diag`, `DM_low_loose`, `DM_low`, and `DM_high`. The purity of the TZCR is $\approx 75\%$, with remaining events due to diboson and tZ single-top production. Figure 14 shows the $p_{\mathrm{T}}^{\ell\ell}$ distribution in the TZCR associated with `tN_med`, as well as $m_{\ell\ell}$ prior to requiring 81 GeV $< m_{\ell\ell} <$ 101 GeV. The $p_{\mathrm{T}}^{\ell\ell}$ distribution serves as a proxy for the $E_{\mathrm{T}}^{\mathrm{miss}}$ distribution in $t\bar{t} + Z(\nu\nu)$ events. The $t\bar{t} + Z(\ell\ell)$ method is cross-checked with an alternative method using the $t\bar{t} + \gamma$ process. The normalisation factors obtained from the $t\bar{t} + \gamma$ events are found to be consistent with those from the $t\bar{t} + Z(\ell\ell)$ method.

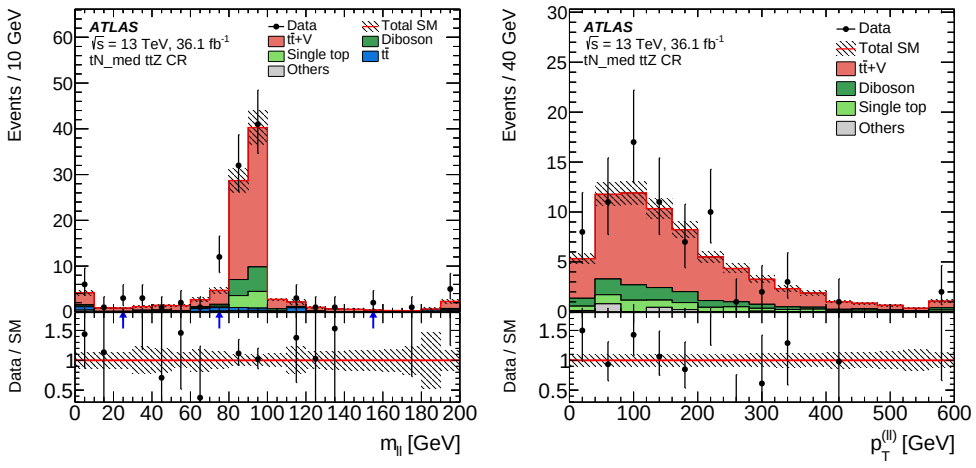

Figure 14: Distribution of (left) the dilepton mass and (right) $p_{\mathrm{T}}^{\ell\ell}$ corresponding to the p_{T} of the reconstructed Z boson in the $t\bar{t} + Z$ control region (TZCR) associated with the `tN_med` signal region. The $t\bar{t} + Z/W$ processes are normalised in the TZCR. The diboson background is normalised to data events with zero b-tagged jets. The hatched area around the total SM prediction and the hatched band in the Data/SM ratio include statistical and experimental uncertainties. The last bin contains overflows.

9 Systematic uncertainties

The systematic uncertainties in the signal and background estimates arise both from experimental sources and from the uncertainty in the theoretical predictions and modelling. Since the yields from the dominant background sources, $t\bar{t}$, single-top Wt, $t\bar{t} + V$, and W+jets, are normalised to data in dedicated CRs, the

uncertainties for these processes affect only the extrapolation from the CRs into the SRs (and amongst the various CRs), but not the overall normalisation. The systematic uncertainties are included as nuisance parameters with Gaussian constraints and profiled in the likelihood fits. The uncertainties are not reduced as a result of the profiling.

The dominant experimental uncertainties arise from imperfect knowledge of the jet energy scale (JES) and jet energy resolution (JER) [146, 164], as well as the modelling of the b-tagging efficiencies and mis-tag rates [165, 166]. From these sources, the resulting uncertainties expressed as relative uncertainties in the total predicted background yield in the SRs are in the range 1.4–7% for JES, 1.5–7% for JER, and 1.6–13% for b-tagging. Other sources of experimental uncertainty include the modelling of the lepton energy scales, energy resolutions, reconstruction and identification efficiencies, trigger efficiencies, and the modelling of pile-up and the integrated luminosity. These uncertainties have a small impact on the final results.

The uncertainty in the modelling of the single-top and $t\bar{t}$ backgrounds include effects related to the MC event generator, the hadronisation modelling, and the amount of initial- and final-state radiation [113]. The MC generator uncertainty is estimated by comparing events produced with Powheg-Box+Herwig++ v2.7.1 with either MG5_aMC@NLO v2.2.3+Herwig++ v2.7.1 (NLO) or Sherpa v2.2.1. Events generated with Powheg-Box are showered and subsequently hadronized with either Pythia6 or Herwig++ to estimate the effect from the modelling of the hadronisation. The impact of altering the amount of initial- and final-state radiation is estimated from comparisons of Powheg-Box+Pythia6 samples with different parton-shower radiation, NLO radiation, and modified factorisation and renormalisation scales. An additional uncertainty stems from the modelling of the interference between the $t\bar{t}$ and Wt processes. The uncertainty is estimated using inclusive $WWbb$ events, generated using MG5_aMC@NLO v2.2.3 (LO), which are compared with the sum of the resonant $t\bar{t}$ and Wt processes [113]. The resulting uncertainties from all the aforementioned sources in the extrapolation factors from the $t\bar{t}$ and Wt CRs to the SRs are 10–45% for $t\bar{t}$, and 10–47% for Wt events, where the latter is dominated by the interference term.

The uncertainty in the modelling of the $t\bar{t}+Z$ background is estimated from independent variations of the renormalisation and factorisation scales, and PDF variations. A MC generator uncertainty is estimated by comparing events produced with MG5_aMC@NLO v2.2.3+Pythia8 (NLO) and Sherpa v2.2.1. The resulting modelling-induced uncertainties in the extrapolation factor are 10–37%, dominated by the MC generator comparison.

The uncertainty in the W+jets background from the choice of MC generator is estimated by comparing Sherpa with MG5_aMC@NLO v2.2.3+Pythia8 (NLO). In addition, the effects of varying the scales for the matching scheme related to the merging of matrix elements and parton showers, renormalisation, factorisation, and resummation are estimated. The total uncertainty is found to be 4–44%.

The sources of uncertainty considered for the diboson background are the effects of varying the renormalisation, factorisation, and resummation scales. Since the diboson background is not normalised in a CR, the analysis is also sensitive to the uncertainty in the total cross-section. The resulting theoretical uncertainty ranges from 13 to 32%.

For the BDT analyses, a systematic-smoothing procedure in BDT score is applied to evaluate the uncertainties in the modelling of $t\bar{t}$ and single-top Wt processes. The procedure gives a reliable estimate of the uncertainties despite statistical fluctuations in the background samples, based on merging statistically insignificant bins and smoothing the result with a Gaussian kernel.

Table 22: Summary of the dominant systematic uncertainties in the total predicted background yields, obtained by the background-only fits as described in Section 10.1, in several representative signal regions: `tN_med`, `bWN`, `bC2x_med`, and `bCsoft_med`. Numbers are given as percentages of the total background estimate.

Signal Region Uncertainty (%)	`tN_med`	`bWN`	`bC2x_med`	`bCsoft_med`
$t\bar{t}+Z$ normalisation	11	–	6.8	–
$t\bar{t}$ (2L) normalisation	4.7	7.5	3.3	2.6
Wt normalisation	3.0	–	17	3.4
W+jets normalisation	2.5	–	2.1	8.1
$t\bar{t}+Z$ modelling	11	2.3	1.2	< 1.0
$t\bar{t}$ radiation	4.3	13	1.9	4.6
$t\bar{t}$ generator	3.6	7.8	1.7	4.6
$t\bar{t}$ hadronisation	2.5	12	5.8	3.9
Wt–$t\bar{t}$ interference	< 1.0	< 1.0	13	< 1.0
Single-top generator	< 1.0	< 1.0	4.9	< 1.0
Single-top hadronisation	< 1.0	< 1.0	11	< 1.0
JER	2.8	1.5	6.8	2.4
JES	2.8	6.6	1.4	2.1
Mis-b-tag (c-quark)	2.3	1.6	4.9	13
Mis-b-tag (light quark)	2.0	< 1.0	2.0	4.6
Pile-up	2.5	1.2	3.8	2.0
Total systematic uncertainty	18	22	28	15

The SUSY signal cross-section uncertainty is taken from an envelope of cross-section predictions using different PDF sets and factorisation and renormalisation scales, as described in Ref. [99], and the resulting uncertainties range from 13% to 23%. The uncertainty in the DM production cross-section is estimated from the effect of varying the renormalisation, factorisation, and matching scales, as well as the PDF choice. The uncertainty is found to be between 12% and 20%. Experimental uncertainties in the signal acceptance have negligible impact on the final results.

Table 22 summarises the dominant systematic uncertainties in selected signal regions. The dominant sources of uncertainty are background modelling and JES/JER uncertainties in most of SRs. The uncertainty related to the description of the b-tagging mis-tag rates in the simulation becomes large in the `bCsoft_med`. This is because the single-top Wt or semileptonic $t\bar{t}$ background events above the am_{T2} kinematic endpoint often have an associated charm-quark misidentified as a b-jet, and thus the background yield is sensitive to the mis-tag modelling.

10 Results

10.1 Observed data and predicted backgrounds

In order to determine the SM background yields in the SRs, a likelihood fit is performed for each SR. The fit is configured to use only the CRs to constrain the fit parameters corresponding to the normalisations of $t\bar{t}$, single-top, W+jets, and $t\bar{t}+V$ processes in the dedicated CRs. This fit configuration is referred to as the background-only fit.

The number of observed events and the predicted number of SM background events from the background-only fits in all SRs and VRs are shown in Figures 15 and 16. The SRs are not mutually exclusive and are therefore not statistically independent. In all SRs, the distributions indicate good agreement between the data and the SM background estimate. The largest excesses over the background-only hypothesis are $1.6\,\sigma$ and $1.4\,\sigma$, observed in `tN_high` and `tN_med`, respectively. The previously observed excess in `DM_low_loose` is reduced with the inclusion of more data to the level of $1.5\,\sigma$.

The number of observed events together with the predicted number of SM background events in all 16 SRs are summarised in Tables 23 and 24, showing the breakdown of the various backgrounds that contribute to the SRs. The tables also list the results for the four fit parameters that control the normalisation of the four main backgrounds (normalisation factors, NFs), together with the associated fit uncertainties including the theoretical modelling uncertainties. In order to quantify the level of agreement of the SM background-only hypothesis with the observations in the SRs, a profile-likelihood-ratio test is performed. The resulting p-values (p_0) are also presented in the tables, and are capped at 0.5. Model-independent upper limits on beyond-SM contributions are derived for each SR. A generic signal model is assumed that contributes only to the SR and for which neither experimental nor theoretical systematic uncertainties except for the luminosity uncertainty are considered. All limits are calculated using the CL_s prescription [167]. Table 25 details the number of observed events and the predicted number of SM background events for each bin of the shape-fit SRs. The NFs are compatible with unity in most cases, except for the single-top NFs in `bCsoft_med` and `bCsoft_high`. The single-top NFs are significantly below unity, possibly due to the effect of interference between the Wt and $t\bar{t}$ processes at NLO.

Figures 17, 18, and 19 show comparisons between the observed data and the SM background prediction with all SR selections applied except the requirement on the plotted variable. Good agreement is found between the observed data and the SM background prediction. The expected distributions from representative signal benchmark models are overlaid.

10.2 Exclusion limits

As no significant excess is observed, exclusion limits are set based on profile-likelihood fits for the stop pair production models and the simplified model for top quarks produced in association with dark-matter particles.

The signal uncertainties and potential signal contributions to all regions are taken into account. All uncertainties except those in the theoretical signal cross-section are included in the fit. Exclusion limits at 95% confidence level (CL) are obtained by selecting *a priori* the signal region with the lowest expected CL_s value for each signal model and the exclusion contours are derived by interpolating in the CL_s value.

Figure 20 shows the expected and observed exclusion contours as a function of stop and neutralino mass for the pure bino LSP scenario. The $\pm 1\,\sigma_{\text{exp}}$ uncertainty band indicates how much the expected limit is affected by the systematic and statistical uncertainties included in the fit. The $\pm 1\,\sigma^{\text{SUSY}}_{\text{theory}}$ uncertainty lines around the observed limit illustrate the change in the observed limit as the nominal signal cross-section is scaled up and down by the theoretical cross-section uncertainty. The exclusion limits are obtained under the hypothesis of mostly right-handed stops in the pure bino LSP scenario. Figure 21 shows the expected and observed exclusion contours as a function of stop mass and the mass splitting $\Delta m(\tilde{t}_1, \tilde{\chi}^0_1)$, providing a greater level of detail for the transitions between the two-, three- and four-body decay regions. Stop masses above 195 GeV are excluded for any value of the neutralino mass within the two-body decay region. The exclusion range extends to stop masses up to 480 GeV or higher depending on the neutralino mass.

The results improve upon previous exclusion limits by excluding the stop mass region up to 940 GeV for a massless lightest neutralino and assuming $\mathcal{B}(\tilde{t}_1 \to t\tilde{\chi}^0_1) = 100\%$. In the three-body scenario, stop masses are excluded up to 500 GeV for a LSP mass of about 300 GeV. In the four-body scenario, stop masses are excluded up to 370 GeV for a mass-splitting between the stop and the LSP as low as 20 GeV.

The non-excluded area between the three- and four-body decay regions is due to a reduction in search sensitivity as the kinematic properties of the signal change significantly when transitioning from a four-body to a three-body decay. In particular, approaching this boundary from the three-body side, the momenta of the two b-jets decrease to zero and hence the acceptance of the p_{T} requirement on the b-tagged jet in the `bWN` signal region decreases rapidly.

The kinematic properties change again at the kinematic boundary between the three-body and on-shell top-quark decay modes. When approaching this diagonal from the on-shell top-quark side, the search sensitivity usually worsens due to the difficulty in disentangling signal from the $t\bar{t}$ background. However, the dedicated BDT analysis (here in particular `tN_diag_high`) recovers partly the sensitivity.

Limits are also set on the masses of the $\tilde{t}_1$ and $\tilde{\chi}^0_1$ in the wino NLSP scenario. Figure 22 shows the exclusion contours based on the combination of all SRs targeting this scenario for positive and negative values of the μ parameter. The stop mass region up to 885 GeV (940 GeV) is excluded in scenarios with $\mu < 0$ ($\mu > 0$) and a 200 GeV neutralino. Figure 23 shows the exclusion limit for the simplified model $\tilde{t}_1 \to b\tilde{\chi}^{\pm}_1$ scenario with $m_{\tilde{t}_1} - m_{\tilde{\chi}^{\pm}_1} = 10$ GeV. The stop mass region is excluded up to 840 GeV for a massless neutralino.

Assuming the higgsino LSP scenario, limits are also set on the masses of the $\tilde{t}_1$ and $\tilde{\chi}^0_1$. Figures 24 and 25 show the exclusion contours for the three signal scenarios, $m_{tR} < m_{q3L}$, $m_{q3L} < m_{tR}$, and $m_{q3L} < m_{tR}$ with large $\tan\beta$, as described in Section 4. The results are based on the combination of two orthogonal hard- and soft-lepton SRs. The stop decay branching ratios to $t\tilde{\chi}^0_1$, $b\tilde{\chi}^{\pm}_1$ and $t\tilde{\chi}^0_2$ vary in these three scenarios. In the scenario with $m_{tR} < m_{q3L}$, the sensitivity is mostly driven by the `bCsoft_med` and `bCsoft_high` SRs, as the branching ratio of the $\tilde{t}_1 \to b\tilde{\chi}^{\pm}_1$ decay (with soft leptons) is large, whereas the sensitivity is driven by the `tN_med` SR for the scenario with $m_{q3L} < m_{tR}$, as the branching ratios of the $\tilde{t}_1 \to t\tilde{\chi}^0_1$ and $\tilde{t}_1 \to t\tilde{\chi}^0_2$ decays (with high-p_{T} leptons from the leptonically decaying top quark) are dominant. The third scenario, $m_{q3L} < m_{tR}$ with large $\tan\beta$, benefits from both the soft- and hard-lepton SRs, with equal branching ratios to all three decay modes.

Figure 26 shows the region $m_b + m_{\tilde{\chi}^{\pm}_1} < m_{\tilde{t}_1} < m_{\text{top}} + m_{\tilde{\chi}^0_1}$. Since the mass-splitting $\Delta m(\tilde{t}_1, \tilde{\chi}^0_1)$ is smaller than the top mass a 100% branching ratio to $\tilde{t}_1 \to b\tilde{\chi}^{\pm}_1$ is assumed, and the exclusion limit is set by a single soft-lepton SR, `bCsoft_diag`. In the gaps between the exclusion contour and diagonal dashed lines indicating the kinematic boundaries ($m_{\tilde{t}_1} = m_b + m_{\tilde{\chi}^{\pm}_1}$ and $m_{\tilde{t}_1} = m_{\text{top}} + m_{\tilde{\chi}^0_1}$), the assumption of a

100% branching ratio may not be accurate due to phase-space effects, hence these gap regions are not considered in the interpretation.

In Figures 25 and 26, $\Delta m(\tilde{\chi}_1^{\pm}, \tilde{\chi}_1^0)$ is fixed to 5 GeV and $\Delta m(\tilde{\chi}_2^0, \tilde{\chi}_1^0)$ is fixed to 10 GeV. In Figure 24, the mass relations $\Delta m(\tilde{\chi}_2^0, \tilde{\chi}_1^0) = 2\times\Delta m(\tilde{\chi}_1^{\pm}, \tilde{\chi}_1^0)$ and $m_{\tilde{\chi}_1^{\pm}} = 150$ GeV are assumed, while $\Delta m(\tilde{\chi}_1^{\pm}, \tilde{\chi}_1^0)$ is varied in the range 0–30 GeV. For the region $\Delta m(\tilde{\chi}_1^{\pm}, \tilde{\chi}_1^0) < 2$ GeV, only the $\tilde{t}_1 \to t\tilde{\chi}_1^0$ process is simulated, with the branching ratio set to account for both the $\tilde{t}_1 \to t\tilde{\chi}_1^0$ and $\tilde{t}_1 \to t\tilde{\chi}_2^0$ decays. In Figure 25, the stop mass region up to 890 GeV (800 GeV) is excluded in scenarios with $m_{q3L} < m_R$ ($m_R < m_{q3L}$).

Limits are also set on the masses of the $\tilde{t}_1$ and $\tilde{\chi}_1^0$ in the well-tempered neutralino scenario as shown in Figure 27. In the scenario with $m_{q3L} < m_{tR}$, the expected sensitivity is better than in the scenario with $m_{tR} < m_{q3L}$ as sbottom pair production can also contribute to the former, roughly doubling the signal acceptance. No observed limit is set in the $m_{tR} < m_{q3L}$ scenario, as a mild excess of data events is seen above the predicted SM background yield in the `bCsoft_high` SR (shape-fit, as shown in Figure 19), which is the most sensitive SR in this scenario. On the other hand, the stop mass region up to 810 GeV is excluded in scenarios with $m_{q3L} < m_{tR}$.

Figure 28 shows the upper limit on the ratio of the DM+$t\bar{t}$ production cross-section to the theoretical cross-section. Limits are shown under the hypothesis of a scalar or pseudoscalar mediator, and for a fixed DM candidate mass or for a fixed mediator mass. A scalar (pseudoscalar) mediator mass of around 100 GeV (20 GeV) is excluded at 95% CL, assuming a 1 GeV dark-matter particle mass and a common coupling of $g = 1$ to SM and dark-matter particles.

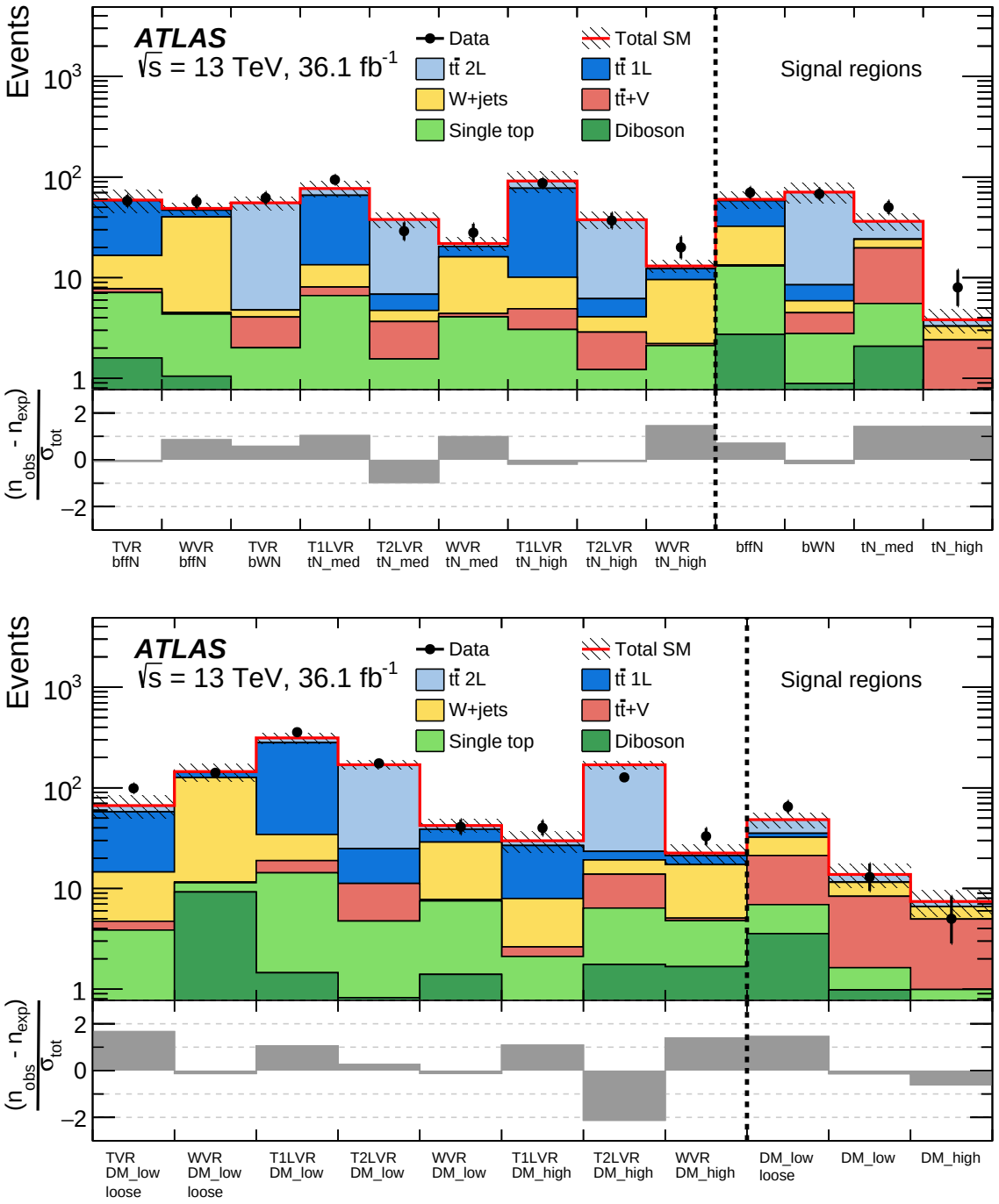

Figure 15: Comparison of the observed data (n_{obs}) with the predicted SM background (n_{exp}) in (top) the `bffN`, `bWN`, `tN_med` and `tN_high` signal regions, and (bottom) the `DM_low_loose`, `DM_low`, and `DM_high` signal regions, and associated VRs. The background predictions are obtained using the background-only fit configuration, and the hatched area around the SM prediction includes all uncertainties. The bottom panels show the difference between data and the predicted SM background divided by the total uncertainty (σ_{tot}).

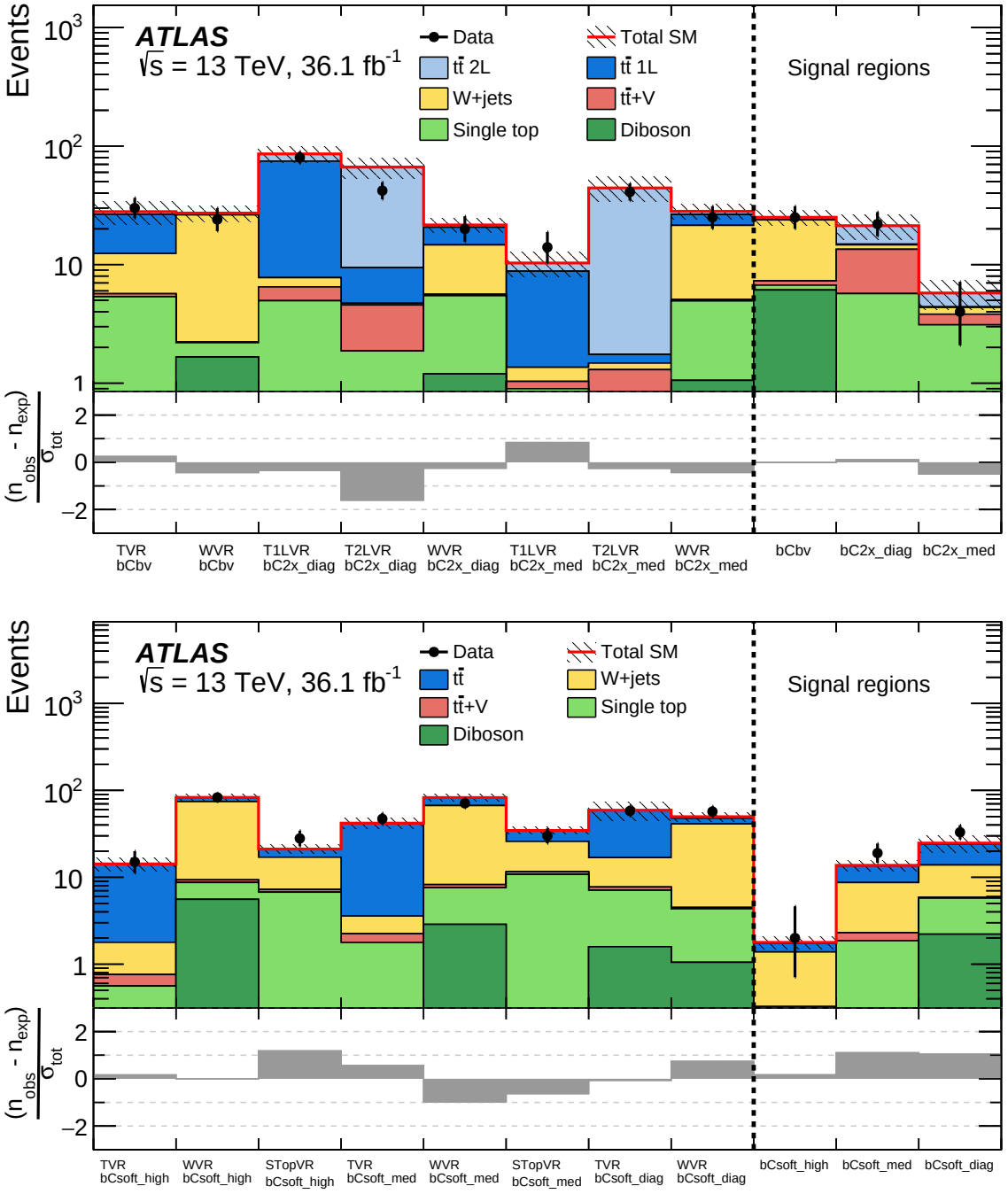

Figure 16: Comparison of the observed data (n_{obs}) with the predicted SM background (n_{exp}) in (top) the `bCbv`, `bC2x_diag`, and `bC2x_med` signal regions, (bottom) the `bCsoft_high`, `bCsoft_med`, and `bCsoft_diag` signal regions, together with associated VRs. The background predictions are obtained using the background-only fit configuration, and the hatched area around the SM prediction includes all uncertainties. The bottom panels show the difference between data and the predicted SM background divided by the total uncertainty (σ_{tot}).

Table 23: The numbers of observed events in the pure bino LSP SRs together with the expected numbers of background events and their uncertainties as predicted by the background-only fits, the normalisation factors (NF) for the background predictions obtained in the fit, the probabilities (represented by p_0 values, and capped at 0.5) that the observed numbers of events are compatible with the background-only hypothesis, and the expected ($N^{\text{limit}}_{\text{non-SM}}$ exp.) and observed ($N^{\text{limit}}_{\text{non-SM}}$ obs.) 95% CL upper limits on the number of beyond-SM events. Some of the SRs where $t\bar{t}$ background events are predominantly semileptonic or dileptonic have only one NF which is also applied to the subdominant $t\bar{t}$ contribution.

Signal region	tN_high	tN_med	tN_diag_high	tN_diag_med	tN_diag_low	bWN	bffN
Observed	8	50	19	115	34	68	70
Total background	3.8 ± 1.0	36.3 ± 6.6	18.3 ± 2.2	115 ± 31	30.3 ± 5.9	71 ± 16	60.5 ± 6.1
$t\bar{t}$ 2ℓ	0.51 ± 0.18	12.1 ± 2.9	15.2 ± 2.4	65.1 ± 9.4	8.5 ± 2.3	65 ± 16	25.5 ± 5.5
$t\bar{t}$ 1ℓ	0.020 ± 0.001	0.19 ± 0.05	-	35.0 ± 8.9	17.5 ± 4.1	-	-
$t\bar{t}+V$	1.86 ± 0.90	14.2 ± 5.5	0.68 ± 0.37	2.5 ± 1.6	0.34 ± 0.20	1.7 ± 1.7	0.35 ± 0.06
Single top	0.13 ± 0.10	3.5 ± 1.2	1.5 ± 1.2	8.1 ± 1.1	2.3 ± 1.2	$1.9^{+2.0}_{-1.9}$	10.3 ± 4.4
W+jets	0.88 ± 0.24	4.3 ± 1.1	0.70 ± 0.56	3.8 ± 1.9	$1.7^{+2.0}_{-1.7}$	1.41 ± 0.88	19.6 ± 4.9
Diboson	0.42 ± 0.16	2.08 ± 0.70	0.21 ± 0.11	$0.69^{+0.73}_{-0.69}$	$0.07^{+0.24}_{-0.07}$	0.89 ± 0.28	2.72 ± 0.99
Z+jets	-	-	-	-	-	-	1.9 ± 1.8
$t\bar{t}$ 2ℓ NF	1.01 ± 0.15	0.96 ± 0.13	1.05 ± 0.06	1.16 ± 0.16	-	1.04 ± 0.07	-
$t\bar{t}$ 1ℓ NF	0.97 ± 0.08	1.05 ± 0.09	-	1.16 ± 0.28	0.85 ± 0.10	-	0.73 ± 0.11
$t\bar{t}+V$ NF	1.11 ± 0.35	1.13 ± 0.32	-	-	-	-	-
Single top NF	0.64 ± 0.37	1.19 ± 0.37	-	-	-	-	-
W+jets NF	0.82 ± 0.17	0.85 ± 0.18	-	-	-	-	1.19 ± 0.26
p_0 (σ)	0.05 (1.6)	0.07 (1.4)	0.44 (0.14)	0.5 (0)	0.33 (0.46)	0.5 (0)	0.17 (0.95)
$N^{\text{limit}}_{\text{non-SM}}$ exp.	5.8	19	11	58	19	33	21
$N^{\text{limit}}_{\text{non-SM}}$ obs.	10	31	11	58	17	31	28

Table 24: The numbers of observed events in DM+$t\bar{t}$, wino NLSP, bCbv, and higgsino LSP SRs together with the expected numbers of background events and their uncertainties as predicted by the background-only fits, the normalisation factors (NF) for the background predictions obtained in the fit, the probabilities (represented by p_0 values, and capped at 0.5) that the observed numbers of events are compatible with the background-only hypothesis, and the expected ($N^{\text{limit}}_{\text{non-SM}}$ exp.) and observed ($N^{\text{limit}}_{\text{non-SM}}$ obs.) 95% CL upper limits on the number of beyond-SM events. Some of the SRs where $t\bar{t}$ background events are predominantly semileptonic or dileptonic have only one NF which is also applied to the subdominant $t\bar{t}$ contribution.

Signal region	DM_high	DM_low	DM_low_loose	bC2x_diag	bC2x_med	bCbv	bCsoft_diag	bCsoft_med	bCsoft_high
Observed	5	13	65	22	4	25	33	19	2
Total background	7.4 ± 2.1	13.8 ± 3.6	48.3 ± 8.2	21.3 ± 5.0	5.8 ± 1.6	25.1 ± 3.8	24.7 ± 3.1	13.7 ± 2.1	1.8 ± 0.3
$t\bar{t}$ 2ℓ	0.82 ± 0.27	2.21 ± 0.58	16.0 ± 5.7	6.4 ± 2.4	1.36 ± 0.49	1.25 ± 0.65	10.3 ± 2.4	4.9 ± 1.5	0.36 ± 0.15
$t\bar{t}$ 1ℓ	0.0 ± 0.0	0.07 ± 0.03	-	0.28 ± 0.18	$0.04^{+0.13}_{-0.04}$	-	-	-	-
$t\bar{t}+V$	4.0 ± 2.0	6.7 ± 3.2	14.3 ± 5.9	7.8 ± 3.3	0.71 ± 0.38	0.58 ± 0.16	0.14 ± 0.06	0.44 ± 0.10	0.05 ± 0.02
Single top	0.33 ± 0.16	0.65 ± 0.57	3.4 ± 1.3	5.5 ± 2.4	3.0 ± 1.5	0.60 ± 0.54	3.5 ± 1.5	1.6 ± 0.5	0.23 ± 0.11
W+jets	1.64 ± 0.53	3.2 ± 1.3	11.0 ± 2.8	1.22 ± 0.35	0.54 ± 0.14	16.5 ± 3.1	8.0 ± 2.0	6.4 ± 2.0	1.06 ± 0.24
Diboson	0.66 ± 0.21	0.98 ± 0.33	3.6 ± 1.3	0.23 ± 0.08	0.07 ± 0.04	6.1 ± 2.0	2.21 ± 0.93	0.31 ± 0.16	0.04 ± 0.01
Z+jets	-	-	-	-	-	-	0.60 ± 0.55	0.17 ± 0.16	0.04 ± 0.04
$t\bar{t}$ 2ℓ NF	1.19 ± 0.13	1.06 ± 0.12	1.13 ± 0.21	1.28 ± 0.17	1.58 ± 0.22	0.78 ± 0.28	-	-	-
$t\bar{t}$ 1ℓ NF	1.08 ± 0.14	0.95 ± 0.04	-	0.96 ± 0.08	0.75 ± 0.15	-	0.73 ± 0.11	0.92 ± 0.07	0.93 ± 0.16
$t\bar{t}+V$ NF	0.98 ± 0.38	1.06 ± 0.38	1.10 ± 0.32	1.18 ± 0.39	0.95 ± 0.52	-	-	-	-
Single top NF	0.94 ± 0.37	1.05 ± 0.35	1.22 ± 0.27	1.59 ± 0.45	1.17 ± 0.37	-	-	0.47 ± 0.14	0.37 ± 0.15
W+jets NF	1.08 ± 0.21	1.04 ± 0.18	0.93 ± 0.10	0.80 ± 0.24	1.11 ± 0.25	1.07 ± 0.09	1.19 ± 0.26	1.35 ± 0.24	1.11 ± 0.19
p_0 (σ)	0.5 (-)	0.5 (-)	0.07 (1.5)	0.45 (0.11)	0.5 (-)	0.5 (-)	0.09 (1.34)	0.12 (1.17)	0.44 (0.16)
$N^{\text{limit}}_{\text{non-SM}}$ exp.	7.2	11	23	14	6.4	13	13	9.6	4.1
$N^{\text{limit}}_{\text{non-SM}}$ obs.	5.7	10	37	14	5.2	13	20	14	4.3

Table 25: The numbers of observed events in each bin of the shape-fit SRs together with the expected numbers of total background events and their uncertainties as predicted by the background-only fits. The bin i (i = 1–5) corresponds to the i-th bin (from left to right) of the variable used in the shape-fit. The bin boundaries of the shape-fits are detailed in Table 6, 7, 8, and 10.

Signal region	Fitted variable		bin1	bin2	bin3	bin4	bin5
tN_med	$E_{\mathrm{T}}^{\mathrm{miss}}$	Observed	21	17	8	4	–
		Total background	14.6 ± 2.8	11.2 ± 2.2	7.3 ± 1.7	3.16 ± 0.74	–
tN_diag_high	BDT_high	Observed	40	41	19	–	–
		Total background	47.3 ± 3.6	37.5 ± 3.5	18.3 ± 2.2	–	–
tN_diag_med	BDT_med	Observed	970	678	366	211	40
		Total background	886 ± 83	618 ± 86	440 ± 71	210 ± 30	51 ± 10
bWN	am_{T2}	Observed	13	19	22	30	36
		Total background	16.5 ± 4.5	16.0 ± 6.0	25.6 ± 5.3	40.1 ± 8.1	38.5 ± 8.3
bffN	$p_{\mathrm{T}}^{\ell}/E_{\mathrm{T}}^{\mathrm{miss}}$	Observed	9	27	34	–	–
		Total background	4.6 ± 1.1	22.9 ± 3.1	32.5 ± 4.1	–	–
bCsoft_diag	$p_{\mathrm{T}}^{\ell}/E_{\mathrm{T}}^{\mathrm{miss}}$	Observed	4	16	13	–	–
		Total background	1.69 ± 0.47	9.3 ± 2.1	13.6 ± 2.8	–	–
bCsoft_med	$p_{\mathrm{T}}^{\ell}/E_{\mathrm{T}}^{\mathrm{miss}}$	Observed	4	15	57	–	–
		Total background	4.92 ± 0.90	8.9 ± 1.3	52.9 ± 6.2	–	–
bCsoft_high	$p_{\mathrm{T}}^{\ell}/E_{\mathrm{T}}^{\mathrm{miss}}$	Observed	1	1	15	–	–
		Total background	0.67 ± 0.13	1.11 ± 0.22	6.98 ± 0.81	–	–

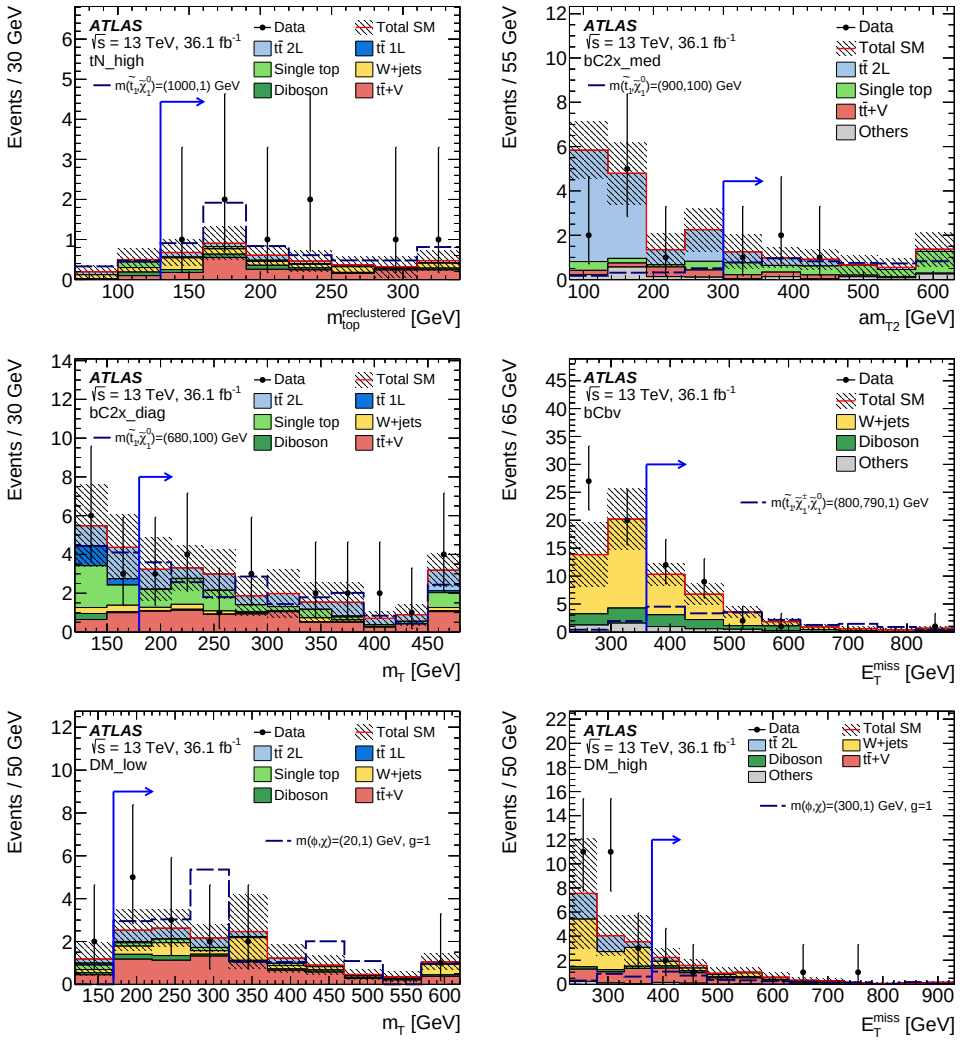

Figure 17: Kinematic distributions in the signal regions: (top left) $m_{\text{top}}^{\text{reclustered}}$ in `tN_high`, (top right) am_{T2} in `bC2x_med`, (middle left) m_{T} in `bC2x_diag`, (middle right) $E_{\text{T}}^{\text{miss}}$ in `bCbv`, (bottom left) m_{T} in `DM_low`, and (bottom right) $E_{\text{T}}^{\text{miss}}$ in `DM_high`. The full event selection in the corresponding signal region is applied, except for the requirement (indicated by an arrow) that is imposed on the variable being plotted. The predicted SM backgrounds are scaled with the normalisation factors obtained from the corresponding control regions in Tables 23 and 24. In addition to the background prediction, a signal model is shown on each plot. In the DM+$t\bar{t}$ signal model, a coupling of $g = 1$ is assumed. The category labelled 'Others' stands for minor SM backgrounds that contribute less than 5% of the total SM background. The hatched area around the total SM prediction includes statistical and experimental uncertainties. The last bin contains overflows.

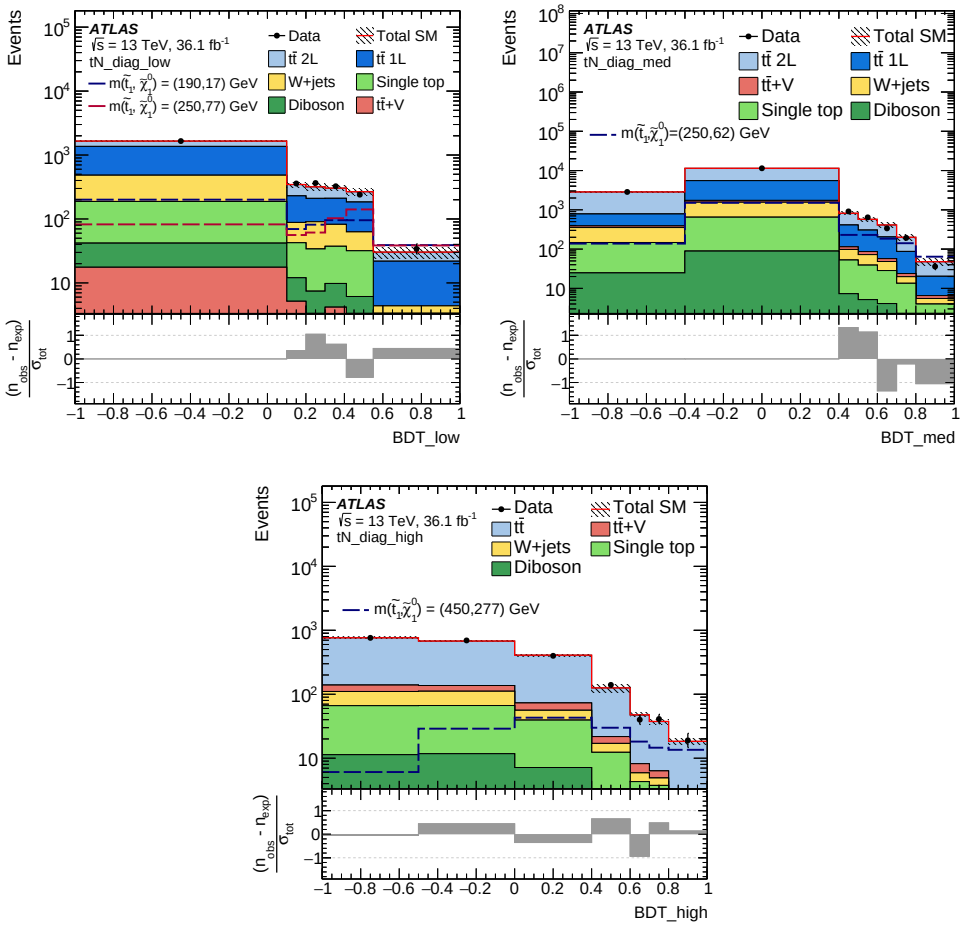

Figure 18: Distributions of BDT score for the `tN_diag_low` (top left), `tN_diag_med` (top right), and `tN_diag_high` (bottom) regions. The SM background predictions are obtained using the background-only fit configuration, and the hatched area around the total SM background prediction includes all uncertainties. In addition to the background prediction, signal models are shown, denoted by $m(\tilde{t}_1, \tilde{\chi}_1^0)$. The bottom panels show the difference between data and the predicted SM background divided by the total uncertainty (σ_{tot}).

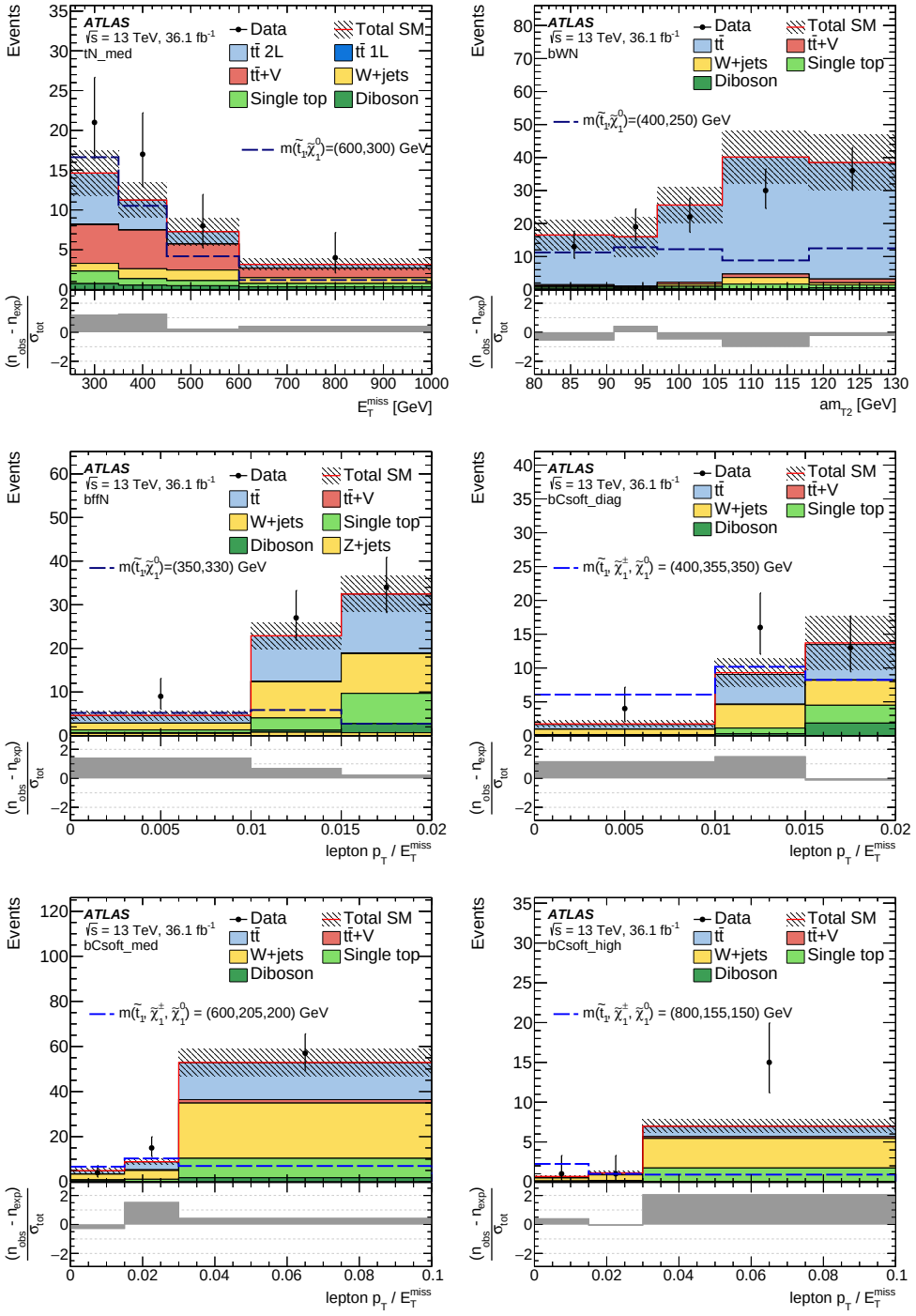

Figure 19: Kinematic distributions for the shape-fit analyses: (top left) $E_{\mathrm{T}}^{\mathrm{miss}}$ in `tN_med`, (top right) am_{T2} in `bWN`, (middle left) $p_{\mathrm{T}}^{\ell}/E_{\mathrm{T}}^{\mathrm{miss}}$ in `bffN`, (middle right) $p_{\mathrm{T}}^{\ell}/E_{\mathrm{T}}^{\mathrm{miss}}$ in `bCsoft_diag`, (bottom left) $p_{\mathrm{T}}^{\ell}/E_{\mathrm{T}}^{\mathrm{miss}}$ in `bCsoft_med`, and (bottom right) $p_{\mathrm{T}}^{\ell}/E_{\mathrm{T}}^{\mathrm{miss}}$ in `bCsoft_high`. The full event selection in the corresponding signal region is applied, except for the requirement that is imposed on the variable being plotted. The predicted SM backgrounds are scaled with the normalisation factors obtained from the corresponding control regions in Tables 23 and 24. The hatched area around the total SM prediction includes statistical and experimental uncertainties. The last bin contains overflows. Benchmark signal models are overlaid for comparison. The bottom panels show the difference between data and the predicted SM background divided by the total uncertainty (σ_{tot}).

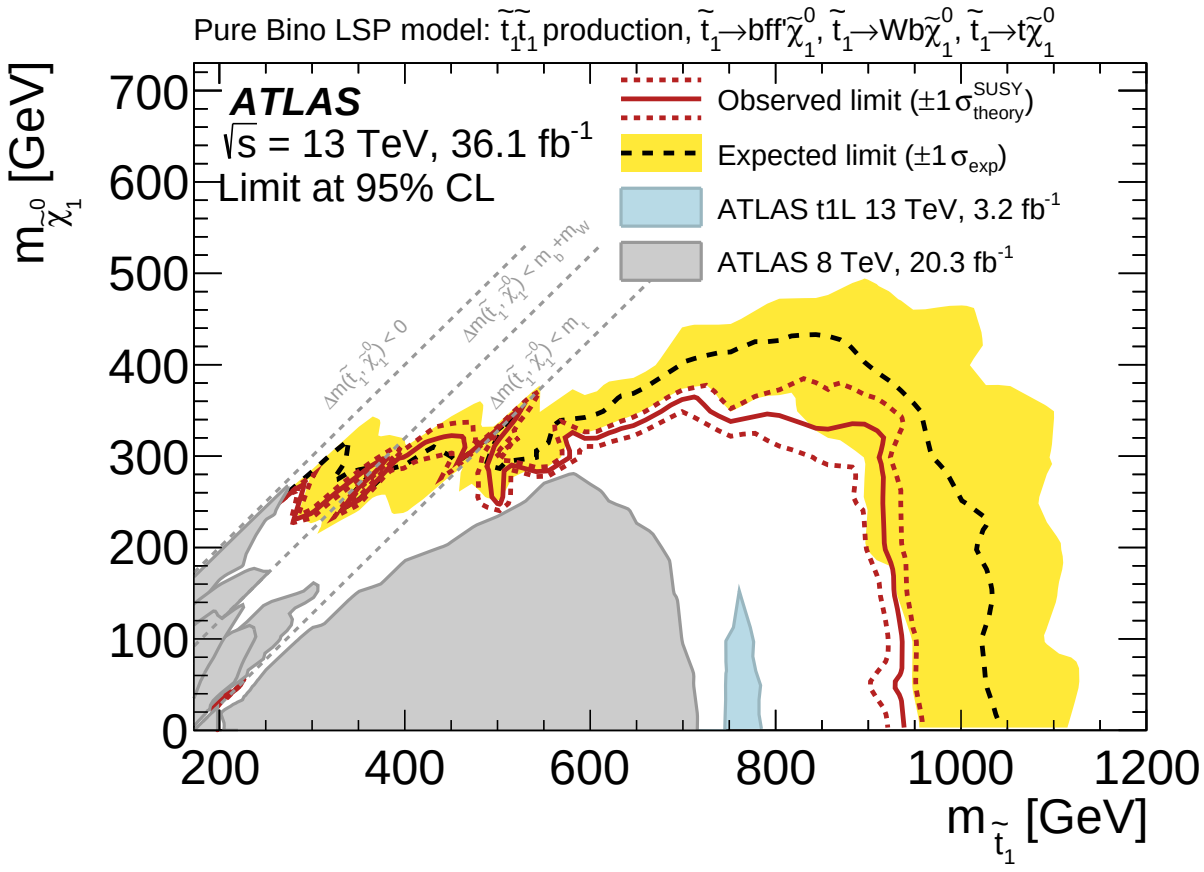

Figure 20: Expected (black dashed) and observed (red solid) 95% excluded regions in the plane of $m_{\tilde{\chi}_1^0}$ versus $m_{\tilde{t}_1}$ for direct stop pair production assuming either $\tilde{t}_1 \to t\tilde{\chi}_1^0$, $\tilde{t}_1 \to bW\tilde{\chi}_1^0$, or $\tilde{t}_1 \to bff'\tilde{\chi}_1^0$ decay with a branching ratio of 100%. The excluded regions from previous publications [37, 158] are shown with the grey and blue shaded areas.

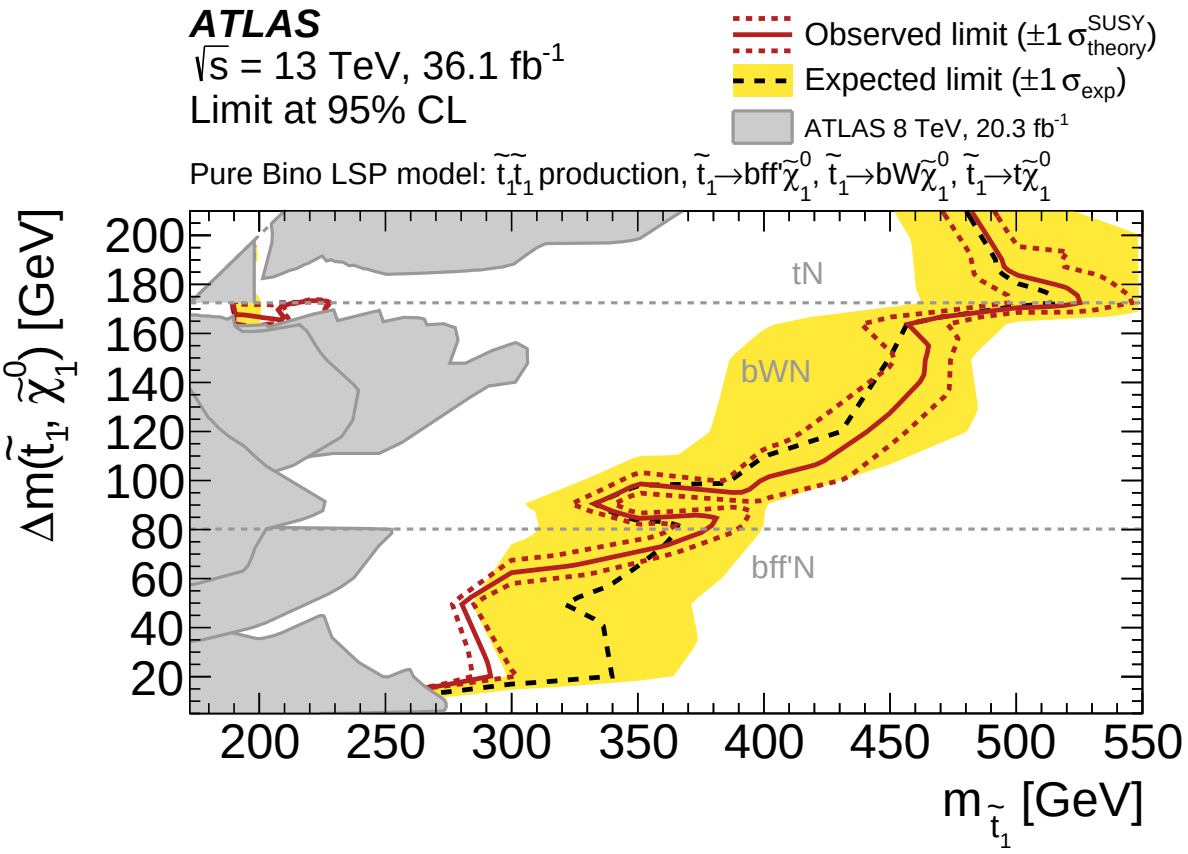

Figure 21: Expected (black dashed) and observed (red solid) 95% excluded regions in the plane of $\Delta m(\tilde{t}_1, \tilde{\chi}_1^0)$ versus $m_{\tilde{t}_1}$ for direct stop pair production assuming either $\tilde{t}_1 \to t\tilde{\chi}_1^0$, $\tilde{t}_1 \to bW\tilde{\chi}_1^0$, or $\tilde{t}_1 \to bff'\tilde{\chi}_1^0$ decay with a branching ratio of 100%. The excluded regions from previous publications [37, 158] are shown with the grey shaded area.

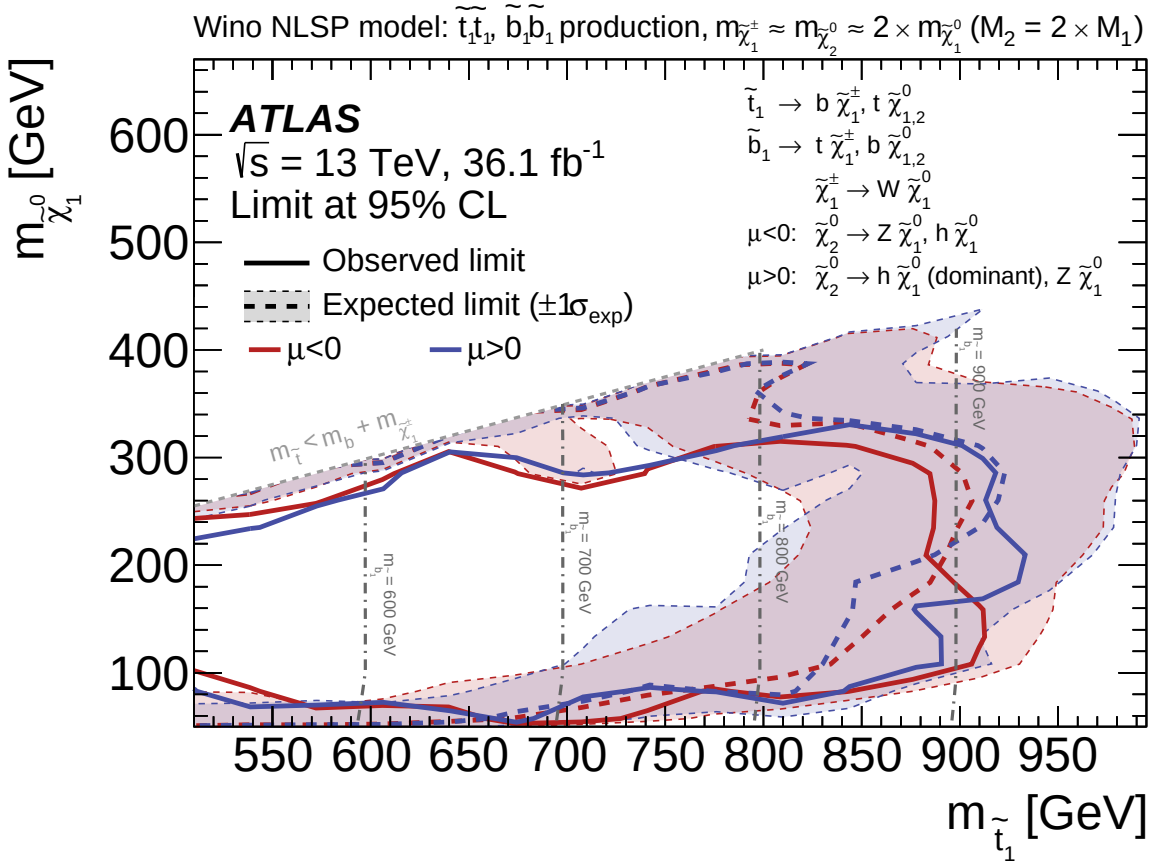

Figure 22: Expected (dashed) and observed (solid) 95% excluded regions in the plane of $m_{\tilde{\chi}_1^0}$ versus $m_{\tilde{t}_1}$ for direct stop/sbottom pair production in the wino NLSP model under the hypothesis of $m_{q^3L} < m_{tR}$, where various decay modes ($\tilde{t}_1 \rightarrow b\tilde{\chi}_1^\pm$, $\tilde{t}_1 \rightarrow t\tilde{\chi}_1^0$, $\tilde{t}_1 \rightarrow t\tilde{\chi}_2^0$, $\tilde{b}_1 \rightarrow t\tilde{\chi}_1^\pm$, $\tilde{b}_1 \rightarrow b\tilde{\chi}_1^0$, and $\tilde{b}_1 \rightarrow b\tilde{\chi}_2^0$) are considered with different branching ratios for each signal point. The $\tilde{\chi}_2^0$ decays into $\tilde{\chi}_1^0$ predominantly via either a Z boson or a Higgs boson depending on the sign of the μ parameter. Contours for the $\mu > 0$ and $\mu < 0$ hypotheses are shown as blue and red lines, respectively. In this model, the $\tilde{\chi}_1^\pm$ and $\tilde{\chi}_2^0$ masses are assumed to be nearly twice as large as the LSP ($\tilde{\chi}_1^0$) mass. The grey vertical dash-dotted lines show the corresponding sbottom mass. The dashed line $m_{\tilde{t}_1} = m_b + m_{\tilde{\chi}_1^\pm}$ is a physical boundary of the $\tilde{t}_1 \rightarrow b\tilde{\chi}_1^\pm$ decay.

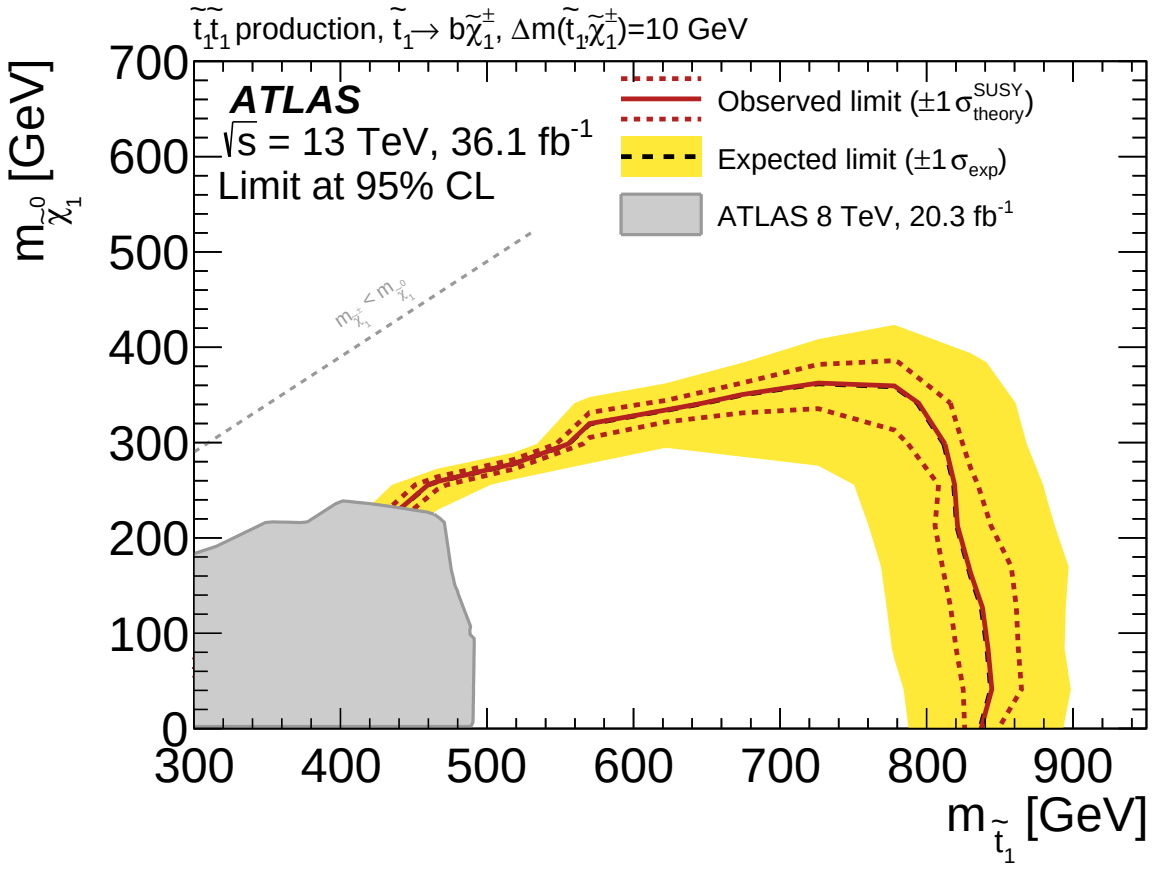

Figure 23: Expected (black dashed) and observed (red solid) 95% excluded regions in the plane of $m_{\tilde{\chi}_1^0}$ versus $m_{\tilde{t}_1}$ for direct stop pair production assuming the $b\tilde{\chi}_1^{\pm}$ decay with a branching ratio of 100%. The chargino mass is assumed to be close to the stop mass, $m_{\tilde{\chi}_1^{\pm}} = m_{\tilde{t}_1} - 10\,\text{GeV}$.

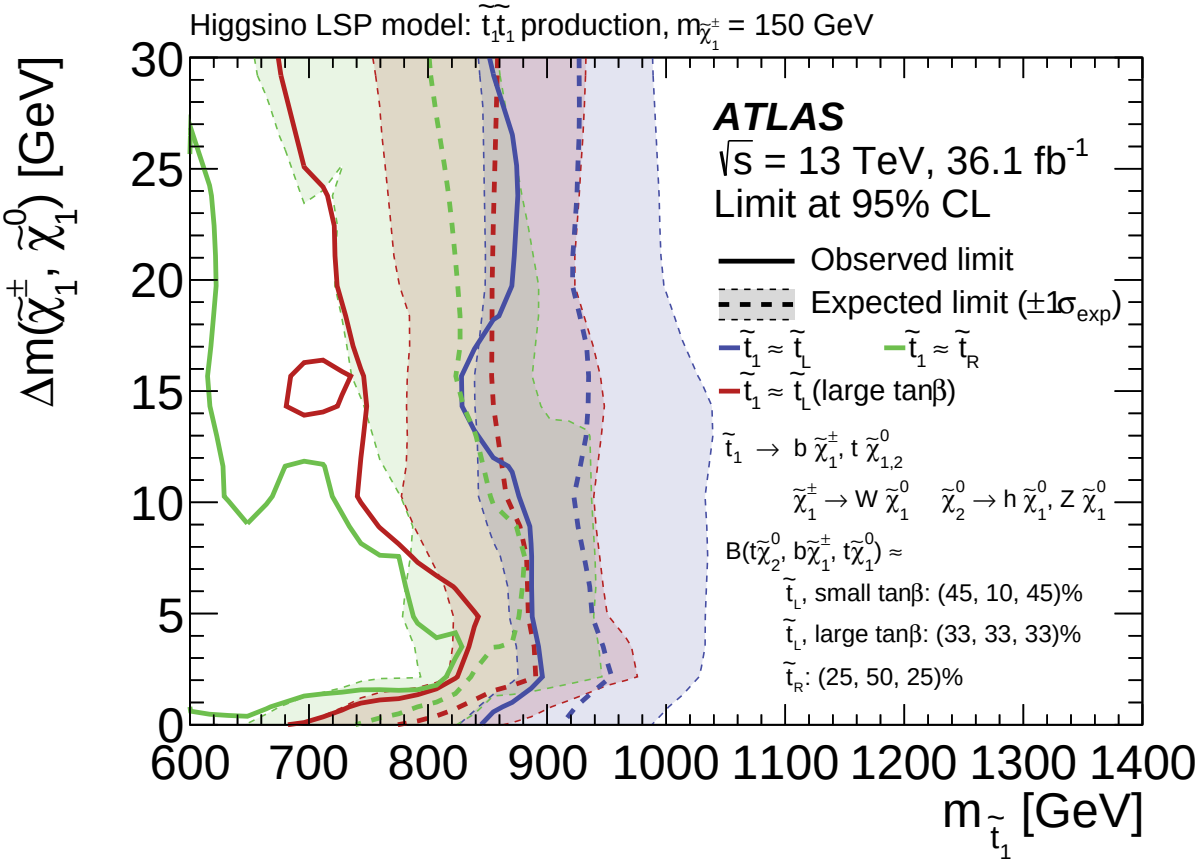

Figure 24: Expected (dashed) and observed (solid) 95% excluded regions in the plane of $\Delta m\,(\tilde{\chi}_1^\pm, \tilde{\chi}_1^0)$ versus $m_{\tilde{t}_1}$ for direct stop pair production in the fixed $m_{\tilde{\chi}_1^\pm} = 150$ GeV higgsino LSP model where various decay modes ($\tilde{t}_1 \rightarrow b\tilde{\chi}_1^\pm$, $\tilde{t}_1 \rightarrow t\tilde{\chi}_1^0$, $\tilde{t}_1 \rightarrow t\tilde{\chi}_2^0$) are considered with different branching ratios, depending on the hypothesis being considered, and overlaid. In this model, the mass relation of $\Delta m(\tilde{\chi}_2^0, \tilde{\chi}_1^0) = 2 \times \Delta m(\tilde{\chi}_1^\pm, \tilde{\chi}_1^0)$ is assumed, varying $\Delta m(\tilde{\chi}_1^\pm, \tilde{\chi}_1^0)$ from 0 GeV to 30 GeV. For the region $\Delta m(\tilde{\chi}_1^\pm, \tilde{\chi}_1^0) < 2$ GeV, only the $\tilde{t}_1 \rightarrow t\tilde{\chi}_1^0$ decay is considered while the branching ratio is set to account for both the $\tilde{t}_1 \rightarrow t\tilde{\chi}_1^0$ and $\tilde{t}_1 \rightarrow t\tilde{\chi}_2^0$ decays.

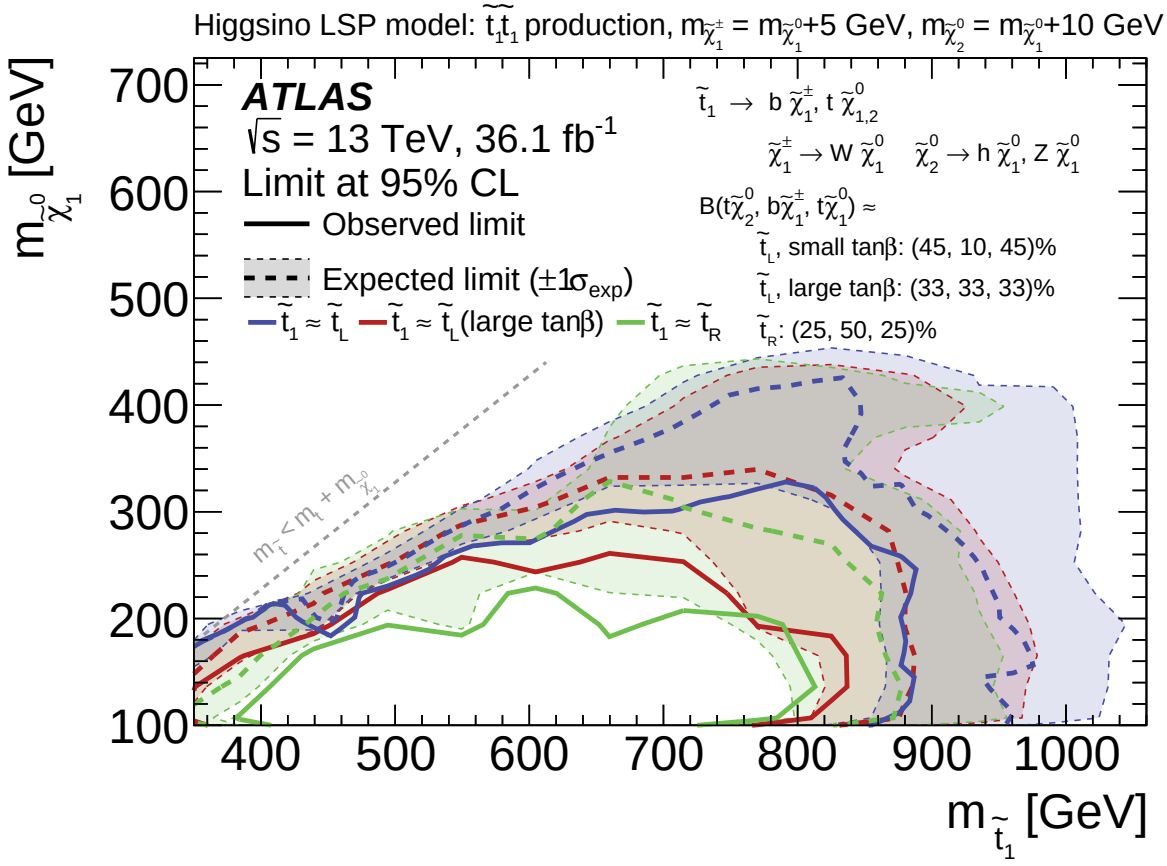

Figure 25: Expected (dashed) and observed (solid) 95% excluded regions in the plane of $m_{\tilde{\chi}_1^0}$ versus $m_{\tilde{t}_1}$ for direct stop pair production in the higgsino LSP model where various decay modes ($\tilde{t}_1 \rightarrow b\tilde{\chi}_1^\pm$, $\tilde{t}_1 \rightarrow t\tilde{\chi}_1^0$, $\tilde{t}_1 \rightarrow t\tilde{\chi}_2^0$) are considered with different branching ratios depending on the hypothesis being considered. In this model, $\Delta m(\tilde{\chi}_1^\pm, \tilde{\chi}_1^0) = 5$ GeV and $\Delta m(\tilde{\chi}_2^0, \tilde{\chi}_1^0) = 10$ GeV are assumed.

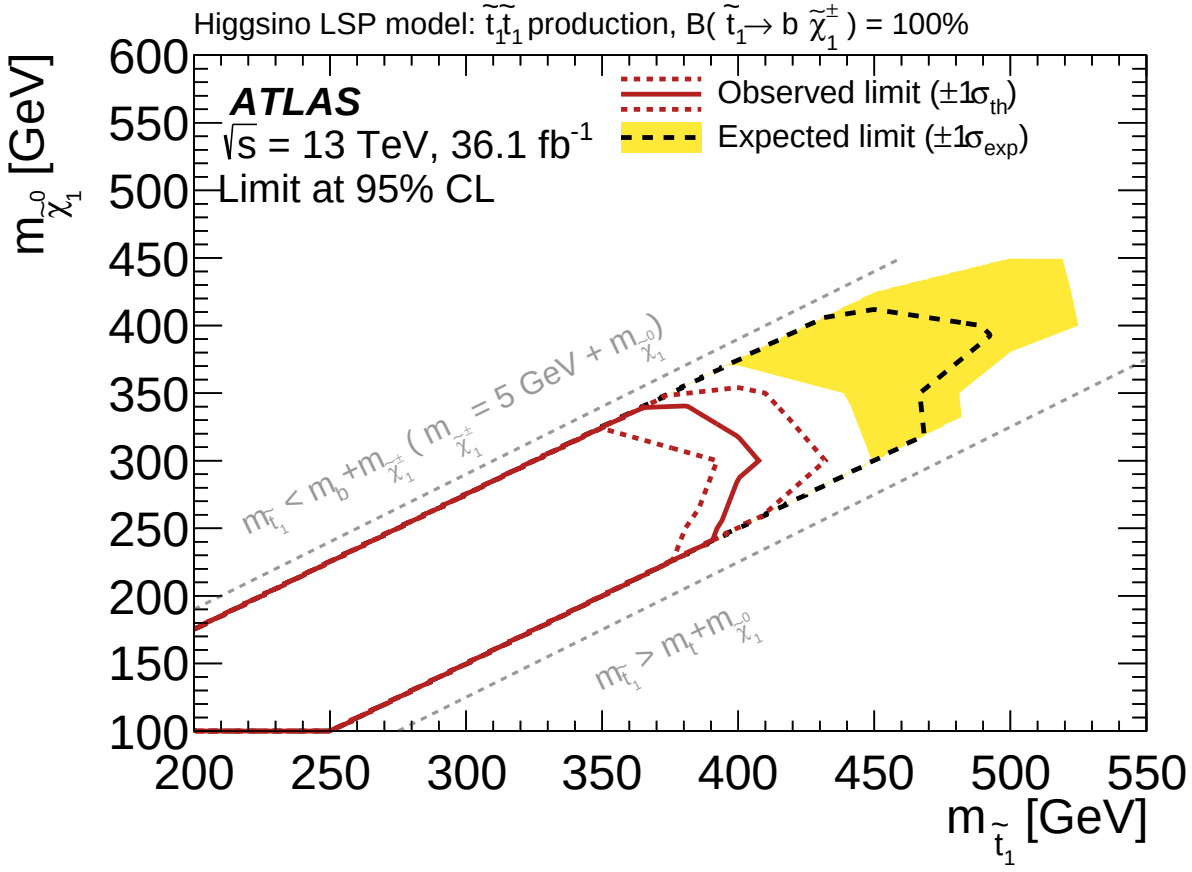

Figure 26: Expected (black dashed) and observed (red solid) 95% excluded regions in the plane of $m_{\tilde{\chi}_1^0}$ versus $m_{\tilde{t}_1}$ for direct stop pair production in the higgsino LSP model where only the $\tilde{t}_1 \rightarrow b\tilde{\chi}_1^{\pm}$ decay mode is kinematically allowed due to the phase space constraint. In this model, $\Delta m(\tilde{\chi}_1^{\pm}, \tilde{\chi}_1^0) = 5$ GeV is assumed.

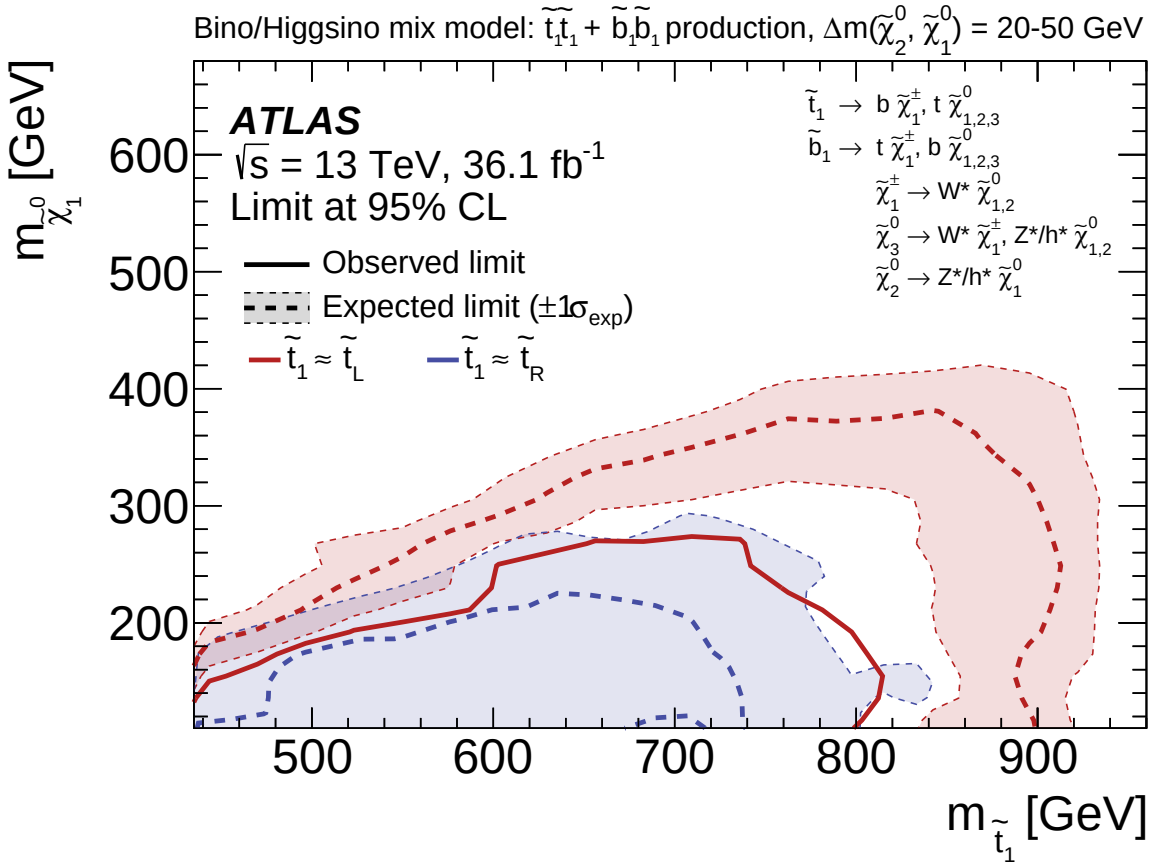

Figure 27: Expected (dashed) and observed (solid) 95% excluded regions in the plane of $m_{\tilde{\chi}^0_1}$ versus $m_{\tilde{t}_1}$ for direct stop/sbottom pair production in the well-tempered neutralino model where various decay modes ($\tilde{t}_1 \rightarrow b\tilde{\chi}^{\pm}_1$, $\tilde{t}_1 \rightarrow t\tilde{\chi}^0_1$, $\tilde{t}_1 \rightarrow t\tilde{\chi}^0_2$, $\tilde{b}_1 \rightarrow t\tilde{\chi}^{\pm}_1$, $\tilde{b}_1 \rightarrow b\tilde{\chi}^0_1$, and $\tilde{b}_1 \rightarrow b\tilde{\chi}^0_2$) are considered with different branching ratios for each signal point. Contours for the $m_{q3L} < m_{tR}$ and $m_{q3L} > m_{tR}$ hypotheses are shown separately as red and blue lines, respectively. For the $m_{q3L} < m_{tR}$ hypothesis, both stop and sbottom pair production is considered while for the $m_{q3L} > m_{tR}$ hypothesis, only stop pair production is considered.

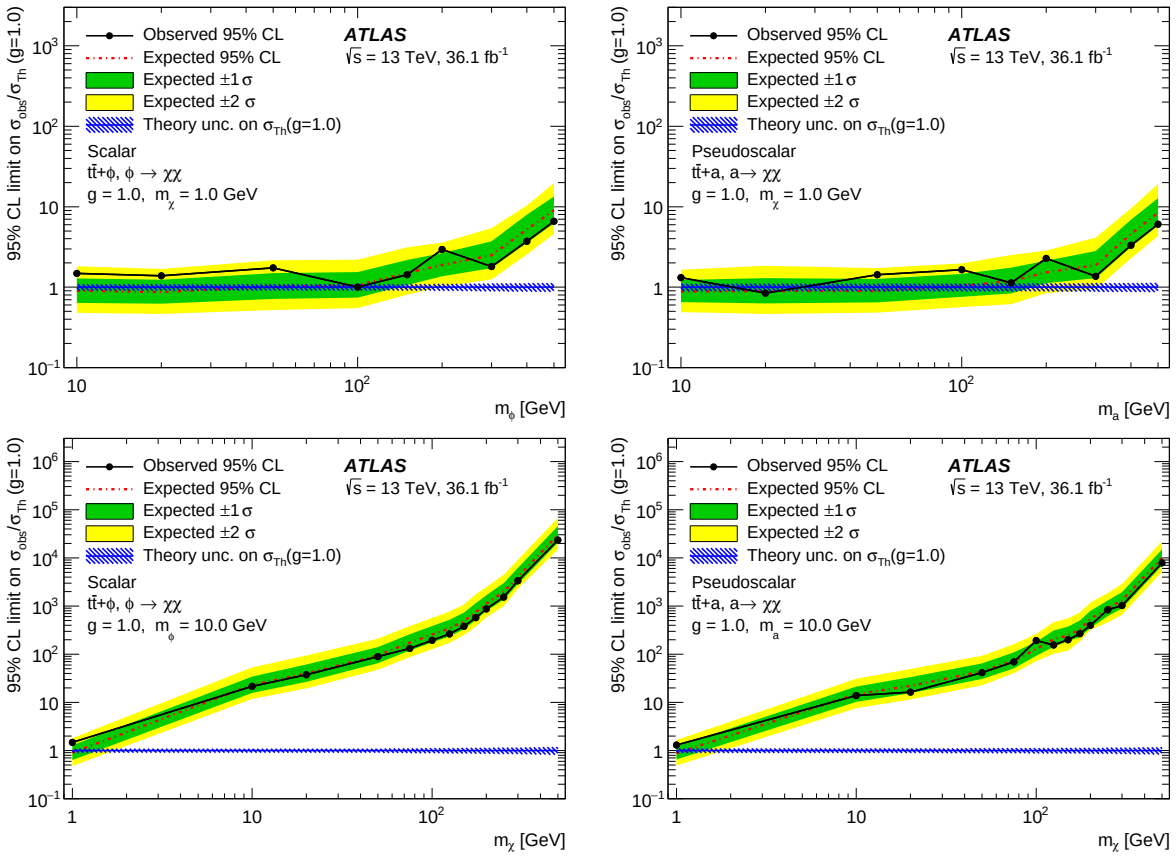

Figure 28: Upper limit on the ratio of the DM production cross-section to the simplified model expectation under the hypothesis of (left) a scalar or (right) a pseudoscalar mediator. The limit is shown as a function of: (top) the mediator mass for a fixed mass of the DM candidate of 1 GeV, or (bottom) the DM candidate mass for a fixed mediator mass of 10 GeV. The coupling of the mediator to SM and DM particles is assumed to be $g = 1$.

11 Summary and conclusions

This paper presents searches for direct top-squark pair production covering various SUSY scenarios and for a spin-0 mediator decaying into pair-produced dark-matter particles produced in association with $t\bar{t}$ using the final state with one isolated lepton, jets, and $E_{\mathrm{T}}^{\mathrm{miss}}$. Thirteen signal-region selections are optimised for the discovery of a top-squark signature. The analysis also defines three signal-region selections for spin-0 mediator models.

The search uses 36.1 fb^{-1} of pp collision data collected by the ATLAS experiment at the LHC at a centre-of-mass energy of $\sqrt{s} = 13$ TeV. No significant excess is observed over the estimated Standard Model backgrounds. Exclusion limits at 95% confidence level are derived for the considered models.

These results improve upon previous exclusion limits by excluding the top-squark mass region up to 940 GeV for a massless lightest neutralino and assuming a 100% branching ratio for $\tilde{t}_1 \to t\tilde{\chi}_1^0$. Exclusion limits are also improved in pMSSM models targeting various sparticle mass spectra. For the wino NLSP model, the top-squark mass region up to 885 GeV (940 GeV) is excluded in scenarios with $\mu < 0$ ($\mu > 0$) and a 200 GeV neutralino. For the higgsino LSP model, the top-squark mass region up to 860 GeV (800 GeV) is excluded in scenarios with $m_{q3L} < m_{tR}$ ($m_{tR} < m_{q3L}$). Furthermore, in a model with well-tempered neutralinos, the top-squark mass region up to 810 GeV is excluded in scenarios with $m_{q3L} < m_{tR}$ while no limit is set in scenarios with $m_{tR} < m_{q3L}$.

For the spin-0 mediator models, a scalar (pseudoscalar) mediator mass of around 100 GeV (20 GeV) is excluded at 95% confidence level, assuming a 1 GeV dark-matter particle mass and a common coupling to SM and dark-matter particles of $g = 1$.

Acknowledgements

We thank CERN for the very successful operation of the LHC, as well as the support staff from our institutions without whom ATLAS could not be operated efficiently.

We acknowledge the support of ANPCyT, Argentina; YerPhI, Armenia; ARC, Australia; BMWFW and FWF, Austria; ANAS, Azerbaijan; SSTC, Belarus; CNPq and FAPESP, Brazil; NSERC, NRC and CFI, Canada; CERN; CONICYT, Chile; CAS, MOST and NSFC, China; COLCIENCIAS, Colombia; MSMT CR, MPO CR and VSC CR, Czech Republic; DNRF and DNSRC, Denmark; IN2P3-CNRS, CEA-DRF/IRFU, France; SRNSF, Georgia; BMBF, HGF, and MPG, Germany; GSRT, Greece; RGC, Hong Kong SAR, China; ISF, I-CORE and Benoziyo Center, Israel; INFN, Italy; MEXT and JSPS, Japan; CNRST, Morocco; NWO, Netherlands; RCN, Norway; MNiSW and NCN, Poland; FCT, Portugal; MNE/IFA, Romania; MES of Russia and NRC KI, Russian Federation; JINR; MESTD, Serbia; MSSR, Slovakia; ARRS and MIZŠ, Slovenia; DST/NRF, South Africa; MINECO, Spain; SRC and Wallenberg Foundation, Sweden; SERI, SNSF and Cantons of Bern and Geneva, Switzerland; MOST, Taiwan; TAEK, Turkey; STFC, United Kingdom; DOE and NSF, United States of America. In addition, individual groups and members have received support from BCKDF, the Canada Council, CANARIE, CRC, Compute Canada, FQRNT, and the Ontario Innovation Trust, Canada; EPLANET, ERC, ERDF, FP7, Horizon 2020 and Marie Skłodowska-Curie Actions, European Union; Investissements d'Avenir Labex and Idex, ANR, Région Auvergne and Fondation Partager le Savoir, France; DFG and AvH Foundation, Germany; Herakleitos, Thales and Aristeia programmes co-financed by EU-ESF and the Greek NSRF; BSF, GIF and

Minerva, Israel; BRF, Norway; CERCA Programme Generalitat de Catalunya, Generalitat Valenciana, Spain; the Royal Society and Leverhulme Trust, United Kingdom.

The crucial computing support from all WLCG partners is acknowledged gratefully, in particular from CERN, the ATLAS Tier-1 facilities at TRIUMF (Canada), NDGF (Denmark, Norway, Sweden), CC-IN2P3 (France), KIT/GridKA (Germany), INFN-CNAF (Italy), NL-T1 (Netherlands), PIC (Spain), ASGC (Taiwan), RAL (UK) and BNL (USA), the Tier-2 facilities worldwide and large non-WLCG resource providers. Major contributors of computing resources are listed in Ref. [168].

References

[1] S. Weinberg, *Implications of Dynamical Symmetry Breaking*, Phys. Rev. D **13** (1976) 974.

[2] E. Gildener, *Gauge Symmetry Hierarchies*, Phys. Rev. D **14** (1976) 1667.

[3] S. Weinberg, *Implications of Dynamical Symmetry Breaking: An Addendum*, Phys. Rev. D **19** (1979) 1277.

[4] L. Susskind, *Dynamics of Spontaneous Symmetry Breaking in the Weinberg-Salam Theory*, Phys. Rev. D **20** (1979) 2619.

[5] ATLAS Collaboration, *Observation of a new particle in the search for the Standard Model Higgs boson with the ATLAS detector at the LHC*, Phys. Lett. B **716** (2012) 1, arXiv: 1207.7214 [hep-ex].

[6] CMS Collaboration, *Observation of a new boson at a mass of 125 GeV with the CMS experiment at the LHC*, Phys. Lett. B **716** (2012) 30, arXiv: 1207.7235 [hep-ex].

[7] L. Evans and P. Bryant, *LHC Machine*, JINST **3** (2008) S08001.

[8] H. Miyazawa, *Baryon Number Changing Currents*, Prog. Theor. Phys. **36** (1966) 1266.

[9] R. Ramond, *Dual Theory for Free Fermions*, Phys. Rev. D **3** (1971) 2415.

[10] Yu. A. Golfand and E. P. Likhtman, *Extension of the Algebra of Poincare Group Generators and Violation of p Invariance*, JETP Lett. **13** (1971) 323, [Pisma Zh. Eksp. Teor. Fiz. 13 (1971) 452].

[11] A. Neveu and J. Schwarz, *Factorizable dual model of pions*, Nucl. Phys. B **31** (1971) 86.

[12] A. Neveu and J. Schwarz, *Quark Model of Dual Pions*, Phys. Rev. D **4** (1971) 1109.

[13] J. Gervais and B. Sakita, *Field theory interpretation of supergauges in dual models*, Nucl. Phys. B **34** (1971) 632.

[14] D. V. Volkov and V. P. Akulov, *Is the Neutrino a Goldstone Particle?*, Phys. Lett. B **46** (1973) 109.

[15] J. Wess and B. Zumino, *A Lagrangian Model Invariant Under Supergauge Transformations*, Phys. Lett. B **49** (1974) 52.

[16] J. Wess and B. Zumino, *Supergauge Transformations in Four-Dimensions*, Nucl. Phys. B **70** (1974) 39.

[17] S. Dimopoulos and H. Georgi, *Softly Broken Supersymmetry and SU(5)*, Nucl. Phys. B **193** (1981) 150.

[18] E. Witten, *Dynamical Breaking of Supersymmetry*, Nucl. Phys. B **188** (1981) 513.

[19] M. Dine, W. Fischler and M. Srednicki, *Supersymmetric Technicolor*, Nucl. Phys. B **189** (1981) 575.

[20] S. Dimopoulos and S. Raby, *Supercolor*, Nucl. Phys. B **192** (1981) 353.

[21] N. Sakai, *Naturalness in Supersymmetric Guts*, Z. Phys. C **11** (1981) 153.

[22] R. Kaul and P. Majumdar, *Cancellation of Quadratically Divergent Mass Corrections in Globally Supersymmetric Spontaneously Broken Gauge Theories*, Nucl. Phys. B **199** (1982) 36.

[23] R. Barbieri and G. F. Giudice, *Upper Bounds on Supersymmetric Particle Masses*, Nucl. Phys. B **306** (1988) 63.

[24] B. de Carlos and J. A. Casas, *One loop analysis of the electroweak breaking in supersymmetric models and the fine tuning problem*, Phys. Lett. B **309** (1993) 320, arXiv: hep-ph/9303291.

[25] K. Inoue, A. Kakuto, H. Komatsu and S. Takeshita, *Aspects of Grand Unified Models with Softly Broken Supersymmetry*, Prog. Theor. Phys. **68** (1982) 927, Erratum: Prog. Theor. Phys. 70 (1983) 330.

[26] J. R. Ellis and S. Rudaz, *Search for Supersymmetry in Toponium Decays*, Phys. Lett. B **128** (1983) 248.

[27] C. Regis et al., *Search for Proton Decay via $p \to \mu^+ K^0$ in Super-Kamiokande I, II, and III*, Phys. Rev. D **86** (2012) 012006, arXiv: 1205.6538 [hep-ex].

[28] P. Fayet, *Supersymmetry and Weak, Electromagnetic and Strong Interactions*, Phys. Lett. B **64** (1976) 159.

[29] P. Fayet, *Spontaneously Broken Supersymmetric Theories of Weak, Electromagnetic and Strong Interactions*, Phys. Lett. B **69** (1977) 489.

[30] G. R. Farrar and P. Fayet, *Phenomenology of the Production, Decay, and Detection of New Hadronic States Associated with Supersymmetry*, Phys. Lett. B **76** (1978) 575.

[31] P. Fayet, *Relations Between the Masses of the Superpartners of Leptons and Quarks, the Goldstino Couplings and the Neutral Currents*, Phys. Lett. B **84** (1979) 416.

[32] H. Goldberg, *Constraint on the Photino Mass from Cosmology*, Phys. Rev. Lett. **50** (1983) 1419, Erratum: Phys. Rev. Lett. 103 (2009) 099905.

[33] J. R. Ellis, J. S. Hagelin, D. V. Nanopoulos, K. A. Olive and M. Srednicki, *Supersymmetric Relics from the Big Bang*, Nucl. Phys. B **238** (1984) 453.

[34] ATLAS Collaboration, *Search for supersymmetry in events with b-tagged jets and missing transverse momentum in pp collisions at $\sqrt{s} = 13$ TeV with the ATLAS detector*, (2017), arXiv: 1708.09266 [hep-ex].

[35] ATLAS Collaboration, *Search for direct top squark pair production in final states with two leptons in $\sqrt{s} = 13$ TeV pp collisions with the ATLAS detector*, (2017), arXiv: 1708.03247 [hep-ex].

[36] ATLAS Collaboration, *Search for direct top squark pair production in events with a Higgs or Z boson, and missing transverse momentum in $\sqrt{s} = 13$ TeV pp collisions with the ATLAS detector*, JHEP **08** (2017) 006, arXiv: 1706.03986 [hep-ex].

[37] ATLAS Collaboration, *Search for top squarks in final states with one isolated lepton, jets, and missing transverse momentum in $\sqrt{s}$ = 13 TeV pp collisions with the ATLAS detector*, Phys. Rev. D **94** (2016) 052009, arXiv: 1606.03903 [hep-ex].

[38] ATLAS Collaboration, *ATLAS Run 1 searches for direct pair production of third-generation squarks at the Large Hadron Collider*, Eur. Phys. J. C **75** (2015) 510, arXiv: 1506.08616 [hep-ex].

[39] CMS Collaboration, *Searches for pair production of third-generation squarks in $\sqrt{s}$ = 13 TeV pp collisions*, Eur. Phys. J. C **77** (2017) 327, arXiv: 1612.03877 [hep-ex].

[40] CMS Collaboration, *A search for new phenomena in pp collisions at $\sqrt{s}$ = 13 TeV in final states with missing transverse momentum and at least one jet using the α_{T} variable*, Eur. Phys. J. C **77** (2017) 294, arXiv: 1611.00338 [hep-ex].

[41] CMS Collaboration, *Inclusive search for supersymmetry using razor variables in pp collisions at $\sqrt{s}$ = 13 TeV*, Phys. Rev. D **95** (2017) 012003, arXiv: 1609.07658 [hep-ex].

[42] CMS Collaboration, *Search for top squark pair production in compressed-mass-spectrum scenarios in proton–proton collisions at $\sqrt{s}$ = 8 TeV using the α_{T} variable*, Phys. Lett. B **767** (2017) 403, arXiv: 1605.08993 [hep-ex].

[43] CMS Collaboration, *Search for top-squark pairs decaying into Higgs or Z bosons in pp collisions at $\sqrt{s}$ = 8 TeV*, Phys. Lett. B **736** (2014) 371, arXiv: 1405.3886 [hep-ex].

[44] CMS Collaboration, *Search for top squark and higgsino production using diphoton Higgs boson decays*, Phys. Rev. Lett. **112** (2014) 161802, arXiv: 1312.3310 [hep-ex].

[45] CMS Collaboration, *Search for top-squark pair production in the single-lepton final state in pp collisions at $\sqrt{s}$ = 8 TeV*, Eur. Phys. J. C **73** (2013) 2677, arXiv: 1308.1586 [hep-ex].

[46] CMS Collaboration, *Search for supersymmetry in hadronic final states with missing transverse energy using the variables α_T and b-quark multiplicity in pp collisions at $\sqrt{s}$ = 8 TeV*, Eur. Phys. J. C **73** (2013) 2568, arXiv: 1303.2985 [hep-ex].

[47] CMS Collaboration, *Search for supersymmetry with razor variables in pp collisions at $\sqrt{s}$ = 7 TeV*, Phys. Rev. D **90** (2014) 112001, arXiv: 1405.3961 [hep-ex].

[48] CDF Collaboration, *Search for Pair Production of Supersymmetric Top Quarks in Dilepton Events from p anti-p Collisions at $\sqrt{s}$ = 1.96 TeV*, Phys. Rev. Lett. **104** (2010) 251801, arXiv: 0912.1308 [hep-ex].

[49] D0 Collaboration, *Search for the lightest scalar top quark in events with two leptons in $p\bar{p}$ collisions at $\sqrt{s}$ = 1.96 TeV*, Phys. Lett. B **675** (2009) 289, arXiv: 0811.0459 [hep-ex].

[50] LEP SUSY Working Group, ALEPH, DELPHI, L3 and OPAL experiments, LEPSUSYWG/04-02.1.

[51] ATLAS Collaboration, *Search for dark matter produced in association with bottom or top quarks in $\sqrt{s}$ = 13 TeV pp collisions with the ATLAS detector*, (2017), arXiv: 1710.11412 [hep-ex].

[52] CMS Collaboration, *Search for dark matter produced in association with heavy-flavor quark pairs in proton–proton collisions at* $\sqrt{s}$ = 13 *TeV*, (2017), arXiv: 1706.02581 [hep-ex].

[53] J. Alwall, M.-P. Le, M. Lisanti and J. G. Wacker, *Searching for Directly Decaying Gluinos at the Tevatron*, Phys. Lett. B **666** (2008) 34, arXiv: 0803.0019.

[54] J. Alwall, P. Schuster and N. Toro, *Simplified Models for a First Characterization of New Physics at the LHC*, Phys. Rev. D **79** (2009) 075020, arXiv: 0810.3921.

[55] D. Alves et al., *Simplified Models for LHC New Physics Searches*, J. Phys. G **39** (2012) 105005, arXiv: 1105.2838.

[56] A. Djouadi et al., *The Minimal supersymmetric standard model: Group summary report*, 1998, arXiv: hep-ph/9901246.

[57] C. F. Berger, J. S. Gainer, J. L. Hewett and T. G. Rizzo, *Supersymmetry Without Prejudice*, JHEP **02** (2009) 023, arXiv: 0812.0980.

[58] ATLAS Collaboration, *Search for charginos nearly mass degenerate with the lightest neutralino based on a disappearing-track signature in pp collisions at* $\sqrt{s}$ = 8 *TeV with the ATLAS detector*, Phys. Rev. D **88** (2013) 112006, arXiv: 1310.3675 [hep-ex].

[59] G. F. Giudice, M. A. Luty, H. Murayama and R. Rattazzi, *Gaugino mass without singlets*, JHEP **12** (1998) 027, arXiv: hep-ph/9810442.

[60] L. Randall and R. Sundrum, *Out of this world supersymmetry breaking*, Nucl. Phys. B **557** (1999) 79, arXiv: hep-th/9810155.

[61] M. Dine and W. Fischler, *A Phenomenological Model of Particle Physics Based on Supersymmetry*, Phys. Lett. B **110** (1982) 227.

[62] L. Alvarez-Gaume, M. Claudson and M. B. Wise, *Low-Energy Supersymmetry*, Nucl. Phys. B **207** (1982) 96.

[63] C. R. Nappi and B. A. Ovrut, *Supersymmetric Extension of the SU(3) x SU(2) x U(1) Model*, Phys. Lett. B **113** (1982) 175.

[64] A. H. Chamseddine, R. L. Arnowitt and P. Nath, *Locally Supersymmetric Grand Unification*, Phys. Rev. Lett. **49** (1982) 970.

[65] R. Barbieri, S. Ferrara and C. A. Savoy, *Gauge Models with Spontaneously Broken Local Supersymmetry*, Phys. Lett. B **119** (1982) 343.

[66] G. L. Kane, C. F. Kolda, L. Roszkowski and J. D. Wells, *Study of constrained minimal supersymmetry*, Phys. Rev. D **49** (1994) 6173, arXiv: hep-ph/9312272.

[67] LEP SUSY Working Group, ALEPH, DELPHI, L3 and OPAL experiments, LEPSUSYWG/01-03.1.

[68] Michele Papucci, Joshua T. Ruderman, Andreas Weiler, *Natural SUSY Endures*, JHEP **09** (2012), arXiv: 1110.6926 [hep-ex].

[69] N. Arkani-Hamed, A. Delgado and G. F. Giudice, *The Well-tempered neutralino*, Nucl. Phys. B **741** (2006) 108, arXiv: hep-ph/0601041 [hep-ph].

[70] R. Barbieri and G. Giudice, *Upper bounds on supersymmetric particle masses*, Nucl. Phys. B **306** (1988) 063.

[71] ATLAS Collaboration, *Summary of the ATLAS experiment's sensitivity to supersymmetry after LHC Run 1 — interpreted in the phenomenological MSSM*, JHEP **10** (2015) 134, arXiv: 1508.06608 [hep-ex].

[72] Planck Collaboration, *Planck 2013 results. XVI. Cosmological parameters*, Astron. Astrophys. **571** (2014) 66, arXiv: 1303.5076 [astro-ph.CO].

[73] D. Abercrombie et al, *Dark Matter Benchmark Models for Early LHC Run-2 Searches: Report of the ATLAS/CMS Dark Matter Forum*, (2015), arXiv: 1507.00966 [hep-ex].

[74] ATLAS Collaboration, *The ATLAS Experiment at the CERN Large Hadron Collider*, JINST **3** (2008) S08003.

[75] ATLAS Collaboration, *ATLAS Insertable B-Layer Technical Design Report*, ATLAS-TDR-19, 2010, URL: https://cds.cern.ch/record/1291633, *ATLAS Insertable B-Layer Technical Design Report Addendum*, ATLAS-TDR-19-ADD-1, 2012, URL: https://cds.cern.ch/record/1451888.

[76] ATLAS Collaboration, *Optimisation of the ATLAS b-tagging performance for the 2016 LHC Run*, ATL-PHYS-PUB-2016-012, 2016, URL: https://cds.cern.ch/record/2160731.

[77] ATLAS Collaboration, *Performance of the ATLAS Trigger System in 2015*, Eur. Phys. J. C **77** (2017) 317, arXiv: 1611.09661 [hep-ex].

[78] ATLAS Collaboration, *Improved luminosity determination in pp collisions at $\sqrt{s}$ = 7 TeV using the ATLAS detector at the LHC*, Eur. Phys. J. C **73** (2013) 2518, arXiv: 1302.4393 [hep-ex].

[79] S. Alioli, P. Nason, C. Oleari and E. Re, *A general framework for implementing NLO calculations in shower Monte Carlo programs: the POWHEG BOX*, JHEP **06** (2010) 043, arXiv: 1002.2581 [hep-ph].

[80] H.-L. Lai et al., *New parton distributions for collider physics*, Phys. Rev. D **82** (2010) 074024, arXiv: 1007.2241 [hep-ph].

[81] T. Sjöstrand, S. Mrenna and P. Z. Skands, *PYTHIA 6.4 Physics and Manual*, JHEP **05** (2006) 026, arXiv: hep-ph/0603175.

[82] P. Z. Skands, *Tuning Monte Carlo Generators: The Perugia Tunes*, Phys. Rev. D **82** (2010) 074018, arXiv: 1005.3457 [hep-ph].

[83] M. Czakon, P. Fiedler and A. Mitov, *Total Top-Quark Pair-Production Cross Section at Hadron Colliders Through $O(\alpha_S^4)$*, Phys. Rev. Lett. **110** (2013) 252004, arXiv: 1303.6254 [hep-ph].

[84] M. Czakon and A. Mitov, *NNLO corrections to top pair production at hadron colliders: the quark-gluon reaction*, JHEP **01** (2013) 080, arXiv: 1210.6832 [hep-ph].

[85] M. Czakon and A. Mitov, *NNLO corrections to top-pair production at hadron colliders: the all-fermionic scattering channels*, JHEP **12** (2012) 054, arXiv: 1207.0236 [hep-ph].

[86] P. Bärnreuther, M. Czakon and A. Mitov, *Percent Level Precision Physics at the Tevatron: First Genuine NNLO QCD Corrections to $q\bar{q} \to t\bar{t} + X$*, Phys. Rev. Lett. **109** (2012) 132001, arXiv: 1204.5201 [hep-ph].

[87] M. Cacciari, M. Czakon, M. Mangano, A. Mitov and P. Nason, *Top-pair production at hadron colliders with next-to-next-to-leading logarithmic soft-gluon resummation*, Phys. Lett. B **710** (2012) 612, arXiv: 1111.5869 [hep-ph].

[88] M. Czakon and A. Mitov, *Top++: A Program for the Calculation of the Top-Pair Cross-Section at Hadron Colliders*, Comput. Phys. Commun. **185** (2014) 2930, arXiv: 1112.5675 [hep-ph].

[89] N. Kidonakis, *Next-to-next-to-leading-order collinear and soft gluon corrections for t-channel single top quark production*, Phys. Rev. D **83** (2011) 091503, arXiv: 1103.2792 [hep-ph].

[90] N. Kidonakis, *Two-loop soft anomalous dimensions for single top quark associated production with a W- or H-*, Phys. Rev. D **82** (2010) 054018, arXiv: 1005.4451 [hep-ph].

[91] N. Kidonakis, *NNLL resummation for s-channel single top quark production*, Phys. Rev. D **81** (2010) 054028, arXiv: 1001.5034 [hep-ph].

[92] T. Gleisberg et al., *Event generation with SHERPA 1.1*, JHEP **02** (2009) 007, arXiv: 0811.4622 [hep-ph].

[93] R. D. Ball et al., *Parton distributions for the LHC Run II*, JHEP **04** (2015) 040, arXiv: 1410.8849 [hep-ph].

[94] S. Catani, L. Cieri, G. Ferrera, D. de Florian and M. Grazzini, *Vector boson production at hadron colliders: a fully exclusive QCD calculation at NNLO*, Phys. Rev. Lett. **103** (2009) 082001, arXiv: 0903.2120 [hep-ph].

[95] J. Alwall et al., *The automated computation of tree-level and next-to-leading order differential cross sections, and their matching to parton shower simulations*, JHEP **07** (2014) 079, arXiv: 1405.0301 [hep-ph].

[96] T. Sjöstrand, S. Mrenna and P. Z. Skands, *A Brief Introduction to PYTHIA 8.1*, Comput. Phys. Commun. **178** (2008) 852, arXiv: 0710.3820 [hep-ph].

[97] ATLAS Collaboration, *ATLAS Pythia 8 tunes to 7 TeV data*, ATL-PHYS-PUB-2014-021, 2014, URL: https://cds.cern.ch/record/1966419.

[98] R. D. Ball et al., *Parton distributions with LHC data*, Nucl. Phys. B **867** (2013) 244, arXiv: 1207.1303 [hep-ph].

[99] C. Borschensky et al., *Squark and gluino production cross sections in pp collisions at $\sqrt{s}$ = 13, 14, 33 and 100 TeV*, Eur. Phys. J. C **74** (2014) 3174, arXiv: 1407.5066.

[100] E. Re, *Single-top Wt-channel production matched with parton showers using the POWHEG method*, Eur. Phys. J. C **71** (2011) 1547, arXiv: 1009.2450 [hep-ph].

[101] S. Frixione, P. Nason and G. Ridolfi, *A Positive-weight next-to-leading-order Monte Carlo for heavy flavour hadroproduction*, JHEP **09** (2007) 126, arXiv: 0707.3088 [hep-ph].

[102] R. Frederix, E. Re and P. Torrielli, *Single-top t-channel hadroproduction in the four-flavour scheme with POWHEG and aMC@NLO*, JHEP **09** (2012) 130, arXiv: 1207.5391 [hep-ph].

[103] S. Alioli, P. Nason, C. Oleari and E. Re,
NLO single-top production matched with shower in POWHEG: s- and t-channel contributions,
JHEP **09** (2009) 111, Erratum: JHEP 02 (2010) 011, arXiv: 0907.4076 [hep-ph].

[104] D. J. Lange, *The EvtGen particle decay simulation package*,
Nucl. Instrum. Meth. A **462** (2001) 152.

[105] ATLAS Collaboration, *The ATLAS Simulation Infrastructure*, Eur. Phys. J. C **70** (2010) 823,
arXiv: 1005.4568 [hep-ex].

[106] S. Agostinelli et al. (GEANT4 Collaboration), *GEANT4: A Simulation toolkit*,
Nucl. Instrum. Meth. A **506** (2003) 250.

[107] M. Bahr et al., *Herwig++ Physics and Manual*, Eur. Phys. J. C **58** (2008) 639,
arXiv: 0803.0883 [hep-ph].

[108] J. Bellm et al., *Herwig 7.0/Herwig++ 3.0 release note*, Eur. Phys. J. C **76** (2016) 196,
arXiv: 1512.01178 [hep-ph].

[109] T. Gleisberg and S. Höche, *Comix, a new matrix element generator*, JHEP **12** (2008) 039,
arXiv: 0808.3674 [hep-ph].

[110] F. Cascioli, P. Maierhofer and S. Pozzorini, *Scattering Amplitudes with Open Loops*,
Phys. Rev. Lett. **108** (2012) 111601, arXiv: 1111.5206 [hep-ph].

[111] S. Schumann and F. Krauss,
A Parton shower algorithm based on Catani-Seymour dipole factorisation, JHEP **03** (2008) 038,
arXiv: 0709.1027 [hep-ph].

[112] S. Höche, F. Krauss, M. Schönherr and F. Siegert,
QCD matrix elements + parton showers: The NLO case, JHEP **04** (2013) 027,
arXiv: 1207.5030 [hep-ph].

[113] ATLAS Collaboration,
Simulation of top-quark production for the ATLAS experiment at $\sqrt{s}$ = 13 *TeV*,
ATL-PHYS-PUB-2016-004, 2016, URL: https://cds.cern.ch/record/2120417.

[114] ATLAS Collaboration, *Monte Carlo Generators for the Production of a W or* Z/γ^* *Boson in Association with Jets at ATLAS in Run 2*, ATL-PHYS-PUB-2016-003, 2016,
URL: https://cds.cern.ch/record/2120133.

[115] ATLAS Collaboration, *Multi-boson simulation for* 13 *TeV ATLAS analyses*,
ATL-PHYS-PUB-2016-002, 2016, URL: https://cds.cern.ch/record/2119986.

[116] ATLAS Collaboration,
Modelling of the $t\bar{t}H$ *and* $t\bar{t}V(V = W, Z)$ *processes for* $\sqrt{s}$ = 13 *TeV ATLAS analyses*,
ATL-PHYS-PUB-2016-005, 2016, URL: https://cds.cern.ch/record/2120826.

[117] B. Allanach, *SOFTSUSY: a program for calculating supersymmetric spectra*,
Comput. Phys. Commun. **143** (2002) 305, arXiv: hep-ph/0104145 [hep-ph].

[118] B. Allanach, P. Athron, L. C. Tunstall, A. Voigt and A. Williams, *Next-to-Minimal SOFTSUSY*,
Comput. Phys. Commun. **185** (2014) 2322, arXiv: 1311.7659 [hep-ph].

[119] A. Djouadi, J. Kalinowski and M. Spira, *HDECAY: A Program for Higgs boson decays in the standard model and its supersymmetric extension*, Comput. Phys. Commun. **108** (1998) 56,
arXiv: hep-ph/9704448 [hep-ph].

[120] A. Djouadi, M. M. Muhlleitner and M. Spira, *Decays of supersymmetric particles: The Program SUSY-HIT (SUspect-SdecaY-Hdecay-InTerface)*, Acta Phys. Polon. B **38** (2007) 635, arXiv: hep-ph/0609292 [hep-ph].

[121] Ian Low, *Polarized Charginos (and Tops) in Stop Decays*, Phys. Rev. D **88** (2013), arXiv: 1304.0491 [hep-ph].

[122] Maxim Perelstein, Andreas Weiler, *Polarized Tops from Stop Decays at the LHC*, JHEP **2009** (2009), arXiv: 0811.1024 [hep-ph].

[123] P. Artoisenet, R. Frederix, O. Mattelaer and R. Rietkerk, *Automatic spin-entangled decays of heavy resonances in Monte Carlo simulations*, JHEP **03** (2013) 015, arXiv: 1212.3460 [hep-ph].

[124] ATLAS Collaboration, *Search for a scalar partner of the top quark in the jets plus missing transverse momentum final state at $\sqrt{s}$=13 TeV with the ATLAS detector*, (2017), arXiv: 1709.04183 [hep-ex].

[125] ATLAS Collaboration, *Search for new phenomena with large jet multiplicities and missing transverse momentum using large-radius jets and flavour-tagging at ATLAS in 13 TeV pp collisions*, (2017), arXiv: 1708.02794 [hep-ex].

[126] ATLAS Collaboration, *Search for pair production of gluinos decaying via stop and sbottom in events with b-jets and large missing transverse momentum in pp collisions at $\sqrt{s}$ = 13 TeV with the ATLAS detector*, Phys. Rev. D **94** (2016) 032003, arXiv: 1605.09318 [hep-ex].

[127] ATLAS Collaboration, *Search for squarks and gluinos in final states with jets and missing transverse momentum at $\sqrt{s}$ = 13 TeV with the ATLAS detector*, Eur. Phys. J. C **76** (2016) 392, arXiv: 1605.03814 [hep-ex].

[128] G. Belanger et al., *MicrOMEGAs 2.0: A Program to calculate the relic density of dark matter in a generic model*, Comput. Phys. Commun. **176** (2007) 367, arXiv: hep-ph/0607059 [hep-ph].

[129] G. Belanger et al., *micrOMEGAs: A Tool for dark matter studies*, Nuovo Cim. C033N2 (2010) 111, arXiv: 1005.4133 [hep-ph].

[130] W. Beenakker, M. Kramer, T. Plehn, M. Spira and P. M. Zerwas, *Stop production at hadron colliders*, Nucl. Phys. **B515** (1998) 3, arXiv: hep-ph/9710451.

[131] W. Beenakker et al., *Supersymmetric top and bottom squark production at hadron colliders*, JHEP **08** (2010) 098, arXiv: 1006.4771.

[132] W. Beenakker et al., *Squark and gluino hadroproduction*, Int. J. Mod. Phys. A **26** (2011) 2637, arXiv: 1105.1110.

[133] O. Mattelaer and E. Vryonidou, *Dark matter production through loop-induced processes at the LHC: the s-channel mediator case*, Eur. Phys. J. C **75** (2015) 436, arXiv: 1508.00564 [hep-ph].

[134] M. Backovic et al., *Higher-order QCD predictions for dark matter production at the LHC in simplified models with s-channel mediators*, Eur. Phys. J. C **75** (2015) 482, arXiv: 1508.05327 [hep-ph].

[135] ATLAS Collaboration, *Electron identification measurements in ATLAS using $\sqrt{s}$ = 13 TeV data with 50 ns bunch spacing*, ATL-PHYS-PUB-2015-041, 2015, URL: https://cds.cern.ch/record/2048202.

[136] ATLAS Collaboration, *Muon reconstruction performance of the ATLAS detector in proton–proton collision data at $\sqrt{s}$ = 13 TeV*, Eur. Phys. J. C **76** (2016) 292, arXiv: 1603.05598 [hep-ex].

[137] ATLAS Collaboration, *Electron efficiency measurements with the ATLAS detector using the 2015 LHC proton–proton collision data*, ATLAS-CONF-2016-024, 2016, URL: https://cds.cern.ch/record/2157687.

[138] ATLAS Collaboration, *Topological cell clustering in the ATLAS calorimeters and its performance in LHC Run 1*, Eur. Phys. J. C **77** (2017) 490, arXiv: 1603.02934 [hep-ex].

[139] ATLAS Collaboration, *Jet energy measurement with the ATLAS detector in proton–proton collisions at $\sqrt{s}$ = 7 TeV*, Eur. Phys. J. C **73** (2013) 2304, arXiv: 1112.6426 [hep-ex].

[140] M. Cacciari, G. P. Salam and G. Soyez, *The Anti-k(t) jet clustering algorithm*, JHEP **04** (2008) 063, arXiv: 0802.1189 [hep-ph].

[141] M. Cacciari, G. P. Salam and G. Soyez, *FastJet User Manual*, Eur. Phys. J. **C72** (2012) 1896, arXiv: 1111.6097 [hep-ph].

[142] M. Cacciari and G. P. Salam, *Pileup subtraction using jet areas*, Phys. Lett. B **659** (2008) 119, arXiv: 0707.1378 [hep-ph].

[143] M. Cacciari, G. P. Salam and G. Soyez, *The Catchment Area of Jets*, JHEP **04** (2008) 005, arXiv: 0802.1188 [hep-ph].

[144] ATLAS Collaboration, *Performance of pile-up mitigation techniques for jets in pp collisions at $\sqrt{s}$ = 8 TeV using the ATLAS detector*, Eur. Phys. J. C **76** (2016) 581, arXiv: 1510.03823 [hep-ex].

[145] ATLAS Collaboration, *Jet energy measurement and its systematic uncertainty in proton–proton collisions at $\sqrt{s}$ = 7 TeV with the ATLAS detector*, Eur. Phys. J. C **75** (2015) 17, arXiv: 1406.0076 [hep-ex].

[146] ATLAS Collaboration, *Jet energy scale measurements and their systematic uncertainties in proton–proton collisions at $\sqrt{s}$ = 13 TeV with the ATLAS detector*, Phys. Rev. D **96** (2017) 072002, arXiv: 1703.09665 [hep-ex].

[147] ATLAS Collaboration, *Characterisation and mitigation of beam-induced backgrounds observed in the ATLAS detector during the 2011 proton–proton run*, JINST **8** (2013) P07004, arXiv: 1303.0223 [hep-ex].

[148] ATLAS Collaboration, *Selection of jets produced in 13 TeV proton–proton collisions with the ATLAS detector*, ATLAS-CONF-2015-029, 2015, URL: https://cds.cern.ch/record/2037702.

[149] ATLAS Collaboration, *Performance of b-Jet Identification in the ATLAS Experiment*, JINST **11** (2016) P04008, arXiv: 1512.01094 [hep-ex].

[150] ATLAS Collaboration, *Reconstruction, Energy Calibration, and Identification of Hadronically Decaying Tau Leptons in the ATLAS Experiment for Run-2 of the LHC*, ATL-PHYS-PUB-2015-045, 2015, URL: https://atlas.web.cern.ch/Atlas/GROUPS/PHYSICS/PUBNOTES/ATL-PHYS-PUB-2015-045.

[151] ATLAS Collaboration, *Performance of missing transverse momentum reconstruction with the ATLAS detector in the first proton–proton collisions at* $\sqrt{s} = 13$ *TeV*, ATL-PHYS-PUB-2015-027, 2015, URL: https://cds.cern.ch/record/2037904.

[152] ATLAS Collaboration, *Expected performance of missing transverse momentum reconstruction for the ATLAS detector at* $\sqrt{s} = 13$ *TeV*, ATL-PHYS-PUB-2015-023, 2015, URL: https://cds.cern.ch/record/2037700.

[153] A. J. Barr, B. Gripaios and C. G. Lester, *Transverse masses and kinematic constraints: from the boundary to the crease*, JHEP **11** (2009) 096, arXiv: 0908.3779 [hep-ph].

[154] P. Konar, K. Kong, K. T. Matchev and M. Park, *Dark Matter Particle Spectroscopy at the LHC: Generalizing M(T2) to Asymmetric Event Topologies*, JHEP **04** (2010) 086, arXiv: 0911.4126 [hep-ph].

[155] Y. Bai, H.-C. Cheng, J. Gallicchio and J. Gu, *Stop the Top Background of the Stop Search*, JHEP **07** (2012) 110, arXiv: 1203.4813 [hep-ph].

[156] C. G. Lester and B. Nachman, *Bisection-based asymmetric* M_{T2} *computation: a higher precision calculator than existing symmetric methods*, JHEP **03** (2015) 100, arXiv: 1411.4312 [hep-ph].

[157] C. G. Lester and D. J. Summers, *Measuring masses of semi-invisibly decaying particles pair produced at hadron colliders*, Phys. Lett. B **463** (1999) 99, arXiv: hep-ph/9906349.

[158] ATLAS Collaboration, *Search for top squark pair production in final states with one isolated lepton, jets, and missing transverse momentum in* $\sqrt{s} = 8$ *TeV pp collisions with the ATLAS detector*, JHEP **11** (2014) 118, arXiv: 1407.0583 [hep-ex].

[159] A. Hoecker et al., *TMVA - Toolkit for Multivariate Data Analysis*, arXiv: physics/0703039 [physics.data-an].

[160] H. An and L.-T. Wang, *Opening up the compressed region of top squark searches at 13 TeV LHC*, Phys. Rev. Lett. **115** (2015) 181602, arXiv: 1506.00653 [hep-ph].

[161] S. Macaluso, M. Park, D. Shih and B. Tweedie, *Revealing Compressed Stops Using High-Momentum Recoils*, JHEP **03** (2016) 151, arXiv: 1506.07885 [hep-ph].

[162] P. Jackson, C. Rogan and M. Santoni, *Sparticles in motion: Analyzing compressed SUSY scenarios with a new method of event reconstruction*, Phys. Rev. D **95** (2017) 035031, arXiv: 1607.08307 [hep-ph].

[163] ATLAS Collaboration, *Observation and measurement of Higgs boson decays to* WW^* *with the ATLAS detector*, Phys. Rev. D **92** (2015) 012006, arXiv: 1412.2641 [hep-ex].

[164] ATLAS Collaboration, *Jet Calibration and Systematic Uncertainties for Jets Reconstructed in the ATLAS Detector at* $\sqrt{s} = 13$ *TeV*, ATL-PHYS-PUB-2015-015, 2015, URL: https://cds.cern.ch/record/2037613.

[165] ATLAS Collaboration, *Calibration of b-tagging using dileptonic top pair events in a combinatorial likelihood approach with the ATLAS experiment*, ATLAS-CONF-2014-004, 2014, URL: https://cds.cern.ch/record/1664335.

[166] ATLAS Collaboration, *Calibration of the performance of b-tagging for c and light-flavour jets in the 2012 ATLAS data*, ATLAS-CONF-2014-046, 2014, URL: https://cds.cern.ch/record/1741020.

[167] A. L. Read, *Presentation of search results: The CL_s technique*, J. Phys. G **28** (2002) 2693.

[168] ATLAS Collaboration, *ATLAS Computing Acknowledgements 2016–2017*, ATL-GEN-PUB-2016-002, URL: https://cds.cern.ch/record/2202407.

The ATLAS Collaboration

M. Aaboud[137d], G. Aad[88], B. Abbott[115], O. Abdinov[12,*], B. Abeloos[119], S.H. Abidi[161], O.S. AbouZeid[139], N.L. Abraham[151], H. Abramowicz[155], H. Abreu[154], R. Abreu[118], Y. Abulaiti[148a,148b], B.S. Acharya[167a,167b,a], S. Adachi[157], L. Adamczyk[41a], J. Adelman[110], M. Adersberger[102], T. Adye[133], A.A. Affolder[139], Y. Afik[154], T. Agatonovic-Jovin[14], C. Agheorghiesei[28c], J.A. Aguilar-Saavedra[128a,128f], S.P. Ahlen[24], F. Ahmadov[68,b], G. Aielli[135a,135b], S. Akatsuka[71], H. Akerstedt[148a,148b], T.P.A. Åkesson[84], E. Akilli[52], A.V. Akimov[98], G.L. Alberghi[22a,22b], J. Albert[172], P. Albicocco[50], M.J. Alconada Verzini[74], S.C. Alderweireldt[108], M. Aleksa[32], I.N. Aleksandrov[68], C. Alexa[28b], G. Alexander[155], T. Alexopoulos[10], M. Alhroob[115], B. Ali[130], M. Aliev[76a,76b], G. Alimonti[94a], J. Alison[33], S.P. Alkire[38], B.M.M. Allbrooke[151], B.W. Allen[118], P.P. Allport[19], A. Aloisio[106a,106b], A. Alonso[39], F. Alonso[74], C. Alpigiani[140], A.A. Alshehri[56], M.I. Alstaty[88], B. Alvarez Gonzalez[32], D. Álvarez Piqueras[170], M.G. Alviggi[106a,106b], B.T. Amadio[16], Y. Amaral Coutinho[26a], C. Amelung[25], D. Amidei[92], S.P. Amor Dos Santos[128a,128c], S. Amoroso[32], G. Amundsen[25], C. Anastopoulos[141], L.S. Ancu[52], N. Andari[19], T. Andeen[11], C.F. Anders[60b], J.K. Anders[77], K.J. Anderson[33], A. Andreazza[94a,94b], V. Andrei[60a], S. Angelidakis[37], I. Angelozzi[109], A. Angerami[38], A.V. Anisenkov[111,c], N. Anjos[13], A. Annovi[126a], C. Antel[60a], M. Antonelli[50], A. Antonov[100,*], D.J. Antrim[166], F. Anulli[134a], M. Aoki[69], L. Aperio Bella[32], G. Arabidze[93], Y. Arai[69], J.P. Araque[128a], V. Araujo Ferraz[26a], A.T.H. Arce[48], R.E. Ardell[80], F.A. Arduh[74], J-F. Arguin[97], S. Argyropoulos[66], M. Arik[20a], A.J. Armbruster[32], L.J. Armitage[79], O. Arnaez[161], H. Arnold[51], M. Arratia[30], O. Arslan[23], A. Artamonov[99,*], G. Artoni[122], S. Artz[86], S. Asai[157], N. Asbah[45], A. Ashkenazi[155], L. Asquith[151], K. Assamagan[27], R. Astalos[146a], M. Atkinson[169], N.B. Atlay[143], K. Augsten[130], G. Avolio[32], B. Axen[16], M.K. Ayoub[119], G. Azuelos[97,d], A.E. Baas[60a], M.J. Baca[19], H. Bachacou[138], K. Bachas[76a,76b], M. Backes[122], P. Bagnaia[134a,134b], M. Bahmani[42], H. Bahrasemani[144], J.T. Baines[133], M. Bajic[39], O.K. Baker[179], E.M. Baldin[111,c], P. Balek[175], F. Balli[138], W.K. Balunas[124], E. Banas[42], A. Bandyopadhyay[23], Sw. Banerjee[176,e], A.A.E. Bannoura[178], L. Barak[155], E.L. Barberio[91], D. Barberis[53a,53b], M. Barbero[88], T. Barillari[103], M-S Barisits[32], J.T. Barkeloo[118], T. Barklow[145], N. Barlow[30], S.L. Barnes[36c], B.M. Barnett[133], R.M. Barnett[16], Z. Barnovska-Blenessy[36a], A. Baroncelli[136a], G. Barone[25], A.J. Barr[122], L. Barranco Navarro[170], F. Barreiro[85], J. Barreiro Guimarães da Costa[35a], R. Bartoldus[145], A.E. Barton[75], P. Bartos[146a], A. Basalaev[125], A. Bassalat[119,f], R.L. Bates[56], S.J. Batista[161], J.R. Batley[30], M. Battaglia[139], M. Bauce[134a,134b], F. Bauer[138], H.S. Bawa[145,g], J.B. Beacham[113], M.D. Beattie[75], T. Beau[83], P.H. Beauchemin[165], P. Bechtle[23], H.P. Beck[18,h], H.C. Beck[57], K. Becker[122], M. Becker[86], C. Becot[112], A.J. Beddall[20e], A. Beddall[20b], V.A. Bednyakov[68], M. Bedognetti[109], C.P. Bee[150], T.A. Beermann[32], M. Begalli[26a], M. Begel[27], J.K. Behr[45], A.S. Bell[81], G. Bella[155], L. Bellagamba[22a], A. Bellerive[31], M. Bellomo[154], K. Belotskiy[100], O. Beltramello[32], N.L. Belyaev[100], O. Benary[155,*], D. Benchekroun[137a], M. Bender[102], K. Bendtz[148a,148b], N. Benekos[10], Y. Benhammou[155], E. Benhar Noccioli[179], J. Benitez[66], D.P. Benjamin[48], M. Benoit[52], J.R. Bensinger[25], S. Bentvelsen[109], L. Beresford[122], M. Beretta[50], D. Berge[109], E. Bergeaas Kuutmann[168], N. Berger[5], J. Beringer[16], S. Berlendis[58], N.R. Bernard[89], G. Bernardi[83], C. Bernius[145], F.U. Bernlochner[23], T. Berry[80], P. Berta[86], C. Bertella[35a], G. Bertoli[148a,148b], F. Bertolucci[126a,126b], I.A. Bertram[75], C. Bertsche[45], D. Bertsche[115], G.J. Besjes[39], O. Bessidskaia Bylund[148a,148b], M. Bessner[45], N. Besson[138], A. Bethani[87], S. Bethke[103], A.J. Bevan[79], J. Beyer[103], R.M. Bianchi[127], O. Biebel[102], D. Biedermann[17], R. Bielski[87], K. Bierwagen[86], N.V. Biesuz[126a,126b], M. Biglietti[136a], T.R.V. Billoud[97], H. Bilokon[50], M. Bindi[57], A. Bingul[20b], C. Bini[134a,134b], S. Biondi[22a,22b], T. Bisanz[57], C. Bittrich[47], D.M. Bjergaard[48], J.E. Black[145], K.M. Black[24], R.E. Blair[6], T. Blazek[146a], I. Bloch[45], C. Blocker[25], A. Blue[56], W. Blum[86,*], U. Blumenschein[79], Dr. Blunier[34a], G.J. Bobbink[109], V.S. Bobrovnikov[111,c], S.S. Bocchetta[84],

A. Bocci[48], C. Bock[102], M. Boehler[51], D. Boerner[178], D. Bogavac[102], A.G. Bogdanchikov[111], C. Bohm[148a], V. Boisvert[80], P. Bokan[168,i], T. Bold[41a], A.S. Boldyrev[101], A.E. Bolz[60b], M. Bomben[83], M. Bona[79], M. Boonekamp[138], A. Borisov[132], G. Borissov[75], J. Bortfeldt[32], D. Bortoletto[122], V. Bortolotto[62a], D. Boscherini[22a], M. Bosman[13], J.D. Bossio Sola[29], J. Boudreau[127], J. Bouffard[2], E.V. Bouhova-Thacker[75], D. Boumediene[37], C. Bourdarios[119], S.K. Boutle[56], A. Boveia[113], J. Boyd[32], I.R. Boyko[68], A.J. Bozson[80], J. Bracinik[19], A. Brandt[8], G. Brandt[57], O. Brandt[60a], U. Bratzler[158], B. Brau[89], J.E. Brau[118], W.D. Breaden Madden[56], K. Brendlinger[45], A.J. Brennan[91], L. Brenner[109], R. Brenner[168], S. Bressler[175], D.L. Briglin[19], T.M. Bristow[49], D. Britton[56], D. Britzger[45], F.M. Brochu[30], I. Brock[23], R. Brock[93], G. Brooijmans[38], T. Brooks[80], W.K. Brooks[34b], J. Brosamer[16], E. Brost[110], J.H Broughton[19], P.A. Bruckman de Renstrom[42], D. Bruncko[146b], A. Bruni[22a], G. Bruni[22a], L.S. Bruni[109], S. Bruno[135a,135b], BH Brunt[30], M. Bruschi[22a], N. Bruscino[23], P. Bryant[33], L. Bryngemark[45], T. Buanes[15], Q. Buat[144], P. Buchholz[143], A.G. Buckley[56], I.A. Budagov[68], F. Buehrer[51], M.K. Bugge[121], O. Bulekov[100], D. Bullock[8], T.J. Burch[110], S. Burdin[77], C.D. Burgard[51], A.M. Burger[5], B. Burghgrave[110], K. Burka[42], S. Burke[133], I. Burmeister[46], J.T.P. Burr[122], E. Busato[37], D. Büscher[51], V. Büscher[86], P. Bussey[56], J.M. Butler[24], C.M. Buttar[56], J.M. Butterworth[81], P. Butti[32], W. Buttinger[27], A. Buzatu[153], A.R. Buzykaev[111,c], Changqiao C.-Q.[36a], S. Cabrera Urbán[170], D. Caforio[130], V.M. Cairo[40a,40b], O. Cakir[4a], N. Calace[52], P. Calafiura[16], A. Calandri[88], G. Calderini[83], P. Calfayan[64], G. Callea[40a,40b], L.P. Caloba[26a], S. Calvente Lopez[85], D. Calvet[37], S. Calvet[37], T.P. Calvet[88], R. Camacho Toro[33], S. Camarda[32], P. Camarri[135a,135b], D. Cameron[121], R. Caminal Armadans[169], C. Camincher[58], S. Campana[32], M. Campanelli[81], A. Camplani[94a,94b], A. Campoverde[143], V. Canale[106a,106b], M. Cano Bret[36c], J. Cantero[116], T. Cao[155], M.D.M. Capeans Garrido[32], I. Caprini[28b], M. Caprini[28b], M. Capua[40a,40b], R.M. Carbone[38], R. Cardarelli[135a], F. Cardillo[51], I. Carli[131], T. Carli[32], G. Carlino[106a], B.T. Carlson[127], L. Carminati[94a,94b], R.M.D. Carney[148a,148b], S. Caron[108], E. Carquin[34b], S. Carrá[94a,94b], G.D. Carrillo-Montoya[32], D. Casadei[19], M.P. Casado[13,j], M. Casolino[13], D.W. Casper[166], R. Castelijn[109], V. Castillo Gimenez[170], N.F. Castro[128a,k], A. Catinaccio[32], J.R. Catmore[121], A. Cattai[32], J. Caudron[23], V. Cavaliere[169], E. Cavallaro[13], D. Cavalli[94a], M. Cavalli-Sforza[13], V. Cavasinni[126a,126b], E. Celebi[20d], F. Ceradini[136a,136b], L. Cerda Alberich[170], A.S. Cerqueira[26b], A. Cerri[151], L. Cerrito[135a,135b], F. Cerutti[16], A. Cervelli[18], S.A. Cetin[20d], A. Chafaq[137a], D. Chakraborty[110], S.K. Chan[59], W.S. Chan[109], Y.L. Chan[62a], P. Chang[169], J.D. Chapman[30], D.G. Charlton[19], C.C. Chau[31], C.A. Chavez Barajas[151], S. Che[113], S. Cheatham[167a,167c], A. Chegwidden[93], S. Chekanov[6], S.V. Chekulaev[163a], G.A. Chelkov[68,l], M.A. Chelstowska[32], C. Chen[36a], C. Chen[67], H. Chen[27], J. Chen[36a], S. Chen[35b], S. Chen[157], X. Chen[35c,m], Y. Chen[70], H.C. Cheng[92], H.J. Cheng[35a,35d], A. Cheplakov[68], E. Cheremushkina[132], R. Cherkaoui El Moursli[137e], E. Cheu[7], K. Cheung[63], L. Chevalier[138], V. Chiarella[50], G. Chiarelli[126a], G. Chiodini[76a], A.S. Chisholm[32], A. Chitan[28b], Y.H. Chiu[172], M.V. Chizhov[68], K. Choi[64], A.R. Chomont[37], S. Chouridou[156], Y.S. Chow[62a], V. Christodoulou[81], M.C. Chu[62a], J. Chudoba[129], A.J. Chuinard[90], J.J. Chwastowski[42], L. Chytka[117], A.K. Ciftci[4a], D. Cinca[46], V. Cindro[78], I.A. Cioara[23], C. Ciocca[22a,22b], A. Ciocio[16], F. Cirotto[106a,106b], Z.H. Citron[175], M. Citterio[94a], M. Ciubancan[28b], A. Clark[52], B.L. Clark[59], M.R. Clark[38], P.J. Clark[49], R.N. Clarke[16], C. Clement[148a,148b], Y. Coadou[88], M. Cobal[167a,167c], A. Coccaro[52], J. Cochran[67], L. Colasurdo[108], B. Cole[38], A.P. Colijn[109], J. Collot[58], T. Colombo[166], P. Conde Muiño[128a,128b], E. Coniavitis[51], S.H. Connell[147b], I.A. Connelly[87], S. Constantinescu[28b], G. Conti[32], F. Conventi[106a,n], M. Cooke[16], A.M. Cooper-Sarkar[122], F. Cormier[171], K.J.R. Cormier[161], M. Corradi[134a,134b], F. Corriveau[90,o], A. Cortes-Gonzalez[32], G. Cortiana[103], G. Costa[94a], M.J. Costa[170], D. Costanzo[141], G. Cottin[30], G. Cowan[80], B.E. Cox[87], K. Cranmer[112], S.J. Crawley[56], R.A. Creager[124], G. Cree[31], S. Crépé-Renaudin[58], F. Crescioli[83], W.A. Cribbs[148a,148b], M. Cristinziani[23], V. Croft[112], G. Crosetti[40a,40b], A. Cueto[85], T. Cuhadar Donszelmann[141], A.R. Cukierman[145], J. Cummings[179], M. Curatolo[50], J. Cúth[86], S. Czekierda[42], P. Czodrowski[32],

G. D'amen[22a,22b], S. D'Auria[56], L. D'eramo[83], M. D'Onofrio[77], M.J. Da Cunha Sargedas De Sousa[128a,128b], C. Da Via[87], W. Dabrowski[41a], T. Dado[146a], T. Dai[92], O. Dale[15], F. Dallaire[97], C. Dallapiccola[89], M. Dam[39], J.R. Dandoy[124], M.F. Daneri[29], N.P. Dang[176], A.C. Daniells[19], N.S. Dann[87], M. Danninger[171], M. Dano Hoffmann[138], V. Dao[150], G. Darbo[53a], S. Darmora[8], J. Dassoulas[3], A. Dattagupta[118], T. Daubney[45], W. Davey[23], C. David[45], T. Davidek[131], D.R. Davis[48], P. Davison[81], E. Dawe[91], I. Dawson[141], K. De[8], R. de Asmundis[106a], A. De Benedetti[115], S. De Castro[22a,22b], S. De Cecco[83], N. De Groot[108], P. de Jong[109], H. De la Torre[93], F. De Lorenzi[67], A. De Maria[57], D. De Pedis[134a], A. De Salvo[134a], U. De Sanctis[135a,135b], A. De Santo[151], K. De Vasconcelos Corga[88], J.B. De Vivie De Regie[119], R. Debbe[27], C. Debenedetti[139], D.V. Dedovich[68], N. Dehghanian[3], I. Deigaard[109], M. Del Gaudio[40a,40b], J. Del Peso[85], D. Delgove[119], F. Deliot[138], C.M. Delitzsch[7], A. Dell'Acqua[32], L. Dell'Asta[24], M. Dell'Orso[126a,126b], M. Della Pietra[106a,106b], D. della Volpe[52], M. Delmastro[5], C. Delporte[119], P.A. Delsart[58], D.A. DeMarco[161], S. Demers[179], M. Demichev[68], A. Demilly[83], S.P. Denisov[132], D. Denysiuk[138], D. Derendarz[42], J.E. Derkaoui[137d], F. Derue[83], P. Dervan[77], K. Desch[23], C. Deterre[45], K. Dette[161], M.R. Devesa[29], P.O. Deviveiros[32], A. Dewhurst[133], S. Dhaliwal[25], F.A. Di Bello[52], A. Di Ciaccio[135a,135b], L. Di Ciaccio[5], W.K. Di Clemente[124], C. Di Donato[106a,106b], A. Di Girolamo[32], B. Di Girolamo[32], B. Di Micco[136a,136b], R. Di Nardo[32], K.F. Di Petrillo[59], A. Di Simone[51], R. Di Sipio[161], D. Di Valentino[31], C. Diaconu[88], M. Diamond[161], F.A. Dias[39], M.A. Diaz[34a], E.B. Diehl[92], J. Dietrich[17], S. Díez Cornell[45], A. Dimitrievska[14], J. Dingfelder[23], P. Dita[28b], S. Dita[28b], F. Dittus[32], F. Djama[88], T. Djobava[54b], J.I. Djuvsland[60a], M.A.B. do Vale[26c], D. Dobos[32], M. Dobre[28b], C. Doglioni[84], J. Dolejsi[131], Z. Dolezal[131], M. Donadelli[26d], S. Donati[126a,126b], P. Dondero[123a,123b], J. Donini[37], J. Dopke[133], A. Doria[106a], M.T. Dova[74], A.T. Doyle[56], E. Drechsler[57], M. Dris[10], Y. Du[36b], J. Duarte-Campderros[155], A. Dubreuil[52], E. Duchovni[175], G. Duckeck[102], A. Ducourthial[83], O.A. Ducu[97,p], D. Duda[109], A. Dudarev[32], A.Chr. Dudder[86], E.M. Duffield[16], L. Duflot[119], M. Dührssen[32], C. Dulsen[178], M. Dumancic[175], A.E. Dumitriu[28b], A.K. Duncan[56], M. Dunford[60a], H. Duran Yildiz[4a], M. Düren[55], A. Durglishvili[54b], D. Duschinger[47], B. Dutta[45], D. Duvnjak[1], M. Dyndal[45], B.S. Dziedzic[42], C. Eckardt[45], K.M. Ecker[103], R.C. Edgar[92], T. Eifert[32], G. Eigen[15], K. Einsweiler[16], T. Ekelof[168], M. El Kacimi[137c], R. El Kosseifi[88], V. Ellajosyula[88], M. Ellert[168], S. Elles[5], F. Ellinghaus[178], A.A. Elliot[172], N. Ellis[32], J. Elmsheuser[27], M. Elsing[32], D. Emeliyanov[133], Y. Enari[157], O.C. Endner[86], J.S. Ennis[173], J. Erdmann[46], A. Ereditato[18], M. Ernst[27], S. Errede[169], M. Escalier[119], C. Escobar[170], B. Esposito[50], O. Estrada Pastor[170], A.I. Etienvre[138], E. Etzion[155], H. Evans[64], A. Ezhilov[125], M. Ezzi[137e], F. Fabbri[22a,22b], L. Fabbri[22a,22b], V. Fabiani[108], G. Facini[81], R.M. Fakhrutdinov[132], S. Falciano[134a], R.J. Falla[81], J. Faltova[32], Y. Fang[35a], M. Fanti[94a,94b], A. Farbin[8], A. Farilla[136a], C. Farina[127], E.M. Farina[123a,123b], T. Farooque[93], S. Farrell[16], S.M. Farrington[173], P. Farthouat[32], F. Fassi[137e], P. Fassnacht[32], D. Fassouliotis[9], M. Faucci Giannelli[49], A. Favareto[53a,53b], W.J. Fawcett[122], L. Fayard[119], O.L. Fedin[125,q], W. Fedorko[171], S. Feigl[121], L. Feligioni[88], C. Feng[36b], E.J. Feng[32], H. Feng[92], M.J. Fenton[56], A.B. Fenyuk[132], L. Feremenga[8], P. Fernandez Martinez[170], S. Fernandez Perez[13], J. Ferrando[45], A. Ferrari[168], P. Ferrari[109], R. Ferrari[123a], D.E. Ferreira de Lima[60b], A. Ferrer[170], D. Ferrere[52], C. Ferretti[92], F. Fiedler[86], A. Filipčič[78], M. Filipuzzi[45], F. Filthaut[108], M. Fincke-Keeler[172], K.D. Finelli[152], M.C.N. Fiolhais[128a,128c,r], L. Fiorini[170], A. Fischer[2], C. Fischer[13], J. Fischer[178], W.C. Fisher[93], N. Flaschel[45], I. Fleck[143], P. Fleischmann[92], R.R.M. Fletcher[124], T. Flick[178], B.M. Flierl[102], L.R. Flores Castillo[62a], M.J. Flowerdew[103], G.T. Forcolin[87], A. Formica[138], F.A. Förster[13], A. Forti[87], A.G. Foster[19], D. Fournier[119], H. Fox[75], S. Fracchia[141], P. Francavilla[83], M. Franchini[22a,22b], S. Franchino[60a], D. Francis[32], L. Franconi[121], M. Franklin[59], M. Frate[166], M. Fraternali[123a,123b], D. Freeborn[81], S.M. Fressard-Batraneanu[32], B. Freund[97], D. Froidevaux[32], J.A. Frost[122], C. Fukunaga[158], T. Fusayasu[104], J. Fuster[170], C. Gabaldon[58], O. Gabizon[154], A. Gabrielli[22a,22b], A. Gabrielli[16], G.P. Gach[41a], S. Gadatsch[32], S. Gadomski[80], G. Gagliardi[53a,53b],

L.G. Gagnon[97], C. Galea[108], B. Galhardo[128a,128c], E.J. Gallas[122], B.J. Gallop[133], P. Gallus[130], G. Galster[39], K.K. Gan[113], S. Ganguly[37], Y. Gao[77], Y.S. Gao[145,g], F.M. Garay Walls[34a], C. García[170], J.E. García Navarro[170], J.A. García Pascual[35a], M. Garcia-Sciveres[16], R.W. Gardner[33], N. Garelli[145], V. Garonne[121], A. Gascon Bravo[45], K. Gasnikova[45], C. Gatti[50], A. Gaudiello[53a,53b], G. Gaudio[123a], I.L. Gavrilenko[98], C. Gay[171], G. Gaycken[23], E.N. Gazis[10], C.N.P. Gee[133], J. Geisen[57], M. Geisen[86], M.P. Geisler[60a], K. Gellerstedt[148a,148b], C. Gemme[53a], M.H. Genest[58], C. Geng[92], S. Gentile[134a,134b], C. Gentsos[156], S. George[80], D. Gerbaudo[13], A. Gershon[155], G. Geßner[46], S. Ghasemi[143], M. Ghneimat[23], B. Giacobbe[22a], S. Giagu[134a,134b], N. Giangiacomi[22a,22b], P. Giannetti[126a], S.M. Gibson[80], M. Gignac[171], M. Gilchriese[16], D. Gillberg[31], G. Gilles[178], D.M. Gingrich[3,d], M.P. Giordani[167a,167c], F.M. Giorgi[22a], P.F. Giraud[138], P. Giromini[59], G. Giugliarelli[167a,167c], D. Giugni[94a], F. Giuli[122], C. Giuliani[103], M. Giulini[60b], B.K. Gjelsten[121], S. Gkaitatzis[156], I. Gkialas[9,s], E.L. Gkougkousis[13], P. Gkountoumis[10], L.K. Gladilin[101], C. Glasman[85], J. Glatzer[13], P.C.F. Glaysher[45], A. Glazov[45], M. Goblirsch-Kolb[25], J. Godlewski[42], S. Goldfarb[91], T. Golling[52], D. Golubkov[132], A. Gomes[128a,128b,128d], R. Gonçalo[128a], R. Goncalves Gama[26a], J. Goncalves Pinto Firmino Da Costa[138], G. Gonella[51], L. Gonella[19], A. Gongadze[68], J.L. Gonski[59], S. González de la Hoz[170], S. Gonzalez-Sevilla[52], L. Goossens[32], P.A. Gorbounov[99], H.A. Gordon[27], I. Gorelov[107], B. Gorini[32], E. Gorini[76a,76b], A. Gorišek[78], A.T. Goshaw[48], C. Gössling[46], M.I. Gostkin[68], C.A. Gottardo[23], C.R. Goudet[119], D. Goujdami[137c], A.G. Goussiou[140], N. Govender[147b,t], E. Gozani[154], L. Graber[57], I. Grabowska-Bold[41a], P.O.J. Gradin[168], J. Gramling[166], E. Gramstad[121], S. Grancagnolo[17], V. Gratchev[125], P.M. Gravila[28f], C. Gray[56], H.M. Gray[16], Z.D. Greenwood[82,u], C. Grefe[23], K. Gregersen[81], I.M. Gregor[45], P. Grenier[145], K. Grevtsov[5], J. Griffiths[8], A.A. Grillo[139], K. Grimm[75], S. Grinstein[13,v], Ph. Gris[37], J.-F. Grivaz[119], S. Groh[86], E. Gross[175], J. Grosse-Knetter[57], G.C. Grossi[82], Z.J. Grout[81], A. Grummer[107], L. Guan[92], W. Guan[176], J. Guenther[65], F. Guescini[163a], D. Guest[166], O. Gueta[155], B. Gui[113], E. Guido[53a,53b], T. Guillemin[5], S. Guindon[32], U. Gul[56], C. Gumpert[32], J. Guo[36c], W. Guo[92], Y. Guo[36a,w], R. Gupta[43], S. Gupta[122], G. Gustavino[115], B.J. Gutelman[154], P. Gutierrez[115], N.G. Gutierrez Ortiz[81], C. Gutschow[81], C. Guyot[138], M.P. Guzik[41a], C. Gwenlan[122], C.B. Gwilliam[77], A. Haas[112], C. Haber[16], H.K. Hadavand[8], N. Haddad[137e], A. Hadef[88], S. Hageböck[23], M. Hagihara[164], H. Hakobyan[180,*], M. Haleem[45], J. Haley[116], G. Halladjian[93], G.D. Hallewell[88], K. Hamacher[178], P. Hamal[117], K. Hamano[172], A. Hamilton[147a], G.N. Hamity[141], P.G. Hamnett[45], L. Han[36a], S. Han[35a,35d], K. Hanagaki[69,x], K. Hanawa[157], M. Hance[139], D.M. Handl[102], B. Haney[124], P. Hanke[60a], J.B. Hansen[39], J.D. Hansen[39], M.C. Hansen[23], P.H. Hansen[39], K. Hara[164], A.S. Hard[176], T. Harenberg[178], F. Hariri[119], S. Harkusha[95], P.F. Harrison[173], N.M. Hartmann[102], Y. Hasegawa[142], A. Hasib[49], S. Hassani[138], S. Haug[18], R. Hauser[93], L. Hauswald[47], L.B. Havener[38], M. Havranek[130], C.M. Hawkes[19], R.J. Hawkings[32], D. Hayakawa[159], D. Hayden[93], C.P. Hays[122], J.M. Hays[79], H.S. Hayward[77], S.J. Haywood[133], S.J. Head[19], T. Heck[86], V. Hedberg[84], L. Heelan[8], S. Heer[23], K.K. Heidegger[51], S. Heim[45], T. Heim[16], B. Heinemann[45,y], J.J. Heinrich[102], L. Heinrich[112], C. Heinz[55], J. Hejbal[129], L. Helary[32], A. Held[171], S. Hellman[148a,148b], C. Helsens[32], R.C.W. Henderson[75], Y. Heng[176], S. Henkelmann[171], A.M. Henriques Correia[32], S. Henrot-Versille[119], G.H. Herbert[17], H. Herde[25], V. Herget[177], Y. Hernández Jiménez[147c], H. Herr[86], G. Herten[51], R. Hertenberger[102], L. Hervas[32], T.C. Herwig[124], G.G. Hesketh[81], N.P. Hessey[163a], J.W. Hetherly[43], S. Higashino[69], E. Higón-Rodriguez[170], K. Hildebrand[33], E. Hill[172], J.C. Hill[30], K.H. Hiller[45], S.J. Hillier[19], M. Hils[47], I. Hinchliffe[16], M. Hirose[51], D. Hirschbuehl[178], B. Hiti[78], O. Hladik[129], X. Hoad[49], J. Hobbs[150], N. Hod[163a], M.C. Hodgkinson[141], P. Hodgson[141], A. Hoecker[32], M.R. Hoeferkamp[107], F. Hoenig[102], D. Hohn[23], T.R. Holmes[33], M. Homann[46], S. Honda[164], T. Honda[69], T.M. Hong[127], B.H. Hooberman[169], W.H. Hopkins[118], Y. Horii[105], A.J. Horton[144], J-Y. Hostachy[58], A. Hostiuc[140], S. Hou[153], A. Hoummada[137a], J. Howarth[87], J. Hoya[74], M. Hrabovsky[117], J. Hrdinka[32], I. Hristova[17], J. Hrivnac[119], T. Hryn'ova[5], A. Hrynevich[96], P.J. Hsu[63], S.-C. Hsu[140], Q. Hu[36a], S. Hu[36c], Y. Huang[35a], Z. Hubacek[130], F. Hubaut[88], F. Huegging[23], T.B. Huffman[122], E.W. Hughes[38],

G. Hughes[75], M. Huhtinen[32], P. Huo[150], N. Huseynov[68,b], J. Huston[93], J. Huth[59], G. Iacobucci[52], G. Iakovidis[27], I. Ibragimov[143], L. Iconomidou-Fayard[119], Z. Idrissi[137e], P. Iengo[32], O. Igonkina[109,z], T. Iizawa[174], Y. Ikegami[69], M. Ikeno[69], Y. Ilchenko[11,aa], D. Iliadis[156], N. Ilic[145], G. Introzzi[123a,123b], P. Ioannou[9,*], M. Iodice[136a], K. Iordanidou[38], V. Ippolito[59], M.F. Isacson[168], N. Ishijima[120], M. Ishino[157], M. Ishitsuka[159], C. Issever[122], S. Istin[20a], F. Ito[164], J.M. Iturbe Ponce[62a], R. Iuppa[162a,162b], H. Iwasaki[69], J.M. Izen[44], V. Izzo[106a], S. Jabbar[3], P. Jackson[1], R.M. Jacobs[23], V. Jain[2], K.B. Jakobi[86], K. Jakobs[51], S. Jakobsen[65], T. Jakoubek[129], D.O. Jamin[116], D.K. Jana[82], R. Jansky[52], J. Janssen[23], M. Janus[57], P.A. Janus[41a], G. Jarlskog[84], N. Javadov[68,b], T. Javůrek[51], M. Javurkova[51], F. Jeanneau[138], L. Jeanty[16], J. Jejelava[54a,ab], A. Jelinskas[173], P. Jenni[51,ac], C. Jeske[173], S. Jézéquel[5], H. Ji[176], J. Jia[150], H. Jiang[67], Y. Jiang[36a], Z. Jiang[145], S. Jiggins[81], J. Jimenez Pena[170], S. Jin[35a], A. Jinaru[28b], O. Jinnouchi[159], H. Jivan[147c], P. Johansson[141], K.A. Johns[7], C.A. Johnson[64], W.J. Johnson[140], K. Jon-And[148a,148b], R.W.L. Jones[75], S.D. Jones[151], S. Jones[7], T.J. Jones[77], J. Jongmanns[60a], P.M. Jorge[128a,128b], J. Jovicevic[163a], X. Ju[176], A. Juste Rozas[13,v], M.K. Köhler[175], A. Kaczmarska[42], M. Kado[119], H. Kagan[113], M. Kagan[145], S.J. Kahn[88], T. Kaji[174], E. Kajomovitz[48], C.W. Kalderon[84], A. Kaluza[86], S. Kama[43], A. Kamenshchikov[132], N. Kanaya[157], L. Kanjir[78], V.A. Kantserov[100], J. Kanzaki[69], B. Kaplan[112], L.S. Kaplan[176], D. Kar[147c], K. Karakostas[10], N. Karastathis[10], M.J. Kareem[57], E. Karentzos[10], S.N. Karpov[68], Z.M. Karpova[68], K. Karthik[112], V. Kartvelishvili[75], A.N. Karyukhin[132], K. Kasahara[164], L. Kashif[176], R.D. Kass[113], A. Kastanas[149], Y. Kataoka[157], C. Kato[157], A. Katre[52], J. Katzy[45], K. Kawade[70], K. Kawagoe[73], T. Kawamoto[157], G. Kawamura[57], E.F. Kay[77], V.F. Kazanin[111,c], R. Keeler[172], R. Kehoe[43], J.S. Keller[31], E. Kellermann[84], J.J. Kempster[80], J Kendrick[19], H. Keoshkerian[161], O. Kepka[129], B.P. Kerševan[78], S. Kersten[178], R.A. Keyes[90], M. Khader[169], F. Khalil-zada[12], A. Khanov[116], A.G. Kharlamov[111,c], T. Kharlamova[111,c], A. Khodinov[160], T.J. Khoo[52], V. Khovanskiy[99,*], E. Khramov[68], J. Khubua[54b,ad], S. Kido[70], C.R. Kilby[80], H.Y. Kim[8], S.H. Kim[164], Y.K. Kim[33], N. Kimura[156], O.M. Kind[17], B.T. King[77], D. Kirchmeier[47], J. Kirk[133], A.E. Kiryunin[103], T. Kishimoto[157], D. Kisielewska[41a], V. Kitali[45], O. Kivernyk[5], E. Kladiva[146b], T. Klapdor-Kleingrothaus[51], M.H. Klein[92], M. Klein[77], U. Klein[77], K. Kleinknecht[86], P. Klimek[110], A. Klimentov[27], R. Klingenberg[46], T. Klingl[23], T. Klioutchnikova[32], E.-E. Kluge[60a], P. Kluit[109], S. Kluth[103], E. Kneringer[65], E.B.F.G. Knoops[88], A. Knue[103], A. Kobayashi[157], D. Kobayashi[159], T. Kobayashi[157], M. Kobel[47], M. Kocian[145], P. Kodys[131], T. Koffas[31], E. Koffeman[109], N.M. Köhler[103], T. Koi[145], M. Kolb[60b], I. Koletsou[5], A.A. Komar[98,*], T. Kondo[69], N. Kondrashova[36c], K. Köneke[51], A.C. König[108], T. Kono[69,ae], R. Konoplich[112,af], N. Konstantinidis[81], R. Kopeliansky[64], S. Koperny[41a], A.K. Kopp[51], K. Korcyl[42], K. Kordas[156], A. Korn[81], A.A. Korol[111,c], I. Korolkov[13], E.V. Korolkova[141], O. Kortner[103], S. Kortner[103], T. Kosek[131], V.V. Kostyukhin[23], A. Kotwal[48], A. Koulouris[10], A. Kourkoumeli-Charalampidi[123a,123b], C. Kourkoumelis[9], E. Kourlitis[141], V. Kouskoura[27], A.B. Kowalewska[42], R. Kowalewski[172], T.Z. Kowalski[41a], C. Kozakai[157], W. Kozanecki[138], A.S. Kozhin[132], V.A. Kramarenko[101], G. Kramberger[78], D. Krasnopevtsev[100], M.W. Krasny[83], A. Krasznahorkay[32], D. Krauss[103], J.A. Kremer[41a], J. Kretzschmar[77], K. Kreutzfeldt[55], P. Krieger[161], K. Krizka[16], K. Kroeninger[46], H. Kroha[103], J. Kroll[129], J. Kroll[124], J. Kroseberg[23], J. Krstic[14], U. Kruchonak[68], H. Krüger[23], N. Krumnack[67], M.C. Kruse[48], T. Kubota[91], H. Kucuk[81], S. Kuday[4b], J.T. Kuechler[178], S. Kuehn[32], A. Kugel[60a], F. Kuger[177], T. Kuhl[45], V. Kukhtin[68], R. Kukla[88], Y. Kulchitsky[95], S. Kuleshov[34b], Y.P. Kulinich[169], M. Kuna[134a,134b], T. Kunigo[71], A. Kupco[129], T. Kupfer[46], O. Kuprash[155], H. Kurashige[70], L.L. Kurchaninov[163a], Y.A. Kurochkin[95], M.G. Kurth[35a,35d], V. Kus[129], E.S. Kuwertz[172], M. Kuze[159], J. Kvita[117], T. Kwan[172], D. Kyriazopoulos[141], A. La Rosa[103], J.L. La Rosa Navarro[26d], L. La Rotonda[40a,40b], F. La Ruffa[40a,40b], C. Lacasta[170], F. Lacava[134a,134b], J. Lacey[45], D.P.J. Lack[87], H. Lacker[17], D. Lacour[83], E. Ladygin[68], R. Lafaye[5], B. Laforge[83], T. Lagouri[179], S. Lai[57], S. Lammers[64], W. Lampl[7], E. Lançon[27], U. Landgraf[51], M.P.J. Landon[79], M.C. Lanfermann[52], V.S. Lang[45], J.C. Lange[13], R.J. Langenberg[32], A.J. Lankford[166], F. Lanni[27],

K. Lantzsch[23], A. Lanza[123a], A. Lapertosa[53a,53b], S. Laplace[83], J.F. Laporte[138], T. Lari[94a], F. Lasagni Manghi[22a,22b], M. Lassnig[32], T.S. Lau[62a], P. Laurelli[50], W. Lavrijsen[16], A.T. Law[139], P. Laycock[77], T. Lazovich[59], M. Lazzaroni[94a,94b], B. Le[91], O. Le Dortz[83], E. Le Guirriec[88], E.P. Le Quilleuc[138], M. LeBlanc[172], T. LeCompte[6], F. Ledroit-Guillon[58], C.A. Lee[27], G.R. Lee[133,ag], S.C. Lee[153], L. Lee[59], B. Lefebvre[90], G. Lefebvre[83], M. Lefebvre[172], F. Legger[102], C. Leggett[16], G. Lehmann Miotto[32], X. Lei[7], W.A. Leight[45], M.A.L. Leite[26d], R. Leitner[131], D. Lellouch[175], B. Lemmer[57], K.J.C. Leney[81], T. Lenz[23], B. Lenzi[32], R. Leone[7], S. Leone[126a], C. Leonidopoulos[49], G. Lerner[151], C. Leroy[97], A.A.J. Lesage[138], C.G. Lester[30], M. Levchenko[125], J. Levêque[5], D. Levin[92], L.J. Levinson[175], M. Levy[19], D. Lewis[79], B. Li[36a,w], H. Li[150], L. Li[36c], Q. Li[35a,35d], Q. Li[36a], S. Li[48], X. Li[36c], Y. Li[143], Z. Liang[35a], B. Liberti[135a], A. Liblong[161], K. Lie[62c], J. Liebal[23], W. Liebig[15], A. Limosani[152], S.C. Lin[182], T.H. Lin[86], R.A. Linck[64], B.E. Lindquist[150], A.E. Lionti[52], E. Lipeles[124], A. Lipniacka[15], M. Lisovyi[60b], T.M. Liss[169,ah], A. Lister[171], A.M. Litke[139], B. Liu[67], H. Liu[92], H. Liu[27], J.K.K. Liu[122], J. Liu[36b], J.B. Liu[36a], K. Liu[88], L. Liu[169], M. Liu[36a], Y.L. Liu[36a], Y. Liu[36a], M. Livan[123a,123b], A. Lleres[58], J. Llorente Merino[35a], S.L. Lloyd[79], C.Y. Lo[62b], F. Lo Sterzo[153], E.M. Lobodzinska[45], P. Loch[7], F.K. Loebinger[87], A. Loesle[51], K.M. Loew[25], A. Loginov[179,*], T. Lohse[17], K. Lohwasser[141], M. Lokajicek[129], B.A. Long[24], J.D. Long[169], R.E. Long[75], L. Longo[76a,76b], K.A. Looper[113], J.A. Lopez[34b], D. Lopez Mateos[59], I. Lopez Paz[13], A. Lopez Solis[83], J. Lorenz[102], N. Lorenzo Martinez[5], M. Losada[21], P.J. Lösel[102], X. Lou[35a], A. Lounis[119], J. Love[6], P.A. Love[75], H. Lu[62a], N. Lu[92], Y.J. Lu[63], H.J. Lubatti[140], C. Luci[134a,134b], A. Lucotte[58], C. Luedtke[51], F. Luehring[64], W. Lukas[65], L. Luminari[134a], O. Lundberg[148a,148b], B. Lund-Jensen[149], M.S. Lutz[89], P.M. Luzi[83], D. Lynn[27], R. Lysak[129], E. Lytken[84], F. Lyu[35a], V. Lyubushkin[68], H. Ma[27], L.L. Ma[36b], Y. Ma[36b], G. Maccarrone[50], A. Macchiolo[103], C.M. Macdonald[141], B. Maček[78], J. Machado Miguens[124,128b], D. Madaffari[170], R. Madar[37], W.F. Mader[47], A. Madsen[45], J. Maeda[70], S. Maeland[15], T. Maeno[27], A.S. Maevskiy[101], V. Magerl[51], J. Mahlstedt[109], C. Maiani[119], C. Maidantchik[26a], A.A. Maier[103], T. Maier[102], A. Maio[128a,128b,128d], O. Majersky[146a], S. Majewski[118], Y. Makida[69], N. Makovec[119], B. Malaescu[83], Pa. Malecki[42], V.P. Maleev[125], F. Malek[58], U. Mallik[66], D. Malon[6], C. Malone[30], S. Maltezos[10], S. Malyukov[32], J. Mamuzic[170], G. Mancini[50], I. Mandić[78], J. Maneira[128a,128b], L. Manhaes de Andrade Filho[26b], J. Manjarres Ramos[47], K.H. Mankinen[84], A. Mann[102], A. Manousos[32], B. Mansoulie[138], J.D. Mansour[35a], R. Mantifel[90], M. Mantoani[57], S. Manzoni[94a,94b], L. Mapelli[32], G. Marceca[29], L. March[52], L. Marchese[122], G. Marchiori[83], M. Marcisovsky[129], C.A. Marin Tobon[32], M. Marjanovic[37], D.E. Marley[92], F. Marroquim[26a], S.P. Marsden[87], Z. Marshall[16], M.U.F Martensson[168], S. Marti-Garcia[170], C.B. Martin[113], T.A. Martin[173], V.J. Martin[49], B. Martin dit Latour[15], M. Martinez[13,v], V.I. Martinez Outschoorn[169], S. Martin-Haugh[133], V.S. Martoiu[28b], A.C. Martyniuk[81], A. Marzin[32], L. Masetti[86], T. Mashimo[157], R. Mashinistov[98], J. Masik[87], A.L. Maslennikov[111,c], L. Massa[135a,135b], P. Mastrandrea[5], A. Mastroberardino[40a,40b], T. Masubuchi[157], P. Mättig[178], J. Maurer[28b], S.J. Maxfield[77], D.A. Maximov[111,c], R. Mazini[153], I. Maznas[156], S.M. Mazza[94a,94b], N.C. Mc Fadden[107], G. Mc Goldrick[161], S.P. Mc Kee[92], A. McCarn[92], R.L. McCarthy[150], T.G. McCarthy[103], L.I. McClymont[81], E.F. McDonald[91], J.A. Mcfayden[32], G. Mchedlidze[57], S.J. McMahon[133], P.C. McNamara[91], C.J. McNicol[173], R.A. McPherson[172,o], S. Meehan[140], T.J. Megy[51], S. Mehlhase[102], A. Mehta[77], T. Meideck[58], K. Meier[60a], B. Meirose[44], D. Melini[170,ai], B.R. Mellado Garcia[147c], J.D. Mellenthin[57], M. Melo[146a], F. Meloni[18], A. Melzer[23], S.B. Menary[87], L. Meng[77], X.T. Meng[92], A. Mengarelli[22a,22b], S. Menke[103], E. Meoni[40a,40b], S. Mergelmeyer[17], C. Merlassino[18], P. Mermod[52], L. Merola[106a,106b], C. Meroni[94a], F.S. Merritt[33], A. Messina[134a,134b], J. Metcalfe[6], A.S. Mete[166], C. Meyer[124], J-P. Meyer[138], J. Meyer[109], H. Meyer Zu Theenhausen[60a], F. Miano[151], R.P. Middleton[133], S. Miglioranzi[53a,53b], L. Mijović[49], G. Mikenberg[175], M. Mikestikova[129], M. Mikuž[78], M. Milesi[91], A. Milic[161], D.A. Millar[79], D.W. Miller[33], C. Mills[49], A. Milov[175], D.A. Milstead[148a,148b], A.A. Minaenko[132], Y. Minami[157], I.A. Minashvili[54b], A.I. Mincer[112],

B. Mindur[41a], M. Mineev[68], Y. Minegishi[157], Y. Ming[176], L.M. Mir[13], K.P. Mistry[124], T. Mitani[174], J. Mitrevski[102], V.A. Mitsou[170], A. Miucci[18], P.S. Miyagawa[141], A. Mizukami[69], J.U. Mjörnmark[84], T. Mkrtchyan[180], M. Mlynarikova[131], T. Moa[148a,148b], K. Mochizuki[97], P. Mogg[51], S. Mohapatra[38], S. Molander[148a,148b], R. Moles-Valls[23], M.C. Mondragon[93], K. Mönig[45], J. Monk[39], E. Monnier[88], A. Montalbano[150], J. Montejo Berlingen[32], F. Monticelli[74], S. Monzani[94a], R.W. Moore[3], N. Morange[119], D. Moreno[21], M. Moreno Llácer[32], P. Morettini[53a], S. Morgenstern[32], D. Mori[144], T. Mori[157], M. Morii[59], M. Morinaga[174], V. Morisbak[121], A.K. Morley[32], G. Mornacchi[32], J.D. Morris[79], L. Morvaj[150], P. Moschovakos[10], M. Mosidze[54b], H.J. Moss[141], J. Moss[145,aj], K. Motohashi[159], R. Mount[145], E. Mountricha[27], E.J.W. Moyse[89], S. Muanza[88], F. Mueller[103], J. Mueller[127], R.S.P. Mueller[102], D. Muenstermann[75], P. Mullen[56], G.A. Mullier[18], F.J. Munoz Sanchez[87], W.J. Murray[173,133], H. Musheghyan[32], M. Muškinja[78], A.G. Myagkov[132,ak], M. Myska[130], B.P. Nachman[16], O. Nackenhorst[52], K. Nagai[122], R. Nagai[69,ae], K. Nagano[69], Y. Nagasaka[61], K. Nagata[164], M. Nagel[51], E. Nagy[88], A.M. Nairz[32], Y. Nakahama[105], K. Nakamura[69], T. Nakamura[157], I. Nakano[114], R.F. Naranjo Garcia[45], R. Narayan[11], D.I. Narrias Villar[60a], I. Naryshkin[125], T. Naumann[45], G. Navarro[21], R. Nayyar[7], H.A. Neal[92], P.Yu. Nechaeva[98], T.J. Neep[138], A. Negri[123a,123b], M. Negrini[22a], S. Nektarijevic[108], C. Nellist[119], A. Nelson[166], M.E. Nelson[122], S. Nemecek[129], P. Nemethy[112], M. Nessi[32,al], M.S. Neubauer[169], M. Neumann[178], P.R. Newman[19], T.Y. Ng[62c], T. Nguyen Manh[97], R.B. Nickerson[122], R. Nicolaidou[138], J. Nielsen[139], V. Nikolaenko[132,ak], I. Nikolic-Audit[83], K. Nikolopoulos[19], J.K. Nilsen[121], P. Nilsson[27], Y. Ninomiya[157], A. Nisati[134a], N. Nishu[36c], R. Nisius[103], I. Nitsche[46], T. Nitta[174], T. Nobe[157], Y. Noguchi[71], M. Nomachi[120], I. Nomidis[31], M.A. Nomura[27], T. Nooney[79], M. Nordberg[32], N. Norjoharuddeen[122], O. Novgorodova[47], M. Nozaki[69], L. Nozka[117], K. Ntekas[166], E. Nurse[81], F. Nuti[91], K. O'connor[25], D.C. O'Neil[144], A.A. O'Rourke[45], V. O'Shea[56], F.G. Oakham[31,d], H. Oberlack[103], T. Obermann[23], J. Ocariz[83], A. Ochi[70], I. Ochoa[38], J.P. Ochoa-Ricoux[34a], S. Oda[73], S. Odaka[69], A. Oh[87], S.H. Oh[48], C.C. Ohm[16], H. Ohman[168], H. Oide[53a,53b], H. Okawa[164], Y. Okumura[157], T. Okuyama[69], A. Olariu[28b], L.F. Oleiro Seabra[128a], S.A. Olivares Pino[34a], D. Oliveira Damazio[27], A. Olszewski[42], J. Olszowska[42], A. Onofre[128a,128e], K. Onogi[105], P.U.E. Onyisi[11,aa], H. Oppen[121], M.J. Oreglia[33], Y. Oren[155], D. Orestano[136a,136b], N. Orlando[62b], R.S. Orr[161], B. Osculati[53a,53b,*], R. Ospanov[36a], G. Otero y Garzon[29], H. Otono[73], M. Ouchrif[137d], F. Ould-Saada[121], A. Ouraou[138], K.P. Oussoren[109], Q. Ouyang[35a], M. Owen[56], R.E. Owen[19], V.E. Ozcan[20a], N. Ozturk[8], K. Pachal[144], A. Pacheco Pages[13], L. Pacheco Rodriguez[138], C. Padilla Aranda[13], S. Pagan Griso[16], M. Paganini[179], F. Paige[27], G. Palacino[64], S. Palazzo[40a,40b], S. Palestini[32], M. Palka[41b], D. Pallin[37], E.St. Panagiotopoulou[10], I. Panagoulias[10], C.E. Pandini[126a,126b], J.G. Panduro Vazquez[80], P. Pani[32], S. Panitkin[27], D. Pantea[28b], L. Paolozzi[52], Th.D. Papadopoulou[10], K. Papageorgiou[9,s], A. Paramonov[6], D. Paredes Hernandez[179], A.J. Parker[75], M.A. Parker[30], K.A. Parker[45], F. Parodi[53a,53b], J.A. Parsons[38], U. Parzefall[51], V.R. Pascuzzi[161], J.M. Pasner[139], E. Pasqualucci[134a], S. Passaggio[53a], Fr. Pastore[80], S. Pataraia[86], J.R. Pater[87], T. Pauly[32], B. Pearson[103], S. Pedraza Lopez[170], R. Pedro[128a,128b], S.V. Peleganchuk[111,c], O. Penc[129], C. Peng[35a,35d], H. Peng[36a], J. Penwell[64], B.S. Peralva[26b], M.M. Perego[138], D.V. Perepelitsa[27], F. Peri[17], L. Perini[94a,94b], H. Pernegger[32], S. Perrella[106a,106b], R. Peschke[45], V.D. Peshekhonov[68,*], K. Peters[45], R.F.Y. Peters[87], B.A. Petersen[32], T.C. Petersen[39], E. Petit[58], A. Petridis[1], C. Petridou[156], P. Petroff[119], E. Petrolo[134a], M. Petrov[122], F. Petrucci[136a,136b], N.E. Pettersson[89], A. Peyaud[138], R. Pezoa[34b], F.H. Phillips[93], P.W. Phillips[133], G. Piacquadio[150], E. Pianori[173], A. Picazio[89], E. Piccaro[79], M.A. Pickering[122], R. Piegaia[29], J.E. Pilcher[33], A.D. Pilkington[87], A.W.J. Pin[87], M. Pinamonti[135a,135b], J.L. Pinfold[3], H. Pirumov[45], M. Pitt[175], L. Plazak[146a], M.-A. Pleier[27], V. Pleskot[86], E. Plotnikova[68], D. Pluth[67], P. Podberezko[111], R. Poettgen[84], R. Poggi[123a,123b], L. Poggioli[119], I. Pogrebnyak[93], D. Pohl[23], G. Polesello[123a], A. Poley[45], A. Policicchio[40a,40b], R. Polifka[32], A. Polini[22a], C.S. Pollard[56], V. Polychronakos[27], K. Pommès[32], D. Ponomarenko[100], L. Pontecorvo[134a], G.A. Popeneciu[28d],

D.M. Portillo Quintero[83], S. Pospisil[130], K. Potamianos[16], I.N. Potrap[68], C.J. Potter[30], H. Potti[11], T. Poulsen[84], J. Poveda[32], M.E. Pozo Astigarraga[32], P. Pralavorio[88], A. Pranko[16], S. Prell[67], D. Price[87], M. Primavera[76a], S. Prince[90], N. Proklova[100], K. Prokofiev[62c], F. Prokoshin[34b], S. Protopopescu[27], J. Proudfoot[6], M. Przybycien[41a], A. Puri[169], P. Puzo[119], J. Qian[92], G. Qin[56], Y. Qin[87], A. Quadt[57], M. Queitsch-Maitland[45], D. Quilty[56], S. Raddum[121], V. Radeka[27], V. Radescu[122], S.K. Radhakrishnan[150], P. Radloff[118], P. Rados[91], F. Ragusa[94a,94b], G. Rahal[181], J.A. Raine[87], S. Rajagopalan[27], C. Rangel-Smith[168], T. Rashid[119], S. Raspopov[5], M.G. Ratti[94a,94b], D.M. Rauch[45], F. Rauscher[102], S. Rave[86], I. Ravinovich[175], J.H. Rawling[87], M. Raymond[32], A.L. Read[121], N.P. Readioff[58], M. Reale[76a,76b], D.M. Rebuzzi[123a,123b], A. Redelbach[177], G. Redlinger[27], R. Reece[139], R.G. Reed[147c], K. Reeves[44], L. Rehnisch[17], J. Reichert[124], A. Reiss[86], C. Rembser[32], H. Ren[35a,35d], M. Rescigno[134a], S. Resconi[94a], E.D. Resseguie[124], S. Rettie[171], E. Reynolds[19], O.L. Rezanova[111,c], P. Reznicek[131], R. Rezvani[97], R. Richter[103], S. Richter[81], E. Richter-Was[41b], O. Ricken[23], M. Ridel[83], P. Rieck[103], C.J. Riegel[178], J. Rieger[57], O. Rifki[115], M. Rijssenbeek[150], A. Rimoldi[123a,123b], M. Rimoldi[18], L. Rinaldi[22a], G. Ripellino[149], B. Ristić[32], E. Ritsch[32], I. Riu[13], F. Rizatdinova[116], E. Rizvi[79], C. Rizzi[13], R.T. Roberts[87], S.H. Robertson[90,o], A. Robichaud-Veronneau[90], D. Robinson[30], J.E.M. Robinson[45], A. Robson[56], E. Rocco[86], C. Roda[126a,126b], Y. Rodina[88,am], S. Rodriguez Bosca[170], A. Rodriguez Perez[13], D. Rodriguez Rodriguez[170], S. Roe[32], C.S. Rogan[59], O. Røhne[121], J. Roloff[59], A. Romaniouk[100], M. Romano[22a,22b], S.M. Romano Saez[37], E. Romero Adam[170], N. Rompotis[77], M. Ronzani[51], L. Roos[83], S. Rosati[134a], K. Rosbach[51], P. Rose[139], N.-A. Rosien[57], E. Rossi[106a,106b], L.P. Rossi[53a], J.H.N. Rosten[30], R. Rosten[140], M. Rotaru[28b], J. Rothberg[140], D. Rousseau[119], A. Rozanov[88], Y. Rozen[154], X. Ruan[147c], F. Rubbo[145], F. Rühr[51], A. Ruiz-Martinez[31], Z. Rurikova[51], N.A. Rusakovich[68], H.L. Russell[90], J.P. Rutherfoord[7], N. Ruthmann[32], Y.F. Ryabov[125], M. Rybar[169], G. Rybkin[119], S. Ryu[6], A. Ryzhov[132], G.F. Rzehorz[57], A.F. Saavedra[152], G. Sabato[109], S. Sacerdoti[29], H.F-W. Sadrozinski[139], R. Sadykov[68], F. Safai Tehrani[134a], P. Saha[110], M. Sahinsoy[60a], M. Saimpert[45], M. Saito[157], T. Saito[157], H. Sakamoto[157], Y. Sakurai[174], G. Salamanna[136a,136b], J.E. Salazar Loyola[34b], D. Salek[109], P.H. Sales De Bruin[168], D. Salihagic[103], A. Salnikov[145], J. Salt[170], D. Salvatore[40a,40b], F. Salvatore[151], A. Salvucci[62a,62b,62c], A. Salzburger[32], D. Sammel[51], D. Sampsonidis[156], D. Sampsonidou[156], J. Sánchez[170], V. Sanchez Martinez[170], A. Sanchez Pineda[167a,167c], H. Sandaker[121], R.L. Sandbach[79], C.O. Sander[45], M. Sandhoff[178], C. Sandoval[21], D.P.C. Sankey[133], M. Sannino[53a,53b], Y. Sano[105], A. Sansoni[50], C. Santoni[37], H. Santos[128a], I. Santoyo Castillo[151], A. Sapronov[68], J.G. Saraiva[128a,128d], B. Sarrazin[23], O. Sasaki[69], K. Sato[164], E. Sauvan[5], G. Savage[80], P. Savard[161,d], N. Savic[103], C. Sawyer[133], L. Sawyer[82,u], J. Saxon[33], C. Sbarra[22a], A. Sbrizzi[22a,22b], T. Scanlon[81], D.A. Scannicchio[166], J. Schaarschmidt[140], P. Schacht[103], B.M. Schachtner[102], D. Schaefer[32], L. Schaefer[124], R. Schaefer[45], J. Schaeffer[86], S. Schaepe[23], S. Schaetzel[60b], U. Schäfer[86], A.C. Schaffer[119], D. Schaile[102], R.D. Schamberger[150], V.A. Schegelsky[125], D. Scheirich[131], M. Schernau[166], C. Schiavi[53a,53b], S. Schier[139], L.K. Schildgen[23], C. Schillo[51], M. Schioppa[40a,40b], S. Schlenker[32], K.R. Schmidt-Sommerfeld[103], K. Schmieden[32], C. Schmitt[86], S. Schmitt[45], S. Schmitz[86], U. Schnoor[51], L. Schoeffel[138], A. Schoening[60b], B.D. Schoenrock[93], E. Schopf[23], M. Schott[86], J.F.P. Schouwenberg[108], J. Schovancova[32], S. Schramm[52], N. Schuh[86], A. Schulte[86], M.J. Schultens[23], H.-C. Schultz-Coulon[60a], H. Schulz[17], M. Schumacher[51], B.A. Schumm[139], Ph. Schune[138], A. Schwartzman[145], T.A. Schwarz[92], H. Schweiger[87], Ph. Schwemling[138], R. Schwienhorst[93], J. Schwindling[138], A. Sciandra[23], G. Sciolla[25], M. Scornajenghi[40a,40b], F. Scuri[126a], F. Scutti[91], J. Searcy[92], P. Seema[23], S.C. Seidel[107], A. Seiden[139], J.M. Seixas[26a], G. Sekhniaidze[106a], K. Sekhon[92], S.J. Sekula[43], N. Semprini-Cesari[22a,22b], S. Senkin[37], C. Serfon[121], L. Serin[119], L. Serkin[167a,167b], M. Sessa[136a,136b], R. Seuster[172], H. Severini[115], T. Šfiligoj[78], F. Sforza[165], A. Sfyrla[52], E. Shabalina[57], N.W. Shaikh[148a,148b], L.Y. Shan[35a], R. Shang[169], J.T. Shank[24], M. Shapiro[16], P.B. Shatalov[99], K. Shaw[167a,167b], S.M. Shaw[87], A. Shcherbakova[148a,148b], C.Y. Shehu[151], Y. Shen[115], N. Sherafati[31],

P. Sherwood[81], L. Shi[153,an], S. Shimizu[70], C.O. Shimmin[179], M. Shimojima[104], I.P.J. Shipsey[122], S. Shirabe[73], M. Shiyakova[68,ao], J. Shlomi[175], A. Shmeleva[98], D. Shoaleh Saadi[97], M.J. Shochet[33], S. Shojaii[94a,94b], D.R. Shope[115], S. Shrestha[113], E. Shulga[100], M.A. Shupe[7], P. Sicho[129], A.M. Sickles[169], P.E. Sidebo[149], E. Sideras Haddad[147c], O. Sidiropoulou[177], A. Sidoti[22a,22b], F. Siegert[47], Dj. Sijacki[14], J. Silva[128a,128d], S.B. Silverstein[148a], V. Simak[130], L. Simic[14], S. Simion[119], E. Simioni[86], B. Simmons[81], M. Simon[86], P. Sinervo[161], N.B. Sinev[118], M. Sioli[22a,22b], G. Siragusa[177], I. Siral[92], S.Yu. Sivoklokov[101], J. Sjölin[148a,148b], M.B. Skinner[75], P. Skubic[115], M. Slater[19], T. Slavicek[130], M. Slawinska[42], K. Sliwa[165], R. Slovak[131], V. Smakhtin[175], B.H. Smart[5], J. Smiesko[146a], N. Smirnov[100], S.Yu. Smirnov[100], Y. Smirnov[100], L.N. Smirnova[101,ap], O. Smirnova[84], J.W. Smith[57], M.N.K. Smith[38], R.W. Smith[38], M. Smizanska[75], K. Smolek[130], A.A. Snesarev[98], I.M. Snyder[118], S. Snyder[27], R. Sobie[172,o], F. Socher[47], A. Soffer[155], A. Søgaard[49], D.A. Soh[153], G. Sokhrannyi[78], C.A. Solans Sanchez[32], M. Solar[130], E.Yu. Soldatov[100], U. Soldevila[170], A.A. Solodkov[132], A. Soloshenko[68], O.V. Solovyanov[132], V. Solovyev[125], P. Sommer[51], H. Son[165], A. Sopczak[130], D. Sosa[60b], C.L. Sotiropoulou[126a,126b], R. Soualah[167a,167c], A.M. Soukharev[111,c], D. South[45], B.C. Sowden[80], S. Spagnolo[76a,76b], M. Spalla[126a,126b], M. Spangenberg[173], F. Spanò[80], D. Sperlich[17], F. Spettel[103], T.M. Spieker[60a], R. Spighi[22a], G. Spigo[32], L.A. Spiller[91], M. Spousta[131], R.D. St. Denis[56,*], A. Stabile[94a,94b], R. Stamen[60a], S. Stamm[17], E. Stanecka[42], R.W. Stanek[6], C. Stanescu[136a], M.M. Stanitzki[45], B.S. Stapf[109], S. Stapnes[121], E.A. Starchenko[132], G.H. Stark[33], J. Stark[58], S.H Stark[39], P. Staroba[129], P. Starovoitov[60a], S. Stärz[32], R. Staszewski[42], M. Stegler[45], P. Steinberg[27], B. Stelzer[144], H.J. Stelzer[32], O. Stelzer-Chilton[163a], H. Stenzel[55], G.A. Stewart[56], M.C. Stockton[118], M. Stoebe[90], G. Stoicea[28b], P. Stolte[57], S. Stonjek[103], A.R. Stradling[8], A. Straessner[47], M.E. Stramaglia[18], J. Strandberg[149], S. Strandberg[148a,148b], M. Strauss[115], P. Strizenec[146b], R. Ströhmer[177], D.M. Strom[118], R. Stroynowski[43], A. Strubig[49], S.A. Stucci[27], B. Stugu[15], N.A. Styles[45], D. Su[145], J. Su[127], S. Suchek[60a], Y. Sugaya[120], M. Suk[130], V.V. Sulin[98], DMS Sultan[162a,162b], S. Sultansoy[4c], T. Sumida[71], S. Sun[59], X. Sun[3], K. Suruliz[151], C.J.E. Suster[152], M.R. Sutton[151], S. Suzuki[69], M. Svatos[129], M. Swiatlowski[33], S.P. Swift[2], I. Sykora[146a], T. Sykora[131], D. Ta[51], K. Tackmann[45], J. Taenzer[155], A. Taffard[166], R. Tafirout[163a], E. Tahirovic[79], N. Taiblum[155], H. Takai[27], R. Takashima[72], E.H. Takasugi[103], T. Takeshita[142], Y. Takubo[69], M. Talby[88], A.A. Talyshev[111,c], J. Tanaka[157], M. Tanaka[159], R. Tanaka[119], S. Tanaka[69], R. Tanioka[70], B.B. Tannenwald[113], S. Tapia Araya[34b], S. Tapprogge[86], S. Tarem[154], G.F. Tartarelli[94a], P. Tas[131], M. Tasevsky[129], T. Tashiro[71], E. Tassi[40a,40b], A. Tavares Delgado[128a,128b], Y. Tayalati[137e], A.C. Taylor[107], A.J. Taylor[49], G.N. Taylor[91], P.T.E. Taylor[91], W. Taylor[163b], P. Teixeira-Dias[80], D. Temple[144], H. Ten Kate[32], P.K. Teng[153], J.J. Teoh[120], F. Tepel[178], S. Terada[69], K. Terashi[157], J. Terron[85], S. Terzo[13], M. Testa[50], R.J. Teuscher[161,o], T. Theveneaux-Pelzer[88], F. Thiele[39], J.P. Thomas[19], J. Thomas-Wilsker[80], P.D. Thompson[19], A.S. Thompson[56], L.A. Thomsen[179], E. Thomson[124], M.J. Tibbetts[16], R.E. Ticse Torres[88], V.O. Tikhomirov[98,aq], Yu.A. Tikhonov[111,c], S. Timoshenko[100], P. Tipton[179], S. Tisserant[88], K. Todome[159], S. Todorova-Nova[5], S. Todt[47], J. Tojo[73], S. Tokár[146a], K. Tokushuku[69], E. Tolley[113], L. Tomlinson[87], M. Tomoto[105], L. Tompkins[145,ar], K. Toms[107], B. Tong[59], P. Tornambe[51], E. Torrence[118], H. Torres[47], E. Torró Pastor[140], J. Toth[88,as], F. Touchard[88], D.R. Tovey[141], C.J. Treado[112], T. Trefzger[177], F. Tresoldi[151], A. Tricoli[27], I.M. Trigger[163a], S. Trincaz-Duvoid[83], M.F. Tripiana[13], W. Trischuk[161], B. Trocmé[58], A. Trofymov[45], C. Troncon[94a], M. Trottier-McDonald[16], M. Trovatelli[172], L. Truong[147b], M. Trzebinski[42], A. Trzupek[42], K.W. Tsang[62a], J.C-L. Tseng[122], P.V. Tsiareshka[95], G. Tsipolitis[10], N. Tsirintanis[9], S. Tsiskaridze[13], V. Tsiskaridze[51], E.G. Tskhadadze[54a], K.M. Tsui[62a], I.I. Tsukerman[99], V. Tsulaia[16], S. Tsuno[69], D. Tsybychev[150], Y. Tu[62b], A. Tudorache[28b], V. Tudorache[28b], T.T. Tulbure[28a], A.N. Tuna[59], S.A. Tupputi[22a,22b], S. Turchikhin[68], D. Turgeman[175], I. Turk Cakir[4b,at], R. Turra[94a], P.M. Tuts[38], G. Ucchielli[22a,22b], I. Ueda[69], M. Ughetto[148a,148b], F. Ukegawa[164], G. Unal[32], A. Undrus[27], G. Unel[166], F.C. Ungaro[91], Y. Unno[69], C. Unverdorben[102], J. Urban[146b], P. Urquijo[91], P. Urrejola[86], G. Usai[8],

J. Usui[69], L. Vacavant[88], V. Vacek[130], B. Vachon[90], K.O.H. Vadla[121], A. Vaidya[81], C. Valderanis[102], E. Valdes Santurio[148a,148b], M. Valente[52], S. Valentinetti[22a,22b], A. Valero[170], L. Valéry[13], S. Valkar[131], A. Vallier[5], J.A. Valls Ferrer[170], W. Van Den Wollenberg[109], H. van der Graaf[109], P. van Gemmeren[6], J. Van Nieuwkoop[144], I. van Vulpen[109], M.C. van Woerden[109], M. Vanadia[135a,135b], W. Vandelli[32], A. Vaniachine[160], P. Vankov[109], G. Vardanyan[180], R. Vari[134a], E.W. Varnes[7], C. Varni[53a,53b], T. Varol[43], D. Varouchas[119], A. Vartapetian[8], K.E. Varvell[152], J.G. Vasquez[179], G.A. Vasquez[34b], F. Vazeille[37], D. Vazquez Furelos[13], T. Vazquez Schroeder[90], J. Veatch[57], V. Veeraraghavan[7], L.M. Veloce[161], F. Veloso[128a,128c], S. Veneziano[134a], A. Ventura[76a,76b], M. Venturi[172], N. Venturi[32], A. Venturini[25], V. Vercesi[123a], M. Verducci[136a,136b], W. Verkerke[109], A.T. Vermeulen[109], J.C. Vermeulen[109], M.C. Vetterli[144,d], N. Viaux Maira[34b], O. Viazlo[84], I. Vichou[169,*], T. Vickey[141], O.E. Vickey Boeriu[141], G.H.A. Viehhauser[122], S. Viel[16], L. Vigani[122], M. Villa[22a,22b], M. Villaplana Perez[94a,94b], E. Vilucchi[50], M.G. Vincter[31], V.B. Vinogradov[68], A. Vishwakarma[45], C. Vittori[22a,22b], I. Vivarelli[151], S. Vlachos[10], M. Vogel[178], P. Vokac[130], G. Volpi[13], H. von der Schmitt[103], E. von Toerne[23], V. Vorobel[131], K. Vorobev[100], M. Vos[170], R. Voss[32], J.H. Vossebeld[77], N. Vranjes[14], M. Vranjes Milosavljevic[14], V. Vrba[130], M. Vreeswijk[109], R. Vuillermet[32], I. Vukotic[33], P. Wagner[23], W. Wagner[178], J. Wagner-Kuhr[102], H. Wahlberg[74], S. Wahrmund[47], J. Walder[75], R. Walker[102], W. Walkowiak[143], V. Wallangen[148a,148b], C. Wang[35b], C. Wang[36b,au], F. Wang[176], H. Wang[16], H. Wang[3], J. Wang[45], J. Wang[152], Q. Wang[115], R. Wang[6], S.M. Wang[153], T. Wang[38], W. Wang[153,av], W. Wang[36a,aw], Z. Wang[36c], C. Wanotayaroj[118], A. Warburton[90], C.P. Ward[30], D.R. Wardrope[81], A. Washbrook[49], P.M. Watkins[19], A.T. Watson[19], M.F. Watson[19], G. Watts[140], S. Watts[87], B.M. Waugh[81], A.F. Webb[11], S. Webb[86], M.S. Weber[18], S.W. Weber[177], S.A. Weber[31], J.S. Webster[6], A.R. Weidberg[122], B. Weinert[64], J. Weingarten[57], M. Weirich[86], C. Weiser[51], H. Weits[109], P.S. Wells[32], T. Wenaus[27], T. Wengler[32], S. Wenig[32], N. Wermes[23], M.D. Werner[67], P. Werner[32], M. Wessels[60a], T.D. Weston[18], K. Whalen[118], N.L. Whallon[140], A.M. Wharton[75], A.S. White[92], A. White[8], M.J. White[1], R. White[34b], D. Whiteson[166], B.W. Whitmore[75], F.J. Wickens[133], W. Wiedenmann[176], M. Wielers[133], C. Wiglesworth[39], L.A.M. Wiik-Fuchs[51], A. Wildauer[103], F. Wilk[87], H.G. Wilkens[32], H.H. Williams[124], S. Williams[109], C. Willis[93], S. Willocq[89], J.A. Wilson[19], I. Wingerter-Seez[5], E. Winkels[151], F. Winklmeier[118], O.J. Winston[151], B.T. Winter[23], M. Wittgen[145], M. Wobisch[82,u], T.M.H. Wolf[109], R. Wolff[88], M.W. Wolter[42], H. Wolters[128a,128c], V.W.S. Wong[171], S.D. Worm[19], B.K. Wosiek[42], J. Wotschack[32], K.W. Wozniak[42], M. Wu[33], S.L. Wu[176], X. Wu[52], Y. Wu[92], T.R. Wyatt[87], B.M. Wynne[49], S. Xella[39], Z. Xi[92], L. Xia[35c], D. Xu[35a], L. Xu[27], T. Xu[138], B. Yabsley[152], S. Yacoob[147a], D. Yamaguchi[159], Y. Yamaguchi[159], A. Yamamoto[69], S. Yamamoto[157], T. Yamanaka[157], F. Yamane[70], M. Yamatani[157], T. Yamazaki[157], Y. Yamazaki[70], Z. Yan[24], H. Yang[36c], H. Yang[16], Y. Yang[153], Z. Yang[15], W-M. Yao[16], Y.C. Yap[83], Y. Yasu[69], E. Yatsenko[5], K.H. Yau Wong[23], J. Ye[43], S. Ye[27], I. Yeletskikh[68], E. Yigitbasi[24], E. Yildirim[86], K. Yorita[174], K. Yoshihara[124], C. Young[145], C.J.S. Young[32], J. Yu[8], J. Yu[67], S.P.Y. Yuen[23], I. Yusuff[30,ax], B. Zabinski[42], G. Zacharis[10], R. Zaidan[13], A.M. Zaitsev[132,ak], N. Zakharchuk[45], J. Zalieckas[15], A. Zaman[150], S. Zambito[59], D. Zanzi[91], C. Zeitnitz[178], G. Zemaityte[122], A. Zemla[41a], J.C. Zeng[169], Q. Zeng[145], O. Zenin[132], T. Ženiš[146a], D. Zerwas[119], D. Zhang[92], F. Zhang[176], G. Zhang[36a,aw], H. Zhang[119], J. Zhang[6], L. Zhang[51], L. Zhang[36a], M. Zhang[169], P. Zhang[35b], R. Zhang[23], R. Zhang[36a,au], X. Zhang[36b], Y. Zhang[35a,35d], Z. Zhang[119], X. Zhao[43], Y. Zhao[36b,ay], Z. Zhao[36a], A. Zhemchugov[68], B. Zhou[92], C. Zhou[176], L. Zhou[43], M. Zhou[35a,35d], M. Zhou[150], N. Zhou[35c], C.G. Zhu[36b], H. Zhu[35a], J. Zhu[92], Y. Zhu[36a], X. Zhuang[35a], K. Zhukov[98], A. Zibell[177], D. Zieminska[64], N.I. Zimine[68], C. Zimmermann[86], S. Zimmermann[51], Z. Zinonos[103], M. Zinser[86], M. Ziolkowski[143], L. Živković[14], G. Zobernig[176], A. Zoccoli[22a,22b], R. Zou[33], M. zur Nedden[17], L. Zwalinski[32].

[1] Department of Physics, University of Adelaide, Adelaide, Australia

[2] Physics Department, SUNY Albany, Albany NY, United States of America

[3] Department of Physics, University of Alberta, Edmonton AB, Canada
[4] [(a)] Department of Physics, Ankara University, Ankara; [(b)] Istanbul Aydin University, Istanbul; [(c)] Division of Physics, TOBB University of Economics and Technology, Ankara, Turkey
[5] LAPP, CNRS/IN2P3 and Université Savoie Mont Blanc, Annecy-le-Vieux, France
[6] High Energy Physics Division, Argonne National Laboratory, Argonne IL, United States of America
[7] Department of Physics, University of Arizona, Tucson AZ, United States of America
[8] Department of Physics, The University of Texas at Arlington, Arlington TX, United States of America
[9] Physics Department, National and Kapodistrian University of Athens, Athens, Greece
[10] Physics Department, National Technical University of Athens, Zografou, Greece
[11] Department of Physics, The University of Texas at Austin, Austin TX, United States of America
[12] Institute of Physics, Azerbaijan Academy of Sciences, Baku, Azerbaijan
[13] Institut de Física d'Altes Energies (IFAE), The Barcelona Institute of Science and Technology, Barcelona, Spain
[14] Institute of Physics, University of Belgrade, Belgrade, Serbia
[15] Department for Physics and Technology, University of Bergen, Bergen, Norway
[16] Physics Division, Lawrence Berkeley National Laboratory and University of California, Berkeley CA, United States of America
[17] Department of Physics, Humboldt University, Berlin, Germany
[18] Albert Einstein Center for Fundamental Physics and Laboratory for High Energy Physics, University of Bern, Bern, Switzerland
[19] School of Physics and Astronomy, University of Birmingham, Birmingham, United Kingdom
[20] [(a)] Department of Physics, Bogazici University, Istanbul; [(b)] Department of Physics Engineering, Gaziantep University, Gaziantep; [(d)] Istanbul Bilgi University, Faculty of Engineering and Natural Sciences, Istanbul; [(e)] Bahcesehir University, Faculty of Engineering and Natural Sciences, Istanbul, Turkey
[21] Centro de Investigaciones, Universidad Antonio Narino, Bogota, Colombia
[22] [(a)] INFN Sezione di Bologna; [(b)] Dipartimento di Fisica e Astronomia, Università di Bologna, Bologna, Italy
[23] Physikalisches Institut, University of Bonn, Bonn, Germany
[24] Department of Physics, Boston University, Boston MA, United States of America
[25] Department of Physics, Brandeis University, Waltham MA, United States of America
[26] [(a)] Universidade Federal do Rio De Janeiro COPPE/EE/IF, Rio de Janeiro; [(b)] Electrical Circuits Department, Federal University of Juiz de Fora (UFJF), Juiz de Fora; [(c)] Federal University of Sao Joao del Rei (UFSJ), Sao Joao del Rei; [(d)] Instituto de Fisica, Universidade de Sao Paulo, Sao Paulo, Brazil
[27] Physics Department, Brookhaven National Laboratory, Upton NY, United States of America
[28] [(a)] Transilvania University of Brasov, Brasov; [(b)] Horia Hulubei National Institute of Physics and Nuclear Engineering, Bucharest; [(c)] Department of Physics, Alexandru Ioan Cuza University of Iasi, Iasi; [(d)] National Institute for Research and Development of Isotopic and Molecular Technologies, Physics Department, Cluj Napoca; [(e)] University Politehnica Bucharest, Bucharest; [(f)] West University in Timisoara, Timisoara, Romania
[29] Departamento de Física, Universidad de Buenos Aires, Buenos Aires, Argentina
[30] Cavendish Laboratory, University of Cambridge, Cambridge, United Kingdom
[31] Department of Physics, Carleton University, Ottawa ON, Canada
[32] CERN, Geneva, Switzerland
[33] Enrico Fermi Institute, University of Chicago, Chicago IL, United States of America
[34] [(a)] Departamento de Física, Pontificia Universidad Católica de Chile, Santiago; [(b)] Departamento de Física, Universidad Técnica Federico Santa María, Valparaíso, Chile

[35] [(a)] Institute of High Energy Physics, Chinese Academy of Sciences, Beijing; [(b)] Department of Physics, Nanjing University, Jiangsu; [(c)] Physics Department, Tsinghua University, Beijing 100084; [(d)] University of Chinese Academy of Science (UCAS), Beijing, China
[36] [(a)] Department of Modern Physics and State Key Laboratory of Particle Detection and Electronics, University of Science and Technology of China, Anhui; [(b)] School of Physics, Shandong University, Shandong; [(c)] School of Physics and Astronomy, Key Laboratory for Particle Physics, Astrophysics and Cosmology, Ministry of Education; Shanghai Key Laboratory for Particle Physics and Cosmology, Tsung-Dao Lee Institute, Shanghai Jiao Tong University, China
[37] Université Clermont Auvergne, CNRS/IN2P3, LPC, Clermont-Ferrand, France
[38] Nevis Laboratory, Columbia University, Irvington NY, United States of America
[39] Niels Bohr Institute, University of Copenhagen, Kobenhavn, Denmark
[40] [(a)] INFN Gruppo Collegato di Cosenza, Laboratori Nazionali di Frascati; [(b)] Dipartimento di Fisica, Università della Calabria, Rende, Italy
[41] [(a)] AGH University of Science and Technology, Faculty of Physics and Applied Computer Science, Krakow; [(b)] Marian Smoluchowski Institute of Physics, Jagiellonian University, Krakow, Poland
[42] Institute of Nuclear Physics Polish Academy of Sciences, Krakow, Poland
[43] Physics Department, Southern Methodist University, Dallas TX, United States of America
[44] Physics Department, University of Texas at Dallas, Richardson TX, United States of America
[45] DESY, Hamburg and Zeuthen, Germany
[46] Lehrstuhl für Experimentelle Physik IV, Technische Universität Dortmund, Dortmund, Germany
[47] Institut für Kern- und Teilchenphysik, Technische Universität Dresden, Dresden, Germany
[48] Department of Physics, Duke University, Durham NC, United States of America
[49] SUPA - School of Physics and Astronomy, University of Edinburgh, Edinburgh, United Kingdom
[50] INFN e Laboratori Nazionali di Frascati, Frascati, Italy
[51] Fakultät für Mathematik und Physik, Albert-Ludwigs-Universität, Freiburg, Germany
[52] Departement de Physique Nucleaire et Corpusculaire, Université de Genève, Geneva, Switzerland
[53] [(a)] INFN Sezione di Genova; [(b)] Dipartimento di Fisica, Università di Genova, Genova, Italy
[54] [(a)] E. Andronikashvili Institute of Physics, Iv. Javakhishvili Tbilisi State University, Tbilisi; [(b)] High Energy Physics Institute, Tbilisi State University, Tbilisi, Georgia
[55] II Physikalisches Institut, Justus-Liebig-Universität Giessen, Giessen, Germany
[56] SUPA - School of Physics and Astronomy, University of Glasgow, Glasgow, United Kingdom
[57] II Physikalisches Institut, Georg-August-Universität, Göttingen, Germany
[58] Laboratoire de Physique Subatomique et de Cosmologie, Université Grenoble-Alpes, CNRS/IN2P3, Grenoble, France
[59] Laboratory for Particle Physics and Cosmology, Harvard University, Cambridge MA, United States of America
[60] [(a)] Kirchhoff-Institut für Physik, Ruprecht-Karls-Universität Heidelberg, Heidelberg; [(b)] Physikalisches Institut, Ruprecht-Karls-Universität Heidelberg, Heidelberg, Germany
[61] Faculty of Applied Information Science, Hiroshima Institute of Technology, Hiroshima, Japan
[62] [(a)] Department of Physics, The Chinese University of Hong Kong, Shatin, N.T., Hong Kong; [(b)] Department of Physics, The University of Hong Kong, Hong Kong; [(c)] Department of Physics and Institute for Advanced Study, The Hong Kong University of Science and Technology, Clear Water Bay, Kowloon, Hong Kong, China
[63] Department of Physics, National Tsing Hua University, Taiwan, Taiwan
[64] Department of Physics, Indiana University, Bloomington IN, United States of America
[65] Institut für Astro- und Teilchenphysik, Leopold-Franzens-Universität, Innsbruck, Austria
[66] University of Iowa, Iowa City IA, United States of America

[67] Department of Physics and Astronomy, Iowa State University, Ames IA, United States of America
[68] Joint Institute for Nuclear Research, JINR Dubna, Dubna, Russia
[69] KEK, High Energy Accelerator Research Organization, Tsukuba, Japan
[70] Graduate School of Science, Kobe University, Kobe, Japan
[71] Faculty of Science, Kyoto University, Kyoto, Japan
[72] Kyoto University of Education, Kyoto, Japan
[73] Research Center for Advanced Particle Physics and Department of Physics, Kyushu University, Fukuoka, Japan
[74] Instituto de Física La Plata, Universidad Nacional de La Plata and CONICET, La Plata, Argentina
[75] Physics Department, Lancaster University, Lancaster, United Kingdom
[76] [(a)] INFN Sezione di Lecce; [(b)] Dipartimento di Matematica e Fisica, Università del Salento, Lecce, Italy
[77] Oliver Lodge Laboratory, University of Liverpool, Liverpool, United Kingdom
[78] Department of Experimental Particle Physics, Jožef Stefan Institute and Department of Physics, University of Ljubljana, Ljubljana, Slovenia
[79] School of Physics and Astronomy, Queen Mary University of London, London, United Kingdom
[80] Department of Physics, Royal Holloway University of London, Surrey, United Kingdom
[81] Department of Physics and Astronomy, University College London, London, United Kingdom
[82] Louisiana Tech University, Ruston LA, United States of America
[83] Laboratoire de Physique Nucléaire et de Hautes Energies, UPMC and Université Paris-Diderot and CNRS/IN2P3, Paris, France
[84] Fysiska institutionen, Lunds universitet, Lund, Sweden
[85] Departamento de Fisica Teorica C-15, Universidad Autonoma de Madrid, Madrid, Spain
[86] Institut für Physik, Universität Mainz, Mainz, Germany
[87] School of Physics and Astronomy, University of Manchester, Manchester, United Kingdom
[88] CPPM, Aix-Marseille Université and CNRS/IN2P3, Marseille, France
[89] Department of Physics, University of Massachusetts, Amherst MA, United States of America
[90] Department of Physics, McGill University, Montreal QC, Canada
[91] School of Physics, University of Melbourne, Victoria, Australia
[92] Department of Physics, The University of Michigan, Ann Arbor MI, United States of America
[93] Department of Physics and Astronomy, Michigan State University, East Lansing MI, United States of America
[94] [(a)] INFN Sezione di Milano; [(b)] Dipartimento di Fisica, Università di Milano, Milano, Italy
[95] B.I. Stepanov Institute of Physics, National Academy of Sciences of Belarus, Minsk, Republic of Belarus
[96] Research Institute for Nuclear Problems of Byelorussian State University, Minsk, Republic of Belarus
[97] Group of Particle Physics, University of Montreal, Montreal QC, Canada
[98] P.N. Lebedev Physical Institute of the Russian Academy of Sciences, Moscow, Russia
[99] Institute for Theoretical and Experimental Physics (ITEP), Moscow, Russia
[100] National Research Nuclear University MEPhI, Moscow, Russia
[101] D.V. Skobeltsyn Institute of Nuclear Physics, M.V. Lomonosov Moscow State University, Moscow, Russia
[102] Fakultät für Physik, Ludwig-Maximilians-Universität München, München, Germany
[103] Max-Planck-Institut für Physik (Werner-Heisenberg-Institut), München, Germany
[104] Nagasaki Institute of Applied Science, Nagasaki, Japan
[105] Graduate School of Science and Kobayashi-Maskawa Institute, Nagoya University, Nagoya, Japan
[106] [(a)] INFN Sezione di Napoli; [(b)] Dipartimento di Fisica, Università di Napoli, Napoli, Italy

[107] Department of Physics and Astronomy, University of New Mexico, Albuquerque NM, United States of America
[108] Institute for Mathematics, Astrophysics and Particle Physics, Radboud University Nijmegen/Nikhef, Nijmegen, Netherlands
[109] Nikhef National Institute for Subatomic Physics and University of Amsterdam, Amsterdam, Netherlands
[110] Department of Physics, Northern Illinois University, DeKalb IL, United States of America
[111] Budker Institute of Nuclear Physics, SB RAS, Novosibirsk, Russia
[112] Department of Physics, New York University, New York NY, United States of America
[113] Ohio State University, Columbus OH, United States of America
[114] Faculty of Science, Okayama University, Okayama, Japan
[115] Homer L. Dodge Department of Physics and Astronomy, University of Oklahoma, Norman OK, United States of America
[116] Department of Physics, Oklahoma State University, Stillwater OK, United States of America
[117] Palacký University, RCPTM, Olomouc, Czech Republic
[118] Center for High Energy Physics, University of Oregon, Eugene OR, United States of America
[119] LAL, Univ. Paris-Sud, CNRS/IN2P3, Université Paris-Saclay, Orsay, France
[120] Graduate School of Science, Osaka University, Osaka, Japan
[121] Department of Physics, University of Oslo, Oslo, Norway
[122] Department of Physics, Oxford University, Oxford, United Kingdom
[123] [(a)] INFN Sezione di Pavia; [(b)] Dipartimento di Fisica, Università di Pavia, Pavia, Italy
[124] Department of Physics, University of Pennsylvania, Philadelphia PA, United States of America
[125] National Research Centre "Kurchatov Institute" B.P.Konstantinov Petersburg Nuclear Physics Institute, St. Petersburg, Russia
[126] [(a)] INFN Sezione di Pisa; [(b)] Dipartimento di Fisica E. Fermi, Università di Pisa, Pisa, Italy
[127] Department of Physics and Astronomy, University of Pittsburgh, Pittsburgh PA, United States of America
[128] [(a)] Laboratório de Instrumentação e Física Experimental de Partículas - LIP, Lisboa; [(b)] Faculdade de Ciências, Universidade de Lisboa, Lisboa; [(c)] Department of Physics, University of Coimbra, Coimbra; [(d)] Centro de Física Nuclear da Universidade de Lisboa, Lisboa; [(e)] Departamento de Fisica, Universidade do Minho, Braga; [(f)] Departamento de Fisica Teorica y del Cosmos, Universidad de Granada, Granada; [(g)] Dep Fisica and CEFITEC of Faculdade de Ciencias e Tecnologia, Universidade Nova de Lisboa, Caparica, Portugal
[129] Institute of Physics, Academy of Sciences of the Czech Republic, Praha, Czech Republic
[130] Czech Technical University in Prague, Praha, Czech Republic
[131] Charles University, Faculty of Mathematics and Physics, Prague, Czech Republic
[132] State Research Center Institute for High Energy Physics (Protvino), NRC KI, Russia
[133] Particle Physics Department, Rutherford Appleton Laboratory, Didcot, United Kingdom
[134] [(a)] INFN Sezione di Roma; [(b)] Dipartimento di Fisica, Sapienza Università di Roma, Roma, Italy
[135] [(a)] INFN Sezione di Roma Tor Vergata; [(b)] Dipartimento di Fisica, Università di Roma Tor Vergata, Roma, Italy
[136] [(a)] INFN Sezione di Roma Tre; [(b)] Dipartimento di Matematica e Fisica, Università Roma Tre, Roma, Italy
[137] [(a)] Faculté des Sciences Ain Chock, Réseau Universitaire de Physique des Hautes Energies - Université Hassan II, Casablanca; [(b)] Centre National de l'Energie des Sciences Techniques Nucleaires, Rabat; [(c)] Faculté des Sciences Semlalia, Université Cadi Ayyad, LPHEA-Marrakech; [(d)] Faculté des Sciences, Université Mohamed Premier and LPTPM, Oujda; [(e)] Faculté des sciences, Université

Mohammed V, Rabat, Morocco
[138] DSM/IRFU (Institut de Recherches sur les Lois Fondamentales de l'Univers), CEA Saclay (Commissariat à l'Energie Atomique et aux Energies Alternatives), Gif-sur-Yvette, France
[139] Santa Cruz Institute for Particle Physics, University of California Santa Cruz, Santa Cruz CA, United States of America
[140] Department of Physics, University of Washington, Seattle WA, United States of America
[141] Department of Physics and Astronomy, University of Sheffield, Sheffield, United Kingdom
[142] Department of Physics, Shinshu University, Nagano, Japan
[143] Department Physik, Universität Siegen, Siegen, Germany
[144] Department of Physics, Simon Fraser University, Burnaby BC, Canada
[145] SLAC National Accelerator Laboratory, Stanford CA, United States of America
[146] [(a)] Faculty of Mathematics, Physics & Informatics, Comenius University, Bratislava; [(b)] Department of Subnuclear Physics, Institute of Experimental Physics of the Slovak Academy of Sciences, Kosice, Slovak Republic
[147] [(a)] Department of Physics, University of Cape Town, Cape Town; [(b)] Department of Physics, University of Johannesburg, Johannesburg; [(c)] School of Physics, University of the Witwatersrand, Johannesburg, South Africa
[148] [(a)] Department of Physics, Stockholm University; [(b)] The Oskar Klein Centre, Stockholm, Sweden
[149] Physics Department, Royal Institute of Technology, Stockholm, Sweden
[150] Departments of Physics & Astronomy and Chemistry, Stony Brook University, Stony Brook NY, United States of America
[151] Department of Physics and Astronomy, University of Sussex, Brighton, United Kingdom
[152] School of Physics, University of Sydney, Sydney, Australia
[153] Institute of Physics, Academia Sinica, Taipei, Taiwan
[154] Department of Physics, Technion: Israel Institute of Technology, Haifa, Israel
[155] Raymond and Beverly Sackler School of Physics and Astronomy, Tel Aviv University, Tel Aviv, Israel
[156] Department of Physics, Aristotle University of Thessaloniki, Thessaloniki, Greece
[157] International Center for Elementary Particle Physics and Department of Physics, The University of Tokyo, Tokyo, Japan
[158] Graduate School of Science and Technology, Tokyo Metropolitan University, Tokyo, Japan
[159] Department of Physics, Tokyo Institute of Technology, Tokyo, Japan
[160] Tomsk State University, Tomsk, Russia
[161] Department of Physics, University of Toronto, Toronto ON, Canada
[162] [(a)] INFN-TIFPA; [(b)] University of Trento, Trento, Italy
[163] [(a)] TRIUMF, Vancouver BC; [(b)] Department of Physics and Astronomy, York University, Toronto ON, Canada
[164] Faculty of Pure and Applied Sciences, and Center for Integrated Research in Fundamental Science and Engineering, University of Tsukuba, Tsukuba, Japan
[165] Department of Physics and Astronomy, Tufts University, Medford MA, United States of America
[166] Department of Physics and Astronomy, University of California Irvine, Irvine CA, United States of America
[167] [(a)] INFN Gruppo Collegato di Udine, Sezione di Trieste, Udine; [(b)] ICTP, Trieste; [(c)] Dipartimento di Chimica, Fisica e Ambiente, Università di Udine, Udine, Italy
[168] Department of Physics and Astronomy, University of Uppsala, Uppsala, Sweden
[169] Department of Physics, University of Illinois, Urbana IL, United States of America
[170] Instituto de Fisica Corpuscular (IFIC), Centro Mixto Universidad de Valencia - CSIC, Spain
[171] Department of Physics, University of British Columbia, Vancouver BC, Canada

[172] Department of Physics and Astronomy, University of Victoria, Victoria BC, Canada
[173] Department of Physics, University of Warwick, Coventry, United Kingdom
[174] Waseda University, Tokyo, Japan
[175] Department of Particle Physics, The Weizmann Institute of Science, Rehovot, Israel
[176] Department of Physics, University of Wisconsin, Madison WI, United States of America
[177] Fakultät für Physik und Astronomie, Julius-Maximilians-Universität, Würzburg, Germany
[178] Fakultät für Mathematik und Naturwissenschaften, Fachgruppe Physik, Bergische Universität Wuppertal, Wuppertal, Germany
[179] Department of Physics, Yale University, New Haven CT, United States of America
[180] Yerevan Physics Institute, Yerevan, Armenia
[181] Centre de Calcul de l'Institut National de Physique Nucléaire et de Physique des Particules (IN2P3), Villeurbanne, France
[182] Academia Sinica Grid Computing, Institute of Physics, Academia Sinica, Taipei, Taiwan
[a] Also at Department of Physics, King's College London, London, United Kingdom
[b] Also at Institute of Physics, Azerbaijan Academy of Sciences, Baku, Azerbaijan
[c] Also at Novosibirsk State University, Novosibirsk, Russia
[d] Also at TRIUMF, Vancouver BC, Canada
[e] Also at Department of Physics & Astronomy, University of Louisville, Louisville, KY, United States of America
[f] Also at Physics Department, An-Najah National University, Nablus, Palestine
[g] Also at Department of Physics, California State University, Fresno CA, United States of America
[h] Also at Department of Physics, University of Fribourg, Fribourg, Switzerland
[i] Also at II Physikalisches Institut, Georg-August-Universität, Göttingen, Germany
[j] Also at Departament de Fisica de la Universitat Autonoma de Barcelona, Barcelona, Spain
[k] Also at Departamento de Fisica e Astronomia, Faculdade de Ciencias, Universidade do Porto, Portugal
[l] Also at Tomsk State University, Tomsk, and Moscow Institute of Physics and Technology State University, Dolgoprudny, Russia
[m] Also at The Collaborative Innovation Center of Quantum Matter (CICQM), Beijing, China
[n] Also at Universita di Napoli Parthenope, Napoli, Italy
[o] Also at Institute of Particle Physics (IPP), Canada
[p] Also at Horia Hulubei National Institute of Physics and Nuclear Engineering, Bucharest, Romania
[q] Also at Department of Physics, St. Petersburg State Polytechnical University, St. Petersburg, Russia
[r] Also at Borough of Manhattan Community College, City University of New York, New York City, United States of America
[s] Also at Department of Financial and Management Engineering, University of the Aegean, Chios, Greece
[t] Also at Centre for High Performance Computing, CSIR Campus, Rosebank, Cape Town, South Africa
[u] Also at Louisiana Tech University, Ruston LA, United States of America
[v] Also at Institucio Catalana de Recerca i Estudis Avancats, ICREA, Barcelona, Spain
[w] Also at Department of Physics, The University of Michigan, Ann Arbor MI, United States of America
[x] Also at Graduate School of Science, Osaka University, Osaka, Japan
[y] Also at Fakultät für Mathematik und Physik, Albert-Ludwigs-Universität, Freiburg, Germany
[z] Also at Institute for Mathematics, Astrophysics and Particle Physics, Radboud University Nijmegen/Nikhef, Nijmegen, Netherlands
[aa] Also at Department of Physics, The University of Texas at Austin, Austin TX, United States of America
[ab] Also at Institute of Theoretical Physics, Ilia State University, Tbilisi, Georgia

[ac] Also at CERN, Geneva, Switzerland
[ad] Also at Georgian Technical University (GTU),Tbilisi, Georgia
[ae] Also at Ochadai Academic Production, Ochanomizu University, Tokyo, Japan
[af] Also at Manhattan College, New York NY, United States of America
[ag] Also at Departamento de Física, Pontificia Universidad Católica de Chile, Santiago, Chile
[ah] Also at The City College of New York, New York NY, United States of America
[ai] Also at Departamento de Fisica Teorica y del Cosmos, Universidad de Granada, Granada, Portugal
[aj] Also at Department of Physics, California State University, Sacramento CA, United States of America
[ak] Also at Moscow Institute of Physics and Technology State University, Dolgoprudny, Russia
[al] Also at Departement de Physique Nucleaire et Corpusculaire, Université de Genève, Geneva, Switzerland
[am] Also at Institut de Física d'Altes Energies (IFAE), The Barcelona Institute of Science and Technology, Barcelona, Spain
[an] Also at School of Physics, Sun Yat-sen University, Guangzhou, China
[ao] Also at Institute for Nuclear Research and Nuclear Energy (INRNE) of the Bulgarian Academy of Sciences, Sofia, Bulgaria
[ap] Also at Faculty of Physics, M.V.Lomonosov Moscow State University, Moscow, Russia
[aq] Also at National Research Nuclear University MEPhI, Moscow, Russia
[ar] Also at Department of Physics, Stanford University, Stanford CA, United States of America
[as] Also at Institute for Particle and Nuclear Physics, Wigner Research Centre for Physics, Budapest, Hungary
[at] Also at Giresun University, Faculty of Engineering, Turkey
[au] Also at CPPM, Aix-Marseille Université and CNRS/IN2P3, Marseille, France
[av] Also at Department of Physics, Nanjing University, Jiangsu, China
[aw] Also at Institute of Physics, Academia Sinica, Taipei, Taiwan
[ax] Also at University of Malaya, Department of Physics, Kuala Lumpur, Malaysia
[ay] Also at LAL, Univ. Paris-Sud, CNRS/IN2P3, Université Paris-Saclay, Orsay, France
[*] Deceased